THE OHIO STATE UNIVERSITY

Department of Materials Science and Engineering

Principal Investigator: Dr. John Lannutti

Advising Graduate Student: Kayla Presley, PhD.

Parameter Optimization to Maximize Luminescent Oxygen Sensor Perfomance Embedded in a Core-Shell Electrospun Nanofiber Design.

By

Ryan Matthew Arnold

Honors Undergraduate Thesis Program

February 2020

Abstract

Oxygen is a critical molecule to several biological processes, making its detection important to several biomedical applications. Oxygen sensors designed using luminescent quenching molecules embedded in an electrospun nanofiber matrix offer several advantages over conventional oxygen sensors, including biocompatibility, ease of miniaturization, and high sensitivity. One of the inherent issues involved with using such a design is the phenomenon of photobleaching, which entails the photochemical degradation of the luminescent quenching probe molecules, resulting in a net loss of emission signal intensity. In this work, several different parameters were explored to determine which would minimize photobleaching to optimize device sensitivity and longevity by measuring changes in sensor molecule emission signal intensity and over time under different conditions. Electrospinning was used to fabricate "core-shell" fiber configurations, where the luminescent oxygen-sensitive molecules were embedded in a polymer "core" with a structurally stable, biocompatible polycaprolactone (PCL) shell. The concentration of luminescent probe molecules was altered and there were two levels of incubation temperature: 37^oC ($\approx$ body temperature) and 50^oC. To examine probe-matrix interaction effects, four polymers were used as core host matrices: Nylon-6, polyether sulfone (PES), polyethylene terephthalate (PET), polysulfone (PSU). All fibers doped with luminescent probes were subjected to long-term continuous light excitation to induce photobleaching. In addition, β-carotene was used as an additive to potentially reduce the detriments caused by photobleaching. Finally, the phosphorescent lifetime of all the aforementioned polymers was examined before and after continuous photoexcitation to explore whether photobleaching and core polymer host had significant effects on the measured phosphorescent lifetimes. Overall, we found that the choice of core polymer matrix and luminescent probe concentration had significant effects on sensor performance in the presence of photobleaching. Also, the choice of polymer matrix and induced photobleaching had significant effects on measured lifetime.

Dedication

This document is dedicated to my friends, family, and significant other.

Acknowledgments

I would like to humbly thank my advisor, Dr.John Lannutti, who gave me the opportunity to work in his lab over the course of 3 years and supported me throughout the entire process. I was treated with fairness and respect in his lab, and am very grateful for that. This work would not have been possible without his insight, advice, and encouragement.

I would also like to express great thanks to Kayla Presley, PhD. for all of her assistance as well. Kayla acted as a mentor throughout the entire process and often challenged me to think in new ways and helped cultivate my lab skills. From her guidance, I was able to become a researcher that I did not know I was capable of. The skills that I gleaned from her help I will take with me on my future endeavours and I will be forever grateful for that.

If it were not for Fransisco J. Chaparro, PhD., I would have never discovered the lab. At the time, Fransisco was a PhD candidate and introduced me to the lab. He took me under his wing and allowed me to assist him in one of his projects in pursuit of his PhD. Eventaully, I eventually began to work on my own projects, but I am still grateful for his teaching, guidance, and kindness and everything he has done for me.

Finally, I would like to thank my friends, family and significant other for all of their gracious support throughout the entire process.

Contents

List of Figures

List of Tables

1 Introduction

1.1 Background and Applications

Molecular oxygen is fundamental to many biological processes, making its detection and time-varying quantification important in biomedical applications. For instance, in cancer research, a common characteristic of advanced tumors is the presence of extremely hypoxic regions distributed within the tumor mass. This is caused by the increased oxygen demand imposed by the cancerous cell mass, insufficient vascularization, increased required oxygen diffusion distances, and the lower rate of oxygen transport caused by tumor blood vessel abnormalities. Furthermore, proper detection of oxygen concentration can indicate a patient's risk of tumor metastasis and provide better insight as to what medical treatment could be necessary. There are numerous other applications to oxygen sensing that include and are not limited to sports medicine applications, breath sensing devices, and oxygen sensing in military pilot apparatus. One conventional oxygen sensing device is the Clark electrode, which offers reliability and lack of heavy metal interference that could prevent oxygen diffusion through the sensing membrane. However, Clark electrodes consume oxygen during measurement and are not well-suited for biological applications due to their lack of miniaturization [2]. A more optimal design is to use luminescent oxygen sensing core-shell nanofibers.

Traditionally, oxygen sensing probes are incorporated into films that are not suited for biological applications, due to their inability to produce the three-dimensional information required by tissue-based engineering applications. Incorporating oxygen sensing probes with electrospun nanofibers offers several advantages, including rapid response times for real-time measurement, high sensitivity, ease of miniaturization, and the capability to mimic morphology resembling an extracellular matrix (ECM). In biological applications, the 3D ECM-like structure promotes cell adhesion, thereby enhancing biocompatibility. In addition, nanofiber-based optical sensors offer higher sensitivity, mass transfer rates, and stability, all of which can yield

more precise oxygen information from the luminescent oxygen sensing probes [3].

1.2 Introduction to Electrospinning

Electrospinning involves flowing a polymer solution held at its surface tension at the end of a capillary tube subjected to an electric field. Charge is then induced on the liquid surface. This causes mutual charge repulsion, resulting in a force opposite of the surface tension. As the magnitude of the electric field is increased, the hemispherical surface of the solution at the capillary tip elongates to form a conical structure known as a Taylor cone. After the electric field reaches the point where the repulsive electric force overcomes the surface tension force, a charged jet of solution forms out of the tip of the Taylor cone. Considering that the jet is charged, its trajectory can be controlled by the electric field. As the jet travels, the solvent of the polymer solution evaporates. What then remains is a charged polymer fiber, which collects randomly on a screen. Typically, the screen is composed of metal and can consequently be used as a grounding source [5]. See Figure 1 for a diagram depicting this process.

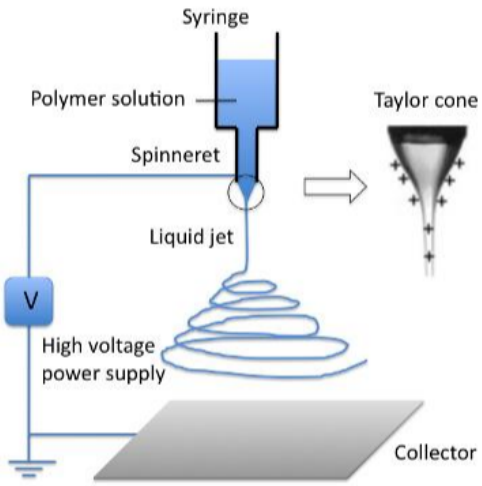

Figure 1: Electrospinning Technique Diagram. retrieved from: *http://www.intechopen.com*

Several experimental parameters affect the quality and diameter of the nanofibers. These include: solution viscosity, conductivity, capillary size, electric potential at the tip, solution flow

rate, and the distance between the tip and collection screen. The electrospinning process can also be sensitive to ambient conditions such as temperature, air velocity in the spinning chamber, and relative humidity. Typically, it is desired to produced small diameter fibers to maintain a high surface area to volume ratio, which facilitates higher rates of mass transport [5]. Maintaining controlled electrospinning parameters is important, as deviations can cause adverse effects on the resulting fibers. For instance, using too high of a voltage potential can cause the formation of multiple jets, which can form undesirable fiber characteristics. Also, other instabilities in the jet can cause beading along the fiber lengths [4].

Another critical electrospinning parameter is the choice of host polymer matrix. The selection influences probe sensor performance based on its solubility in the host matrix, stability, and oxygen permeability. In our work, we electrospun using coaxial spinning to produce a "core-shell" configuration. Not all polymer hosts are stable on their own, so this configuration makes it possible to embed a sensor compatible polymer host within a more structurally or more biocompatible shell. In our application, we used polycaprolactone (PCL) as a shell material combined with various other core polymer matrices. PCL offers both structural stability and excellent biocompatibility. Without the PCL shell, the core fibers deposit with low efficiency and form brittle, cotton-like mats. Overall, it is crucial to carefully choose electrospinning parameters that produce biocompatible, high-performance fibers [3].

1.3 Photochemistry of Luminescent Oxygen Probes

Oxygen detection using luminescent oxygen is possible due to their photochemistry. The principal optical method behind this is based on phosphorescence lifetime quenching. The mechanism involves an excited state luminescent probe being quenched by molecular oxygen. In terms of a luminescent oxygen sensor specifically, phosphorescence is the preferred excitation mechanism over fluorescence. In fluorescence, the probe absorbs light energy, and an electron is promoted to a higher energy state. The electron then fluoresces by immediately

returning to its ground state at a high rate, usually faster than the rate at which oxygen can quench the excited probe. On the contrary, phosphorescence has a much longer excited lifetime. In this case, after an electron is excited by light energy, it gets promoted to a higher energy singlet spin state (S_1). Then, instead of directly returning to ground state (S_0), the electron transitions to its lowest excited triplet state (T_1) via intersystem crossing (ISC) before eventually returning to its ground state configuration. The transition from the first singlet state to ground state and subsequent emission of photon energy is what is known as phosphorescence. However, the transition from the first excited state to ground state ($T_1 \rightarrow S_0$) is spin forbidden, making the lifetime of phosphorescence much longer than for fluorescence (e.g., 10^{-6} to several seconds). The longer duration excited state of phosphorescence grants enough time for molecular oxygen to quantifiably quench the excited probe [7]. See the Jablonski Diagram in Figure 2 for a diagram of this process.

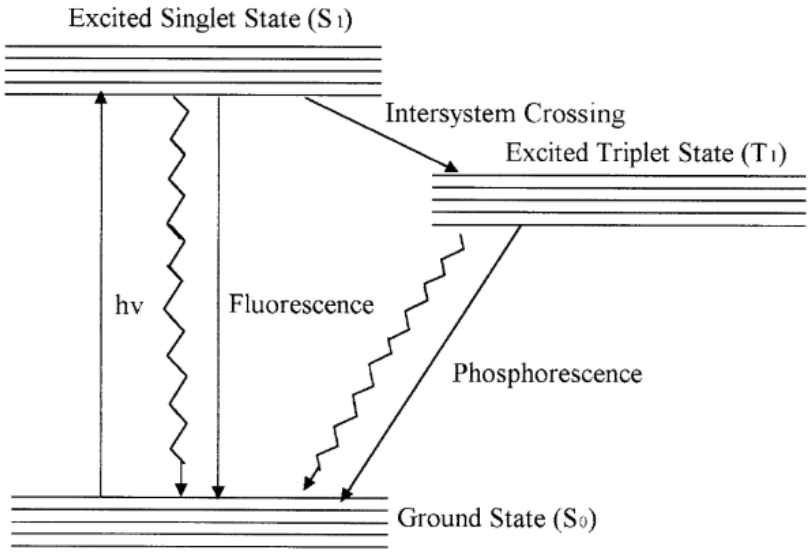

Figure 2: Jablonski Diagram depicting phosphorescence in luminescent oxygen probe [6].

When molecular oxygen comes in contact with the photoexcited probe, energy can be transferred to the oxygen molecule, such that it becomes promoted to singlet oxygen: $^1O_2$. Oxygen's ground state exists as a triplet spin state: $^3O_2$. Upon excitation, electrons are

promoted to the LUMO singlet state $^1O_2$. The event of energy transfer to oxygen results in a lower overall phosphorescent light intensity in the overall oxygen probe population [8]. Furthermore, since the amount of energy transfer depends on the amount of oxygen present, the quenching can be described by a Stern-Volmer relationship in Equations (1)-(2):

$$I_0/I = 1 + K_{SV}[O_2] \tag{1}$$

$$K_{SV} = k_2\tau_0 \tag{2}$$

where I and I_0 are the luminescent intensities with and without quencher, $[O_2]$ is the concentration of oxygen, k_2 is the bimolecular quenching rate constant, and τ_0 is the decay lifetime without any quencher present. Moreover, these equations can be calibrated in an oxygen sensor design to accurately determine a system's oxygen concentration [9]. See Figure 3 for a Diagram depicting the phosphorescent quenching process.

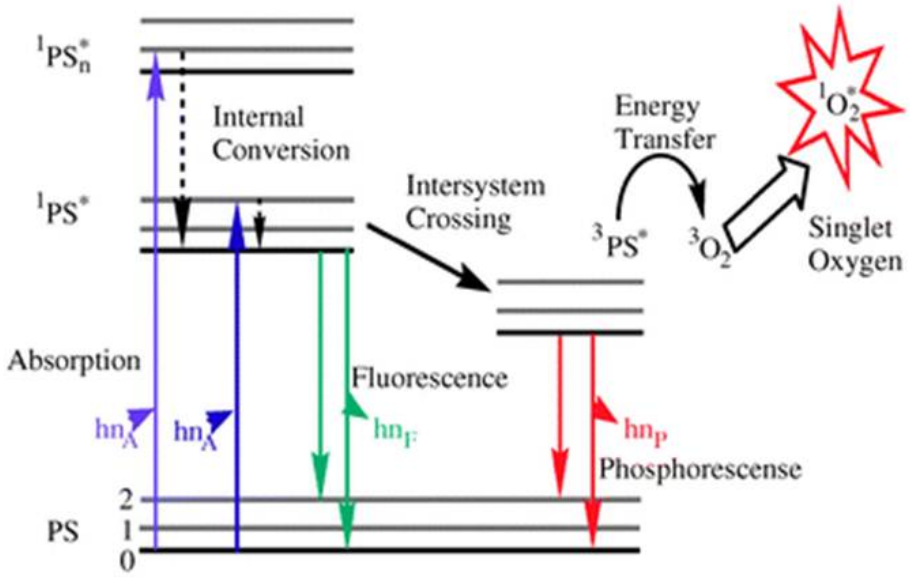

Figure 3: Diagram depicting phosphorescent quenching by molecular oxygen [8].

1.4 Oxygen Sensing Probe Selection

Several key factors have to be considered when selecting a sensing probe. The probe must first have good quantum yield and a distinct separation between the excitation and emission peaks (Stoke's shift). Having this property allows for easier measurement and detection of the luminescent signals. It is also desirable to have a long triplet lifetime (τ_0), so that there is ample time for photochemical energy transfer to occur via collision between the probe molecules and molecular oxygen. Other important characteristics include photostability, compatibility with the carrier, and low-energy excitation wavelength. Based on these criteria, three primary luminescent oxygen probes were selected to be used throughout the project. Two of the probes used were classified as metalloporphyrin dyes: PtTFPP {Pt (II) meso-tetra(pentafluorophenyl) porphine} and PdTFPP {Pd (II) meso-tetra(pentafluorophenyl) porphine}. The third dye chosen was a transition metal-complex dye: ($Ru(dpp)_3Cl_2$) {Tris (4,7-diphenyl-1,10-phenanthroline) ruthenium(II) dichloride)} [10].

One practical characteristic of all three dyes was they have excitation wavelengths within the visible light spectrum, namely within the blue wavelength region, with bright emission peaks. All three dyes are fundamentally similar upon excitation where either a metal d-orital or π electron is excited by visible light to a ligand π^* antibonding orbital. The central metal then helps facilitate intersystem crossing to a lower energy triplet spin state, thereby having a long duration of τ_0. Compared to the Pt and Pd porphyrins, however, the Ru complex has a much shorter lifetime and consequently lower detection sensitivity [11]. The Pt and Pd porphyrins also offer better stability due to the electron withdrawing nature of the perfluorophenyl substituents, being able to raise redox potentials and reduce the density of the porphyrin rings, making them stable against photo-oxidation and photo-reduction [6].

Comparing PtTFPP and PdTFPP, there are tradeoffs when using either one in a sensor design. PtTFPP offers excellent stability and performance longevity under continuous excitation. However, it lacks the high sensitivity and longer lifetime that PdTFPP offers. The

choice of dye strongly depends on the application and required levels of continuous light exposure. Nonetheless, both dyes demonstrate superior performance over the Ru complex. However, the Ru complex still has utility ironically because of its lower lifetime. Based on the lifetime spectrometer instrument that was available (mini-tau: Edinbergh Instruments), the lifetime of the Ru complex was within the device's constrained detection window. Thus, the Ru complex was a suitable selection for experiments exploring phosphorescent lifetime, τ_0 [3]. See Figures A.2-A.4 for the sensor chemical structures.

Although the blue light excitation wavelength of the proposed oxygen probes is low-energy and not technologically difficult to obtain as an excitation source, this compromises their performance for *in vivo* and *in vitro* sensing applications. Moreover, visible wavelengths do not properly transmit through adherent cell layers or tissue. However, near-infrared light (NIR) possesses the capability to fully penetrate tissue with minimal damage. In separate works, Presley proposed combining an oxygen sensing probe ($Ru(dpp)_3Cl_2$) in conjunction with upconverting nanoparticles composed of $Y_2O_2S : Yb, Tm$. Upon excitation by a NIR light source (980nm), the upconverting nanoparticles exhibit a blue light emission wavelength (480nm). These particles can then demonstrate a "handshake" interaction with the oxygen sensing probe by acting as a blue light excitation source, allowing the oxygen probe to adequately detect oxygen content. This technology makes the luminescent oxygen sensing design more practical, especially in biological/biomedical applications [12]. See Figure 4 for a diagram that depicts the "handshake" interaction.

1.5 Photobleaching

1.5.1 Photobleaching Description

An inherent underreported problem that occurs with luminescent oxygen sensors, namely the aforementioned probes, is the phenomenon of photobleaching. In short, this results in the

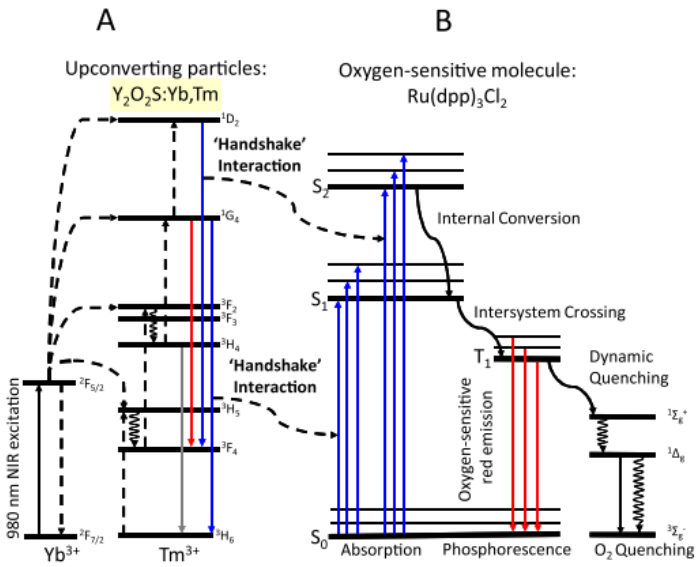

Figure 4: Diagram depicting ”handshake” interaction between oxygen sensing probe and nanoparticle upconverters [12].

sensor molecule gradually degrading over time under continuouous light excitation. Extended exposures to an excitation source can create severe photobleaching that would at the very least result in a net loss in emission signal. In the event that an adequate signal remains, new calibration curves would likely be required. It is therefore a critical goal to minimize photobleaching, especially in long-term sensing applications [14].

The major source of photobleaching in our application is the presence of singlet oxygen, which can be produced by the quenching process that is exploited to detect oxygen content. Singlet oxygen photochemically interacts with the sensor molecule and is involved in the production of a nonemissive photoproduct. The exact mechanism of the photochemical reaction and photoproduct identity are unclear, but singlet oxygen is at least known to enhance the processes involved in the photodegradation of the sensor molecules [15]. In our work, we visually observed the photoproduct by the presence of a distinct green portion of our polymer scaffolds, directly where the excitation source was applied. This is also shown visually in Figures D.2-D.3 in Appendix D.

There are several parameters that affect the rate of photobleaching. For instance, the chemistry of the luminescent molecules themselves is significant. As an example, PdTFPP experiences a higher rate of photobleaching than PtTFPP, mostly due to its longer lifetime [3]. The chemical interactions involved with the polymer matrix plays a large role in this as well. One factor is the differing oxygen permeabilities between polymer hosts. Another factor is the varying sensor molecule solubility in the host. Moreover, Xue demonstrated that the photobleaching of a Ru(II) polypyridyl complex decreased when incorporated with a polyethersulfone (PES) and polysulfone (PSU) matrix over a polycaprolactone (PCL) matrix [17]. Having a low or poor solubility in the host polymer matrix can alter the aggregation state of the molecule. Furthermore, this can result in clustered sensor molecule populations.

We hypothesized that highly aggregated populations have lower photostability due to self-quenching and higher probabilities of singlet oxygen photodegradation. Tightly aggregated populations have small distances between neighboring molecules, thus making the distance from an excited singlet oxygen molecule to another sensing molecule short. Moreover, this makes singlet oxygen collision probability much higher, resulting in a higher rate of photobleaching for systems that contain populations that are tightly aggregated [18, 19]. In the case of the experiment by Xue, PES and PSU possess relatively glassy, amorphous structures that likely helped facilitate a more uniform host environment compared to PCL as a host [17]. Presley also explored how solvent variation affected photobleaching rates. During the electrospinning process, solvent type and concentration are typically chosen based on volatility and conductivity, along with capability to dissolve the polymer. However, they hypothesized that the solvent could also influence the state of probe molecule aggregation; the high rates of solvent evaporation could leave the probe molecules fixed in aggregated states. Overall, they were able to demonstrate that both polymer and solvent selection have strong effects on the rate of photobleaching [13].

The oxygen sensing lifetime influences the rate of photobleaching as well. If the

luminescent molecule stays excited in the triplet state longer, there is a higher chance that an interaction with singlet oxygen will occur [16]. Different sensor molecules have their own natural lifetimes. However, we hypothesized that the host environment could also have a significant effect on lifetime and therefore photobleaching rates.

1.5.2 Proposed Investigations of Photobleaching

In this work, the previously discussed aggregation hypothesis is tested further. This was done in an experiment where PdTFPP and PtTFPP dyes were both selected as oxygen sensing probes, embedded in a PSU host matrix. The scaffolds were also electrospun in a core-shell configuration, using PSU as the core and PCL and the shell for added stability. Samples were prepared for each type of dye that had varying levels of dye concentration. Finally, each set of samples were replicated at two different temperatures: $37°C$ and $50°C$. Two dyes were tested to explore whether the different performing dyes experience similar effects on emission intensity caused by aggregation and self-quenching [29, 30]. Then, dye concentration was varied in both sets to explore if increasing dye load significantly affects dye performance and photostability.

We hypothesized that a higher dye concentration would increase the number of dye populations with a tightly aggregated state. Finally, we also examined two different temperatures because we hypothesized that an increased temperature could increase the solubility of the dyes in their host polymer, and therefore change the aggregation state of the dye populations. With higher solubility, we expected the dye populations to be more dispersed and less aggregated. We predicted self-quenching would occur at higher rates in more aggregated samples at lower temperatures. If self-quenching was occurring substantially, then it would follow that photobleaching could occur substantially in the same sensor configuration as well, since self-quenching indicates close sensor molecule proximity, making the distance to collision with singlet oxygen shorter [18, 19].

We also explored the interactions that could occur when the luminescent dyes were combine

with different polymer hosts. We chose a number of polymers that offer potential as hosts with different material properties, including oxygen permeability and modulus of elasticity. The following polymers were selected as candidate hosts: PSU, PET, PES, and Nylon-6. All of the polymers were electrospun using the same core-shell configuration, where each polymer acted as the core with a PCL shell. We also tested every polymer with PdTFPP dye as the oxygen sensor probe. All samples were also continuously excited by a green light source to induce photobleaching. The samples were then periodically examined under stimulation by blue light to evaluate sensor performance throughout the course of the period of induced photobleaching. Based on a combination of factors, we expected significant results between polymer levels, which could then be used as a basis for an oxygen sensor design. The exact selection would depend on the required performance characteristics, but would largely depend on level of sensitivity. Therefore, the aim of this particular experiment was to gain more insight on oxygen sensing performance across multiple polymers to make better design choices for applications that impose specific sensor design requirements.

Since phosphorescent lifetime has a critical role in the extent at which photobleaching occurs, we designed an experiment to further explore this and determine if lifetime varies in different polymer matrix hosts. These differences, if significant, could then be compared and contrasted with the oxygen sensitivity performance results of the polymer matrices from the previous experiment. These results are hypothesized to provide better insight on how significant the lifetime is and the potential interaction with polymer host. We expected higher lifetime systems to experience higher rates of photobleaching over time. We also tested lifetime before and after extended continuous excitation by a blue light source to induce photobleaching. This was done to explore whether or not photobleaching had any effect on the inherent lifetime of the sensor systems. We hypothesized that there could be some sort of significant effect in this regard.

One method to minimize photobleaching is to incorporate chemical stabilizers that quench

singlet oxygen. For example, Enko et al. demonstrated that incorporating the physical singlet oxygen quenching molecule: 1,4-Diazabicyclo[2.2.2] octane (DABCO) was found to significantly improve photostability of PtTFPP across multiple polymer hosts. This was proven by demonstrating that the total photon emissions were decreased when using DABCO, indicating that less singlet oxygen molecules were present as a result of interaction with the sensor molecule upon excitation [15]. In our experiment, we proposed to use $\beta-$Carotene as a singlet oxygen quencher. According to Stratton et al., $\beta-$Carotene is known to scavenge singlet oxygen primarily as a physical quencher with some quenching that occurs chemically. Chemical quenching is not as desirable, since it consumes $\beta-$Carotene during the photochemical process [20]. Despite this drawback, $\beta-$Carotene was chosen to experiment with due to its excellent solvent compatibility with the oxygen sensing probes and polymer matrix hosts that we examined. We hypothesized that by incorporating $\beta-$Carotene, we could slow the rate of photobleaching over time during continuous excitation. See Figure A.1 for the chemical structure of $\beta-$Carotene.

In summary, the overall aim of this project was to explore the different parameters that may significantly contribute to photobleaching and sensor performance. One unique facet of this project was some of the experiments were conducted over the course of 1000 hours up to a year, which was a lengthy duration not examined previously by anyone working in this field. After gaining insight as to what parameters significantly exacerbate photobleaching, we can then set the parameters to optimally design an electrospun core-shell luminescent oxygen sensing device.

2 Experimental Methodology

2.1 Materials / Apparatus

See Table 1 for all of the materials and equipment used throughout the course of the experiments.

Table 1: Equipment/Instrumentation used in experiments.

Equipment/Instrumentation	**Manufacturer**
High Voltage Power Supply	Gamma High Voltage Research
Auotmated Syringe Pumps	Kd Scientific
20 mL Syringes	Becton Dickinson and Company (BD)
12.5*12.5*45 mm Cuvettes	BRAND GMBH + CO KG
20 GA Precision Syringe Tips	Nordson EFD
Direct Heat CO2 Incubator	Thermo Electron Corporation
Jaz Spectral Sensing Suite (Spectrometer)	Ocean Optics
Accu Temp-09 Vacuum Oven	Across International
Dram Clear Vials	glassvials.com
Super Magnetic Stirrer	Fauske & Associates, LLC.
Magnetic Stirring Rods	Fisher Scientific
Discovery Precision Balance	OHAUS
Mini-tau fluorescent lifetime spectrometer	Edinburgh Instruments
Nova NanoSEM 400 (scanning electron microscopy)	FEI
Green LEDs (525nm)	LED Supply

See Table 2 for all materials used throughout the course of the experiments.

Table 2: Materials used in experiments.

Category	Material	Description	Manufacturer
General Materials	Compressed O2/N2	-	Praxair
	Aluminum Foil	-	Fisher Scientific
	Dessicant	$\geq 98\%$ CaSO4 ; $< 2\%$ CoCl2	W.A. Hammond Drierite Company LTD.
Polymers	Nylon-6	-	Sigma Aldrich
	PSU	Polysulfone	Sigma Aldrich
	PCL	Polycaprolactone	sigma Aldrich
	PES	Polyethersulfone	Good Fellow Cambridge Limited
	PET	polyethylene terephthalate	Good Fellow Cambridge Limited
Dyes	PdTFPP	Pd (II) meso-tetra(pentafluorophenyl) porphine	Frontier Scientific
	PtTFPP	Pt (II) meso-tetra(pentafluorophenyl) porphine	Frontier Scientific
	$Ru(dpp)_3Cl_2$	Tris (4,7-diphenyl-1,10-phenanthroline) ruthenium(II) dichloride	Alfa Aesar
Solvents	DCM	Methylene Chloride	Fisher Chemical
	Chloroform	Dichloromethane	Mallinckrodt Chemicals
	HFP	1,1,1,3,3,3 - hexafluoro-2-propanol	Oakwood Chemical

2.2 Experimental Procedures

2.2.1 Solution Preparation

Prior to electrospinning, solutions were prepared combining the polymer host, dye sensing molecule, and solvent. In addition, a solution was prepared for each sample group that acted as the shell. The shell solution was ubiquitous to all experiments, comprised of 5 wt% PCL dissolved in HFP. For the case of all different solution blends for the array of polymers tested throughout the experiments, two solvents were used. The reason for this was most of the solvents that were best suited to dissolve the polymers and dyes were not the best suited for electrospinning, based on volatility, conductivity, and other parameters. Furthermore, the first solution was typically present in smaller amounts for the purpose of homogeneity. They were also selected such that they were miscible in the second solvent to ensure that the solution was well-mixed during the electrospinning process. For example, HFP dissolves the polymer and dye very well, but is not as good of an electrospinning solvent as DCM.

In every case, each solution was prepared first by weighing out the dye using a precision balance and depositing it in a 15-mL glass vial. After this, the first of two solvents would be added, allowing the dye to completely dissolve. Proceeding this, the second solvent was measured out and added to the solution. Finally, polymer was weighed out and then added to the solution. The combined solution was allowed to dissolve overnight. In the case of solutions requiring PET as a host polymer, a stirring rod was added and the solution was mixed at a temperature of 40C overnight due to low solubility in the selected solvents at room temperature. See Table 3 for all solution compositions organized by experiment. Note that the weight composition of the polymer is relative to the entire solution mass, whereas the dye weight composition is relative to the total mass of polymer exclusively. Also, in the case of the PET solutions, the polymer weight composition was 5 wt.% instead of 12 wt.%. This was due to its low solubility, making 12 wt.% infeasible for our experiments. In the cases of PET and Nylon-6

solutions, the HFP solvent content is 75% compared to 25% DCM, contradicting the other solution compositions. Both Nylon-6 and PET experience better homogeneity, due to their higher HFP solubility. Finally, the solution prepared for the $\beta-$Carotene quencher analysis, 100% chloroform was used, since this better dissolves $\beta-$Carotene, is capable of dissolving the host polymer/PdTFPP dye, and served as an adequate electrospinning solvent.

Table 3: All experimental solution compositions.

Group	**Experiment**	**Polymer**	**wt.% Polymer**	**Dye Used**	**wt.% dye (relative to polymer mass)**	**Solvent mass ratios**
1	Aggregation	PSU	12	PdTFPP	[0.1, 0.5, 3, 10]	75% DCM 25% HFP
2		PSU	12	PtTFPP	[0.1, 0.5, 3, 10]	75% DCM 25% HFP
1	Aging	Nylon-6	12	PdTFPP	0.5	75% HFP 25% DCM
2		PES	12	PdTFPP	0.5	75% DCM 25% HFP
3		PET	5	PdTFPP	0.5	75% HFP 25% DCM
4		PSU	12	PdTFPP	0.5	75% DCM 25% HFP
1	Lifetime	Nylon-6	12	$Ru(dpp)_3Cl_2$	0.5	75% HFP 25% DCM
2		PES	12	$Ru(dpp)_3Cl_2$	0.5	75% DCM 25% HFP
3		PET	5	$Ru(dpp)_3Cl_2$	0.5	75% HFP 25% DCM
4		PSU	12	$Ru(dpp)_3Cl_2$	0.5	75% DCM 25% HFP
5		PSU	12	$Ru(dpp)_3Cl_2$	3	75% DCM 25% HFP
1	$\beta-$Carotene Analysis	PSU	12	PdTFPP	0.5+0.06wt.% $\beta-$Carotene	100% Chloroform

2.2.2 Electrospinning Procedure

Once the solutions were prepared and well-mixed, they were then prepped for electrospinning. Inside of a fume hood with proper ventilation, the core solutions were dispensed into a 20-mL syringe. Attached to the tip of the syringe was a coaxial needle that also had a port for a shell solution. The shell solution was always 5 wt.% PCL in HFP, also fed into a separate 20-mL syringe. To extend the reach of the shell solution, the syringe was connected to the coaxial needle with small diameter plastic tubing. Each of the two syringes was also configured to a kd-Scientific automated syringe pump. The flow rates were set to 2 and 4 mL/hr for the core and shell solutions respectively. The solutions were dispensed vertically

from the syringes to a small metal plate covered in aluminum foil. The displacement between the coaxial needle tip and the plate was set to 20cm. Before allowing the solutions to dispense, alligator clips were used to electrically connect the coaxial needle tip and metal plate, facilitating a voltage potential. The positive source was connected to the coaxial needle tip, while the plate was connection acted as the ground source. The source of power stemmed from the listed HVPS (High Voltage Power Supply). Once all preparation was complete, the power supply was set to 25 kV promptly after activating the syringe pumps.

After proper setup and application of the HVPS, nanofibers could clearly be observed in the gap between the needle and plate and would subsequently collect on the plate. The time that the nanofibers were allowed to collect varied, but averaged approximately 20 minutes. The criteria was based on a visual evaluation of the deposited electrospun scaffold thickness. We assumed for our purposes that the variation in thickness would have negligible effects on oxygen sensing signal performance. Once all fibers were deposited, the scaffolds were placed under vacuum for 24 hours to remove any excess moisture that could affect sensor performance.

2.2.3 Optical Signaling Characterization

Optical characterization was performed using a JAZ spectrometer with an accompanying software suite developed by Ocean Optics. The spectrometer had a built-in 470nm blue LED source connected to a 600 μm optical fiber. The process first involved placing any given sample inside a cuvette, flush against the inner surface. The samples were mounted in the cuvette by means of electrical tape. Once the samples were mounted properly inside the cuvettes, the software was calibrated to the conditions of a dark room. Any residual ambient light was zeroed out. After the software was setup, the sample would then be excited by the built-in blue light source, and the output emission intensity peaks were recorded to data files to be analyzed later. In some experiments, samples were subjected to different levels of oxygen. In cases where this applied, a custom cuvette cap was sealed to the top to allow gas to be charged via a needle inside

the small volume of the cuvette containing the sample. When gas was charged, the samples were given approximately 30 seconds to equilibrate before being excited by the blue light source.

2.2.4 Aggregation Experiments

The intent of the aggregation experiments was to see if hypothesized aggregation conditions significantly affected the performance of the oxygen sensing dyes over time. For this experiment, measurements were taken over varying intervals over the course of one year. There were two main sample groups that were held at two different constant temperatures during the entire time interval. The temperatures were $37°C$ and $50°C$. $37°C$ is close to the internal temperature of the human body, thereby helping simulate bodily conditions if the device were to be used in an application such as hypoxic tumor detection. $50°C$ was used as a higher temperature group to contrast with $37°C$ and examine whether higher temperatures would enhance the dye solubility state in the host polymer and allow for dye molecule populations that were less dense. Next, each temperature group was then blocked by the two selected porphyrin dyes electrospun with PSU-PCL fibers: PdTFPP and PtTFPP. Within each dye block, four levels of dye concentration were tested: 0.1, 0.5, 3, and 10 wt.% relative to host polymer mass. Each sample level as described had three replicates. The three replicates would originate from the same electrospun scaffold (can be referred to as a "fiber mat"). In other words, three samples would be cut from one electrospun scaffold. Cuts were made such that the samples would be flush with the cuvette when mounted for spectrometer analysis.

The samples were incubated over the course of a year. Emission intensity peaks were recorded upon blue light excitation in air (i.e., 21% oxygen) at the following intervals: day 0 (initial measurement), day 1, day 3, day 7, day 14, day 28, 1000 hours, 1 year. During the initial period, more emission samples were taken, since we wanted to capture probe solubility stabilization behavior that we expected to occur more rapidly up front. The time spacing towards the later intervals was larger since we were primarily interested in examining associated

long-term behavior. Once all the emission peaks were recorded, the intensity data points for each day were normalized by the initial values recorded at day 0.

2.2.5 Polymer Aging Experiments

The intent of this experiment was to subject different polymers containing an oxygen sensing dye to continuous excitation to induce photobleaching. We attempt to show the differences in dye sensing performance, based on polymer core host. The sample groups contained four levels of polymer: Nylon-6(PdTPP)-PCL, PES(PdTFPP)-PCL, PET(PdTFPP)-PCL, and PSU(PdTFPP)-PCL. Each polymer level contained three replicates. PdTFPP dye was concentrated at 0.5 wt% relative to polymer mass for every sample. PdTFPP was chosen for this experiment due to its higher sensitivity over PtTFPP, making the polymers groups more distinguishable from each other, provided they contribute statistically significant effects on sensing performance. Each replicate was taken from the same unique electrospun scaffold for each given configuration.

The long-term photobleaching tests were performed using 525 nm green LEDs. The continuous excitation wavelength was chosen based on its alignment with the PdTFPP absorption curve [21]. The tests were conducted using a 3D printed bay containing an array of 12 LEDs inside of cylinders with heights of 16mm. Furthermore, the samples were displaced approximately 16 mm away from the green LED excitation sources. Samples of each fiber were punched out of their respective scaffolds in the shape of circles so that they could be fastened to the top of the cylinders, allowing them to be fully exposed to the green light LEDs. The samples were held flush to the cylinder tops using electrical tape, the same tape that would be also be used to mount the samples to the cuvettes during spectrometer analysis. Emission intensity measurements for each sample were taken over the course of 1000 hours at the following time intervals: day 0 (initial measurement), 1 week, 2 weeks, 4 weeks, and 1000 hours. An additional day 1 measurement was taken exclusively for the Nylon-6 sample, due to its observed rapid rate

of photobleaching.

For this experiment, the intensity measurements were taken at three levels of oxygen concentration: 0%, 21%, and 100%. Prior to each spectrometer measurement, the 0% oxygen level was achieved by charging each cuvette with pure nitrogen, 21% was achieved using ambient air, and 100% was achieved by charging with pure oxygen. Having access to the pure nitrogen and oxygen intensities allowed us to measure oxygen sensitivity. Moreover, this was achieved by taking all nitrogen intensity values and dividing them by the pure oxygen environment measurements, producing data sets that were representative of oxygen sensitivity. To better demonstrate how photobleaching affects the relative sensitivity values, the data sets were also normalized by their initial values. A higher value of the ratio of indicates a higher sensitivity, meaning that the configuration would be more equipped to detect small changes in oxygen concentration. In application of a biomedical diagnostic device, high sensitivity is typically required. In addition to this, having measurements for three different oxygen concentrations made it possible to produce Stern-Volmer plots. Stern-Volmer plots with high slopes indicate high sensitivity. Also, having a high degree of linearity, as determined by evaluating the R^2 term after fitting a linear least squares regression model, indicates good probe-matrix compatibility and means more accurate calibration can be provided. Without accurate calibration, data analysis is no longer straightforward, rendering the sensor inadequate in biomedical applications [3].

2.2.6 Experiment Exploring $\beta-$Carotene as a Singlet Oxygen Quencher

The setup for this experiment was very similar to the setup in the aging experiments with a few notable differences. First, the solution solvent was purely chloroform. Also, in addition to a 0.5 wt.% PdTFPP dye load, 0.06 wt.% of total polymer mass of $\beta-$Carotene was added to act as a singlet oxygen quencher. β-Carotene can act as a quencher by absorbing excited state energy from singlet oxygen and dissipating it through its polyene chain [20]. The mass composition

was originally chosen to be close to 1:1 molar ratio with PdTFPP. However, $\beta-$Carotene posed several challenges during the electrospinning process, namely the formation of crystalline particles that clogged the needle tip, which then cause jet splitting. Furthermore, the 0.06 wt.%, (about $1/4$ equimolar amount) was found to produce reasonable fibers for testing. Measurements were taken at the following intervals: Day 0, 1, 2, 3, 7. The intent was then to prove if $\beta-$Carotene could significantly improve oxygen sensing performance by analyzing the same aforementioned normalized sensitivity ratios.

2.2.7 Lifetime Experiments

In the lifetime experiments, the objective was to determine if phosphorescent lifetime was significantly affected by either varying the polymer host or inducing photobleaching. This could then supplement the results obtained through the aging experiments. In this experiment, samples were grouped by the following polymer hosts: Nylon-6-PCL, PES-PCL, PET-PCL, and PSU-PCL. All hosts were contained within a shell composed of 5 wt.% PCL in HFP. The oxygen sensing probe used in this experiment was $Ru(dpp)_3Cl_2$, since the lifetime was more compatible with the detection window constraint of the Mini-Tau spectrometer used for lifetime characterization. All samples had a Ruthenium dye load of 0.5 wt.%, with the exception of PSU($Ru(dpp)_3Cl_2$)-PCL samples. The PSU samples had two levels of dye load: 0.5 wt.% and 3 wt.%. This allowed us to also analyze if aggregation was contributing to a difference in lifetime. PSU($Ru(dpp)_3Cl_2$)-PCL was the host selected to have two levels of dye concentration due to its high stability. Each sample subset contained three replicates, each of which came from the same unique electrospun fiber scaffold. The scaffold samples were then aged using a blue LED (470 nm) bay in the same manner as the previous experiment, and were optically examined over the course of a week. Blue light better overlaps with the $Ru(dpp)_3Cl_2$ absorption spectrum, hence why blue was used over green compared to the previous experiment. The measurements were taken in two batches: unaged and aged. The aged samples were continuously excited for 28

days. The duration was chosen based on what time span would induce a substantial amount of photobleaching, as indicated by a pale green discoloration.

Once all samples were prepared, lifetime was analyzed in the Mini-Tau spectrometer, which used a vertical pulsation laser as an excitation source. Pulses were sent at a wavelength of 444.4 nm with an 84.4 ps pulse width and a 50 μs pulse period. The device used 1024 channels that acted as photon bins to measure excited electron lifetimes. If the lifetime fell within a given bin time width, then a photon was counted in that bin. After letting the measurement take its course, the resulting data contained a data output file with a scatter plot where each point represented the counts in each discrete bin of lifetime. The resulting plots were then fitted to an exponential decay curve according to Equation (3), where a, b and c were fit parameters and x was time. The equations were fit using the SciPy library in Python 3 code. From Equation (3), the magnitude of the fit parameter b was used to estimate the lifetime in each data set. The source code can be retrieved from the following Git repository: *https://github.com/rarnold97/Research.git*.

$$a \times e^{-b \times x} + c \tag{3}$$

3 Results and Discussion

3.1 Aggregation Experiment Results and Discussion

The first set of analyzed data for the aggregation experiment includes the normalized intensity data for each set of dye loads and incubation temperature. The samples were divided into two different groups based on which dye was used: PdTFPP or PtTFPP. Also, to better demonstrate the early curve behavior, a separate plot was generated for both the first 1000 hour and the entire year time intervals for each sensing dye group. See Figures 5-B.4. Note that in all the plots, the points shown are based on the prediction values of a discrete model fit in JMP software. The

error bars are reflective of the 95% confidence intervals of the prediction, which takes the data spread into account. See Figures B.1-B.8 in Appendix B for the decay plots of emission intensity in an air environment.

Statistically, it was important to evaluate whether the effects of temperature, dye load, and day were significant. This was determined using ANOVA tables and parameter effect tests from the statistical models generated using JMP software. The following model in Equation (4) was hypothesized in the software, where all the effect terms were treated as discrete. Treating the terms as discrete made it possible to compare the differences between time levels, which can explain the observed early behavior of the data sets.

$$\hat{y} = \mu + \tau_{temperature} + \tau_{day} + \tau_{dyeload} + \tau_{day}\tau_{dyeload} + \epsilon \qquad (4)$$

In Equation (4), the $\hat{y}$ term is the estimate for normalized intensity (I_{Air}/I_{Air_0}), the μ term is the intercept estimate, the ϵ term accounts for random error, and all τ terms are parameter effect estimates for day, temperature, dye load, and the interaction between day and dye load. Other interaction terms were originally included, but were statistically insignificant by having p-values < 0.05, and were therefore omitted before arriving at the fully reduced model. In fact, for the PdTFPP dye group, all interaction terms were insignificant and omitted from the model in Equation (4). The first set of results in Tables 4-5 show the statistical significance of all the effects as a whole when taking every data series into account for each dye group.

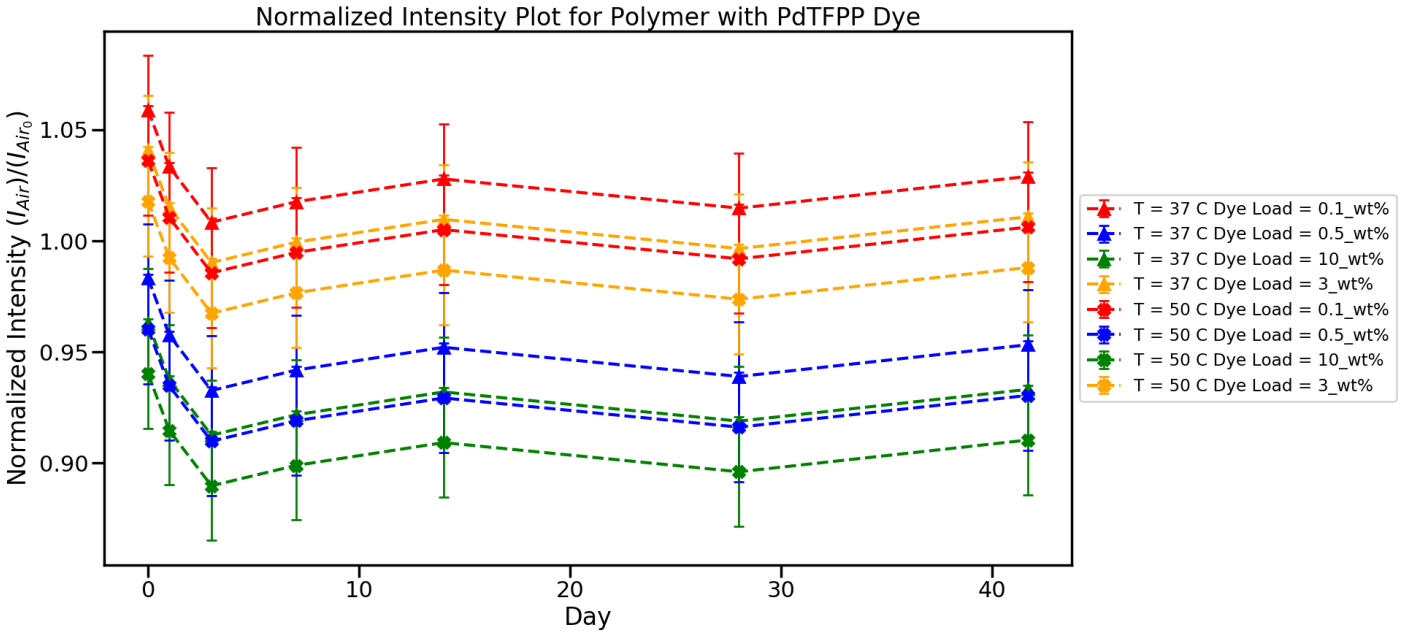

(a) Beginning normalized curve behavior for PdTFPP aggregation experiment group.

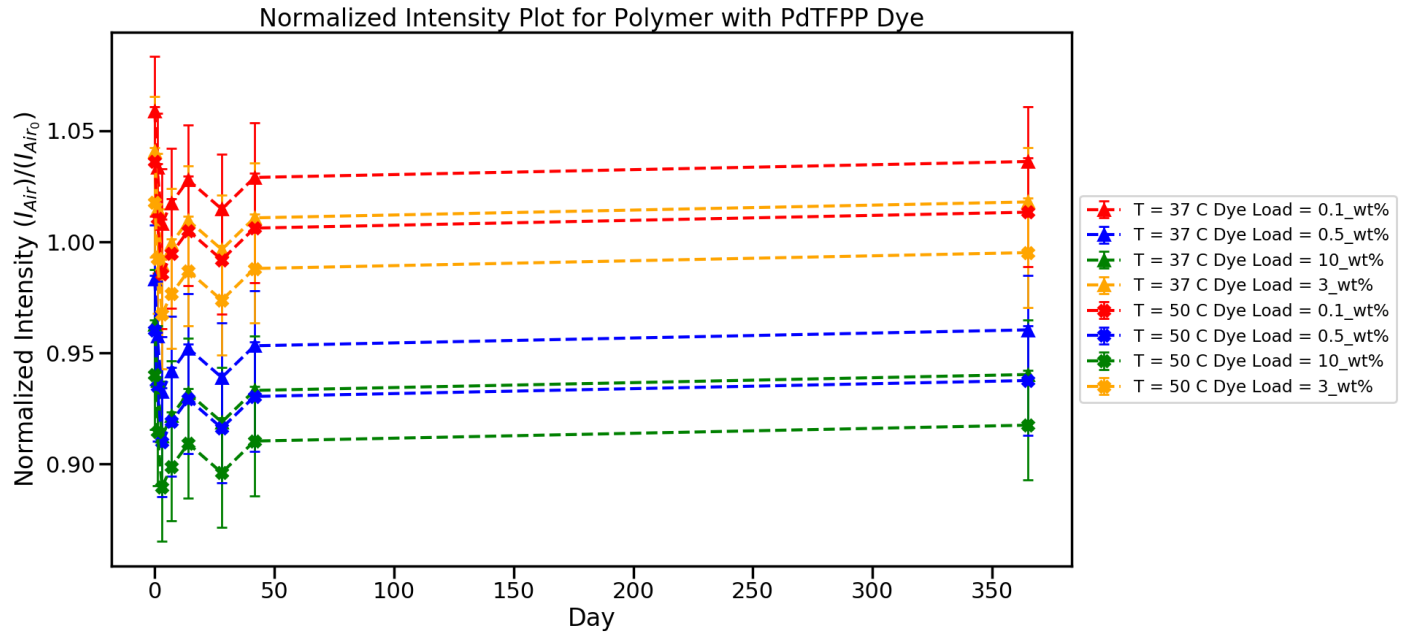

(b) End normalized curve behavior for PdTFPP aggregation experiment group.

Figure 5: Short and long term normalized intensity plots for PdTFPP dye aggregation experiment group.

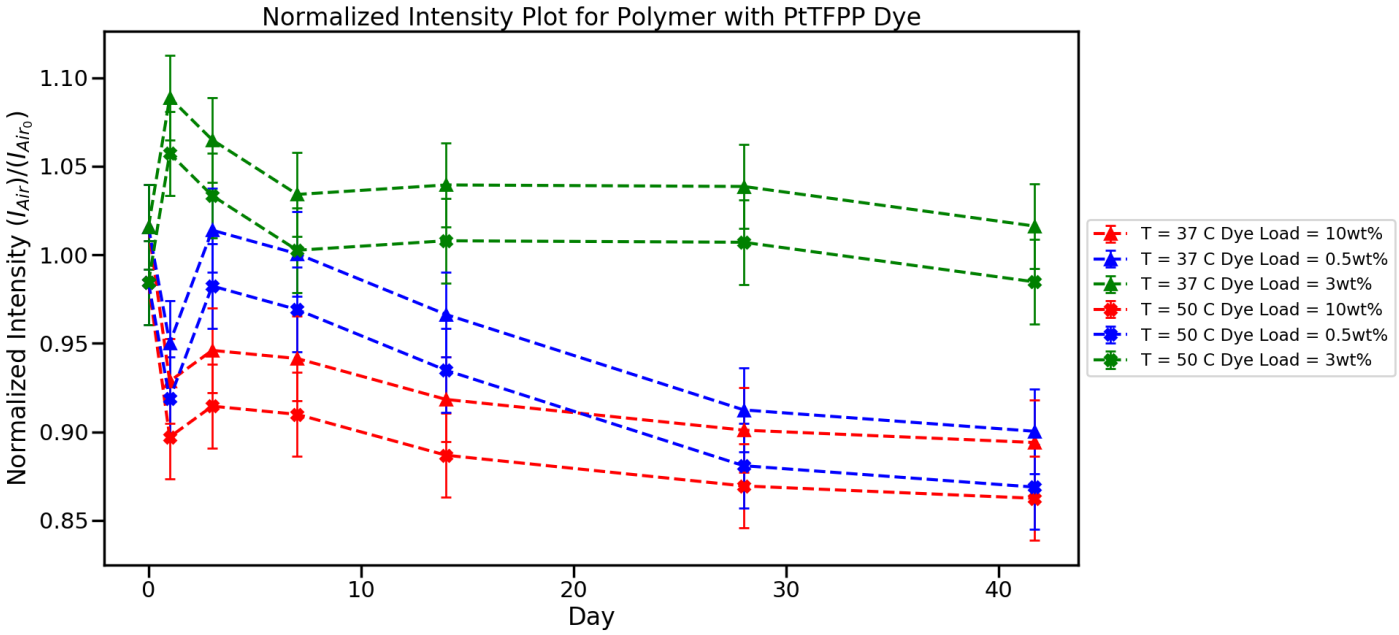

(a) Beginning normalized curve behavior for PtTFPP aggregation experiment group.

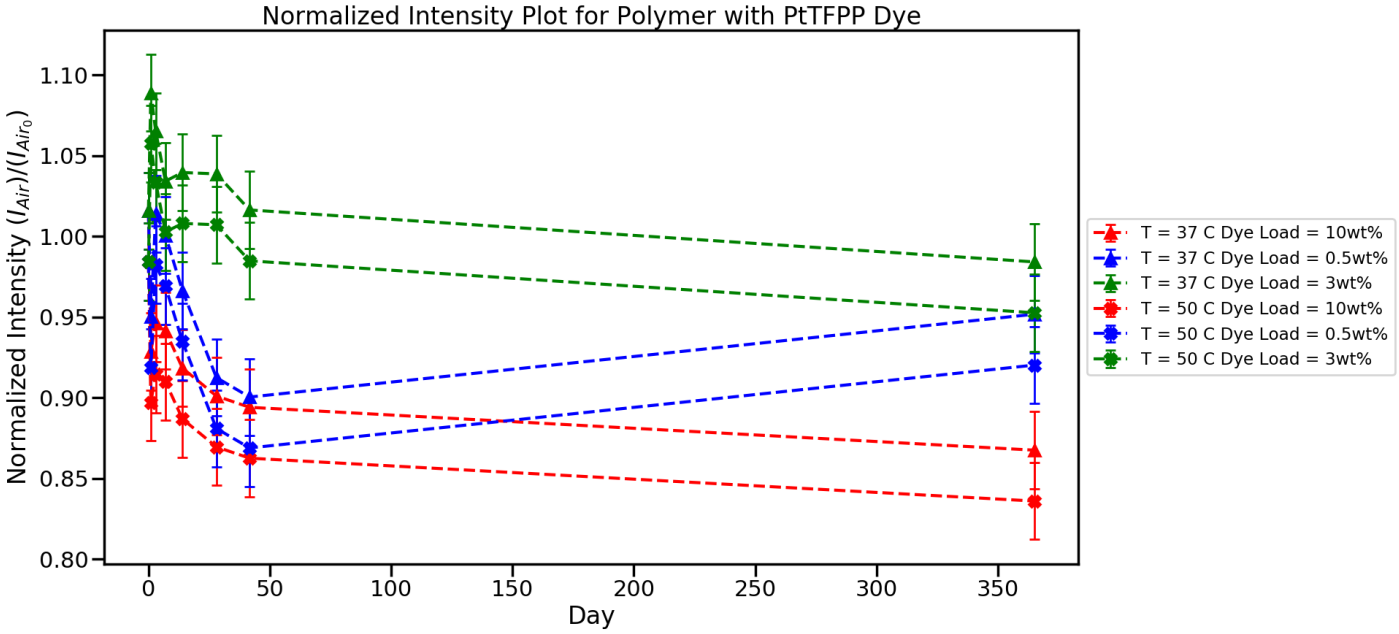

(b) End normalized curve behavior for PtTFPP aggregation experiment group.

Figure 6: Short and long term normalized intensity plots for PtTFPP dye aggregation experiment group.

Table 4: ANOVA Effect Tests Results for PtTFPP dye group

Effect Tests

Source	Nparm	DF	Sum of Squares	F Ratio	Prob > F
Day	7	7	0.12519436	5.4626	<.0001*
Dye Load Group	2	2	0.29278590	44.7127	<.0001*
Temperature	1	1	0.03577962	10.9281	0.0013*
Dye Load Group*Day	14	14	0.08208008	1.7907	0.0476*

Table 5: ANOVA Effect Tests Results for PdTFPP dye group

Effect Tests

Source	Nparm	DF	Sum of Squares	F Ratio	Prob > F
Day	7	7	0.04117441	2.3688	0.0244*
Dye Load Group	3	3	0.29966315	40.2270	<.0001*
Temperature	1	1	0.02491759	10.0349	0.0018*

From Tables 4-5, it can be concluded that the effects of time, dye load, and temperature all had significant effects on the normalized intensity response for both groups, as indicated by the p-values all being < 0.05. Also, the interaction term between day and dye load was significant exclusively in the PtTFPP group data set, indicating that the response change for any given day simultaneously depends on the dye load . In the case of the PdTFPP data set, a significant interaction term was not observed. The dye load level for 0.1 wt.% was omitted, since it was considered an outlier set. This was evaluated by analyzing the scaled residuals of the model for the data set and observing that most had a magnitude greater than 3. According to Montgomery et al., this is one heuristic used in determining data outliers [26].

After determining that all effect parameters were significant, we then examined what levels were significant from each other within the parameter effects by applying Tukey-HSD tests. Note that since the temperature parameter effect only contained two levels, a Tukey-HSD test was not necessary and we concluded that the series for T=50$^{\circ}C$ were significantly different than T=37$^{\circ}C$ for both groups, according to p-values from Tables 4 and 5. Tables 6 and 8 show the results

for levels of dye load and Tables 7 and 9 show the results for levels of day for the PtTFPP and PdTFPP sample groups respectively. The Tables are presented as connecting letters reports, where levels connected by the same letter are statistically insignificant.

Table 6: Dye load Effect Tukey-HSD results for PtTFPP dye group

Dye Load Effect

Level				Least Sq Mean
3wt%Pt	A			1.0195063
0.5wt%Pt		B		0.9481385
10wt%Pt			C	0.9108187

Table 7: Day Effect Tukey-HSD results for PtTFPP dye group

Day Effect

Level				Least Sq Mean
0	A			1.0000000
3	A	B		0.9925503
7	A	B	C	0.9762867
1	A	B	C	0.9734349
14	A	B	C	0.9589468
28		B	C	0.9349190
41.67			C	0.9211235
365			C	0.9186416

Table 8: Dye load Effect Tukey-HSD results for PdTFPP dye group

Dye Load Effect

Level			Least Sq Mean
0.1_wt%_PdTFPP	A		1.0168175
3_wt%_PdTFPP	A		0.9986434
0.5_wt%_PdTFPP		B	0.9411090
10_wt%_PdTFPP		B	0.9210367

Table 9: Day Effect Tukey-HSD results for PdTFPP dye group

Day Effect

Level			Least Sq Mean
0	A		1.0000000
365	A	B	0.9773102
1	A	B	0.9745335
41.67	A	B	0.9701556
14	A	B	0.9690167
7	A	B	0.9587428
28	A	B	0.9558937
3		B	0.9495606

We observed interesting behaviors of the normalized values during the early time points, specifically days 0-14. The observed values did not conform to any pattern and seemed to oscillate. We postulated that this could be a result of stabilization of the dye aggregates within the host polymer matrices with the onset of time. Then, after the 14 day time point, the points stabilized as observed by the data trends towards 1000 hours and 1 year. Since these samples were not subjected to any intentional excitation, we did not expect significant photobleacing to occur, hence why the long-term behavior converged towards the initial values. One plausible explanation for the overall behavior is that the probe molecules aggregates were equilibrating in their host environment, due to a different levels of solubility caused by elevated incubation

temperatures of $37°C$ and $50°C$. After sufficient amount of time elapsed, the molecules stabilized and began plateauing. However, the p-values of the day-to-day effect estimates indicate that the values for days 0-14 are in fact statistically insignificant, as presented in Tables 9 and 7. Furthermore, there is evidence that suggests that there was no significant equilibrating behavior at all during the early time points.

In terms of the dye load effects, there were significant differences. In the PtTFPP group, all dye loads had significant effects on the normalized intensity response. The ordering of the general magnitudes of normalized intensity from highest to lowest were the following: 3wt.%> 0.5 wt.% > 10 wt.%. For the PdTFPP group, 0.1 wt.% was insignificant from 3 wt.% and 0.5 wt.% was insignificant from 10 wt.%. However, the the two insignificant pairs were significant from each other. The ordering of magnitude of normalized intensity by dye load for PdTFPP was the following: 0.1 wt.% > 3 wt.% > 0.5 wt.% > 10 wt.%.

In either case, the 10 wt.% dye load samples demonstrated the lowest overall values of normalized intensity. This was expected, since these samples had the highest probability of containing aggregate populations, due to their high concentrations of probe sensor molecules. Within such tightly packed populations of dye molecules, we suspect that self-quenching readily occurred. Moreover, the activated sensor molecules photochemically deactivate themselves when in such close proximity to each other by absorbing activated photon energy [29, 30]. By that logic, it would be reasonable to assume that the 0.1 wt.% and 0.5 wt.% levels would have the highest values, since there would be a lower probability of tightly aggregated populations with lower concentrations. In the case of the PdTFPP group, the 0.1 wt.% level is the highest. However, the 3 wt.% level is higher than the 0.5 wt.% level. In the PtTFPP group, the 3 wt.% level is also higher than the 0.5 wt.% group. One plausible explanation for this is that despite the 3 wt.% level having a higher probability of self-quenching, there was an order of magnitude more sensor molecules present, therefore having a higher emission intensity contribution. Furthermore, the 3 wt.% dye load is likely low enough such that the overall cumulative

contribution to emission has an overall greater net effect than the decrease in intensity due to self-quenching from tight-packing within aggregate populations.

The temperature levels demonstrated that the lower temperatures produced overall higher normalized intensities for both dye groups. In contrast, Presley demonstrated that intensity increases when PSU(PdTFPP)-PCL fibers are subjected to temperatures of $50°C$ [13]. However, this was demonstrated at a different solvent ratio of 90/10 DCM/HFP. It is possible that with the higher ratio of DCM, the higher temperature exhibits a stabilizing effect, dispersing any self-aggregated populations that formed as a result of the solvent insolubility because of higher diffusion rates . In contrast, this experiment may have exhibited a destabilizing effect at the higher temperature level, which produced significantly lower normalized intensity outputs. Therefore, at the solvent ratio of 75/25 DCM/HFP used in this experiment, there may have been other factors that had to do with polymer-host stability that may have contributed to a destabilizing effect upon exposure to a $50°C$ incubation environment. Finally, despite the significant differences in temperature levels, all normalized intensities did not deviate more than 10% from 1.0 and the differences between temperature levels of the same dye load were relatively small.

3.2 Polymer Aging Results and Discussion

The first data set to be discussed is the sensitivity ratios, calculated by taking emission intensity subjected to pure nitrogen divided by emission values subjected to pure oxygen ($I_{N_2}.I_{O_2}$). The data was also normalized by the initial ratios for each set of core host polymers. Normalizing the data allowed us to examine the relative loss in sensitivity due to photobleaching. We expected a loss in sensitivity as a result of photobleaching, since less sensor molecules could produce emission peaks after photochemical degradation by singlet oxygen, creating an inactive photoproduct [27]. We were also confident that photobleaching occurred, based on the fiber scaffold color change from light pink to pale green for all samples after

continuous excitation. The discoloration can be seen in Figure D.2 in Appendix D.

The graph shown in Figure 7 was constructed by fitting a second-order regression model to each data series classified by host polymer using JMP software. Moreover, each individual data point is reflective of three sample replicates. The points displayed are the model prediction points, which are similar in value to the averages. Also, the error bars displayed are based on the 95% confidence interval of the mean model predictions. This also takes into account the data spread of each polymer host series as a whole, rather than constructing error bars by exclusively focusing on the spread at each time point. The plot in Figure 8 shows the same data normalized by the initial values of each series. Since the overall objective was to display significant differences between the polymer host effects as a whole rather than individual variations between time points, we decided this was the most adequate representation of the data. The raw emission decay curves recorded in a pure nitrogen environment can be found in Figures B.12-B.10 in Appendix B.

Based on the normalized results, after the full excitation period, the rank ordering of long-term percent of original sensitivity was the following: PSU(PdTFPP)-PCL > PES(PdTFPP)-PCL > PET(PdTFPP)-PCL > Nylon-6(PdTFPP)-PCL. This is indicative of the fact that PSU(PdTFPP)-PCL, PES(PdTFPP)-PCL, and PET(PdTFPP)-PCL experienced similar amounts of relative long-term photobleaching, while Nylon-6(PdTFPP)-PCL was heavily bleached over the same period. Based on observation during experimentation, we expected this result for Nylon-6(PdTFPP)-PCL considering that the samples turned green much faster than the other samples. This also indicates that the PES(PdTFPP)-PCL, PSU(PdTFPP)-PCL, and PET(PdTFPP)-PCL systems have the highest oxygen concentration sensitivity in a long-term time period, and could measure changes more preciscely than Nylon-6(PdTFPP)-PCL long-term, considering its much lower sensitivity. PSU(PdTFPP)-PCL and PES(PdTFPP)-PCL possess similar chemical structures, so it was expected that they would be close in sensitivity, as demonstrated by Figure 7. Also, the sensitivity trend followed the oxygen permeability trend.

The oxygen permeabilities were the following in units of $(cm^3 - mm)/(m^2 - day - atm)$: PSU-91, PES-14.6, PET-0.223, Nylon-6-1.2. Furthermore, the polymers with lower oxygen permeability (e.g., Nylon-6 and PET) showed lower sensitivities. Since less oxygen was able to diffuse in the core polymer, the sensor interacted with less oxygen, which would result in lower detection events. The trends for PSU and Nylon-6 are similar to results that Presley produced for the same host polymers as well [13]. The normalized intensities show the relative decreases in sensitivity caused by photobleaching.

The rank ordering of relative decrease in sensitivity from lowest to highest was the following: PSU < PES(PdTFPP)-PCL < PET(PdTFPP)-PCL < Nylon-6(PdTFPP)-PCL. With a higher oxygen permeability, we expected more photobleaching to occur, due to the presence of more singlet oxygen. However, this was not the case for the normalized intensity measurements in Figure 8. It was possible that probe-matrix compatibility and solubility dictated the trend and had a greater net effect than permeability, as suggested by Presley [13]. The ordering on relative sensitivity decrease is therefore reflective of compatibility. A supporting observation to this was that PSU(PdTFPP)-PCL and PES(PdTFPP)-PCL had a more definitive pink color than PET, both of which had lower relative decreases in sensitivity. The pink color is representative of good probe solubility, considering the emission spectrum of both dyes fall in within red visible light range. The actual polymer fibers are typically white, so the combination of the two produces pink coloration. Nonetheless, Nylon-6(PdTFPP)-PCL did show definitive pink color, so there must have been other effects contributing to the rapid rate of sensitivity decrease in that specific case. Poor probe-matrix compatibility likely results in more tightly packed aggregate sensor molecule populations, raising the singlet oxygen/sensor molecule collision rate and therefore raising the rate of photobleaching [13].

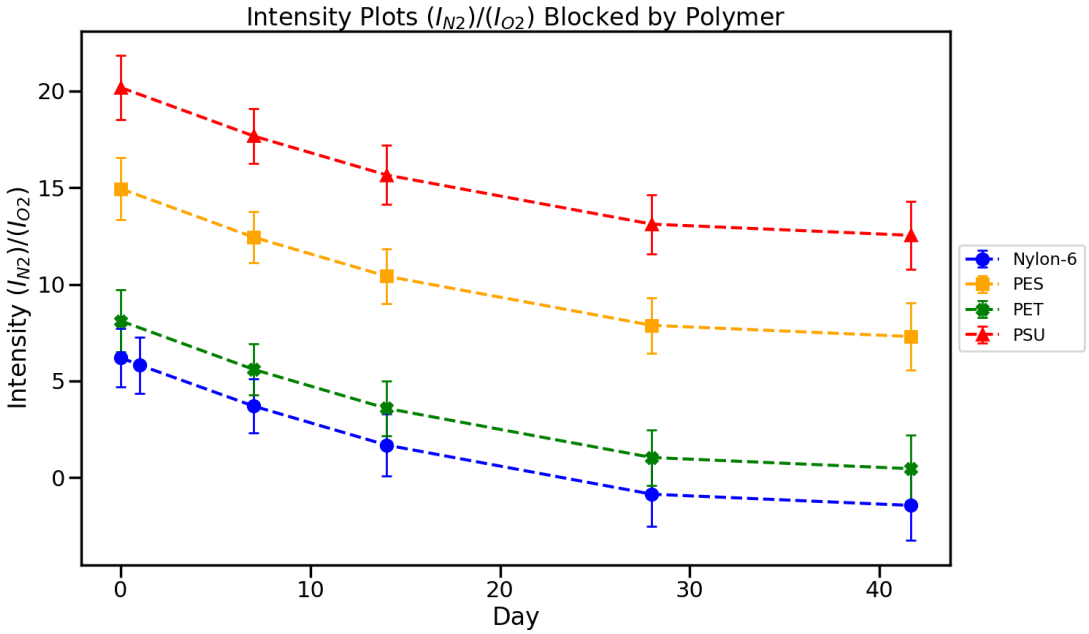

Figure 7: Emission intensity sensitivities: I_{N_2}/I_{O_2} from aging experiment.

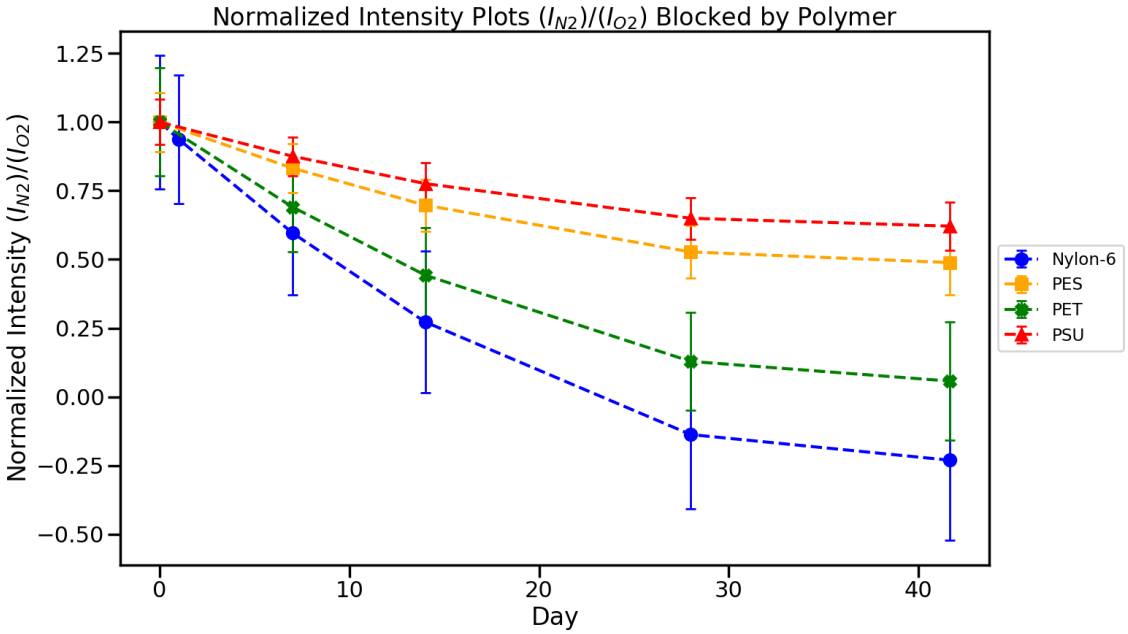

Figure 8: Normalized emission intensity sensitivities: I_{N_2}/I_{O_2} from aging experiment.

It is, however, not appropriate to draw the previous conclusions based on the plots alone. We investigated this further by using ANOVA tables and statistical reports generated from the statistical models fitted to the data using JMP software. The combined discrete-continuous effect model hypothesized is represented by Equation (5).

$$\hat{y} = \beta_0 + \beta_1 x_1 + \beta_{1,1} x_1^2 + \tau_{polymer} + \epsilon \tag{5}$$

In Equation (5), the $\hat{y}$ term is the estimated normalized intensity response term, β_0 is the intercept estimate, β_1 is the linear regression coefficient term with respect to time, $\beta_{1,1}$ is the quadratic regression coefficient term with respect to time, x_1 is the continuous variable for time in days, $\tau_{polymer}$ is the discrete effect term for the host polymer classification, and ϵ is the random error term. After running a report in JMP software, the model revealed an $R^2 = 0.67$, implying the model was able to account for 67% of the data variability. The ANOVA tables from the model testing each effect in the hypothesized model. The intent of this was to determine whether overall effects of day and polymer host were significant on the response normalized intensity. The Tables displaying these results with p-values can be found in Tables 10 for the normalized I_{N_2}/I_{O_2} response.

Table 10: ANOVA effects test report for I_{N_2}/I_{O_2} response.

Expanded Estimates

Nominal factors expanded to all levels

Term	Estimate	Std Error	t Ratio	Prob>|t|	Lower 95%	Upper 95%
Intercept	10.590941	0.736895	14.37	<.0001*	9.1093156	12.072567
Polymer[Nylon-6]	-6.354985	0.76408	-8.32	<.0001*	-7.89127	-4.818699
Polymer[PES]	2.6565123	0.700588	3.79	0.0004*	1.2478854	4.0651392
Polymer[PET]	-4.179076	0.700588	-5.97	<.0001*	-5.587703	-2.770449
Polymer[PSU]	7.8775485	0.757998	10.39	<.0001*	6.3534917	9.4016052
Day Cts	-0.204283	0.030167	-6.77	<.0001*	-0.264938	-0.143627
(Day Cts-18.1365)*(Day Cts-18.1365)	0.0046955	0.002438	1.93	0.0601	-0.000207	0.0095979

From Table 10, we concluded that the day-to-day variability is significant due to p-values

Table 11: Tukey-HSD test report for the I_{N_2}/I_{O_2} response.

Level				Least Sq Mean
PSU	A			14.763521
PES		B		9.542485
PET			C	2.706896
Nylon-6			C	0.530988

Levels not connected by same letter are significantly different.

being less than 0.05 for the time effects. We also know that photobleaching increased as time advanced, therefore we expected the time effect to be significant. Table 10 shows that the discrete effect terms for polymer host were significant (p-values <0.05) for all four levels: PSU(PdTFPP)-PCL, PES(PdTFPP)-PCL, PET(PdTFPP)-PCL, and Nylon-6(PdTFPP)-PCL. Taking the analysis a step further, Tukey-HSD tests were performed to determine whether the sensitivity response values for each polymer host data series were significant when compared to the other levels. See Table 11 for the results for the I_{N_2}/I_{O_2} response. Based on Table 11, the report indicates that the PSU(PdTFPP)-PCL level was significant from PES(PdTFPP)-PCL and the insignificant PET/Nylon-6(PdTFPP)-PCL pair.

After the data was collected from the spectrometer, we observed that the blue light excitation source produced an intensity peak over-saturated compared with respect to the target dye emission peaks. Therefore, subtracting out the excitation peak contribution of intensity can provide data that would yield sensitivity ratios possibly closer to the true values. Thus, we made an effort to eliminate this contribution by developing an involved Python 3 program to account for this. The underlying strategy behind the algorithm involved using the SciPy optimize library to fit high order polynomials to the region of overlap. By using data ranges prior to and after the overlap range, it was possible to optimize curves via interpolation, which is more accurate and reliable than extrapolation. See Figure 9 for a sample output graph constructed using the Python 3 program. Note in Figure 9, the large curve in the left of the plot is the over-saturated blue light excitation peak and the dotted green curve is the best fit representing the overlap generated by

the program. All source code, including Jupyter notebooks, can be retrieved from the following Git repository: *https://github.com/rarnold97/Research.git*.

The blue light overlap fit algorithm was used for each sample, generating interpolated blue light intensities that were subtracted from every pure oxygen and nitrogen environment emission intensity. The fit adjusted sensitivity plot can be found in Figure 10 and the normalized version of the plot can be found in Figure 11.The same statistical reports as before were generated for the fitted data to determine if the fitted values still produced significant results. See Table 12 and Table 16 for the effect tests and Tukey-HSD report results.

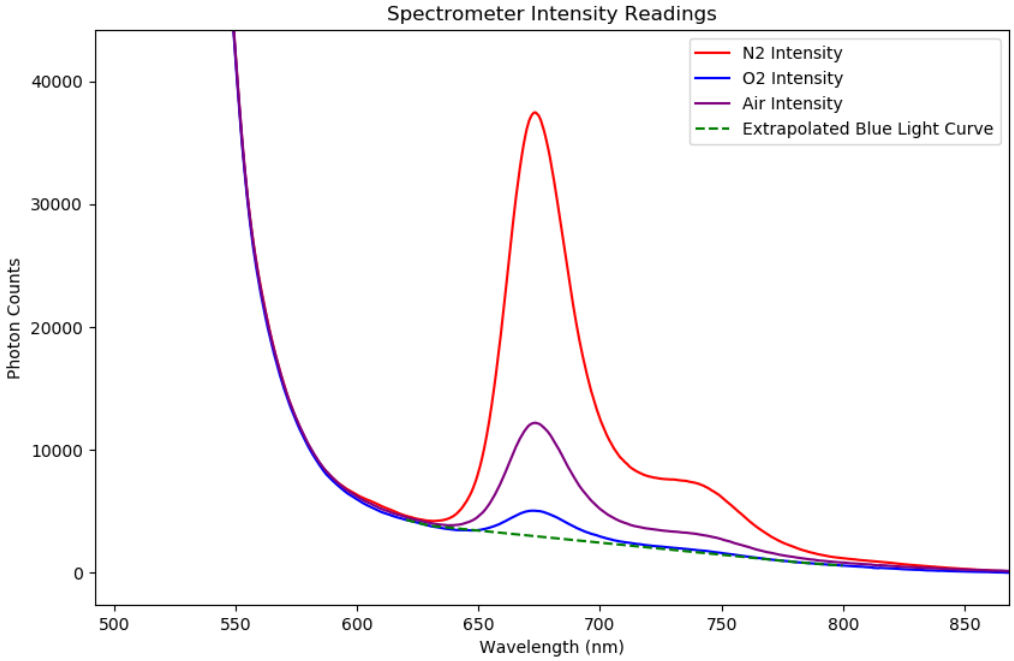

Figure 9: Sample output from Python program that optimizes a high order polynomial fit to account for blue light excitation source overlap.

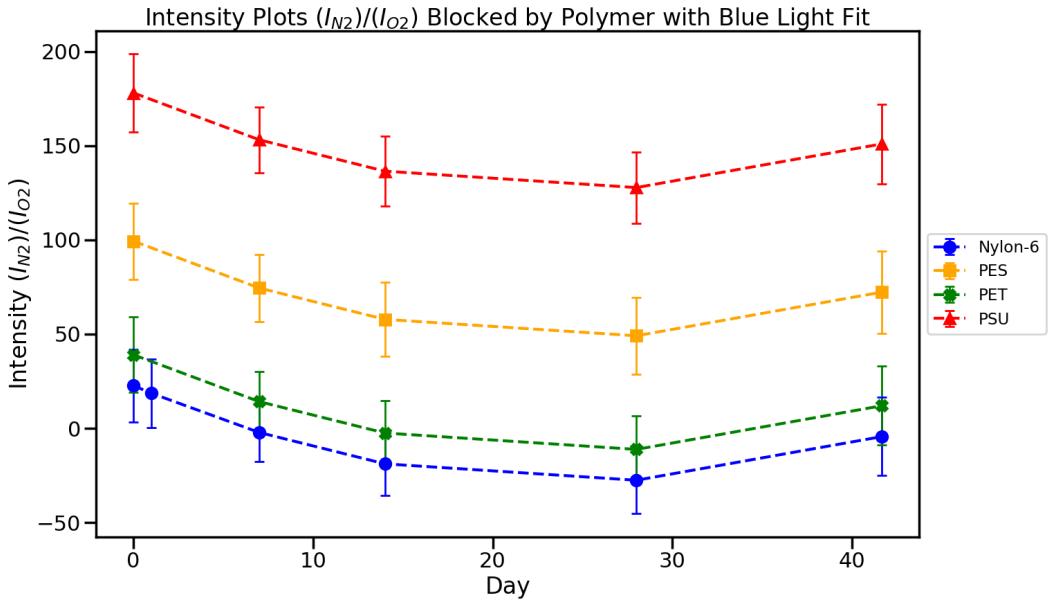

Figure 10: Emission intensities: I_{N_2}/I_{O_2} after subtracting blue light overlap fitted values.

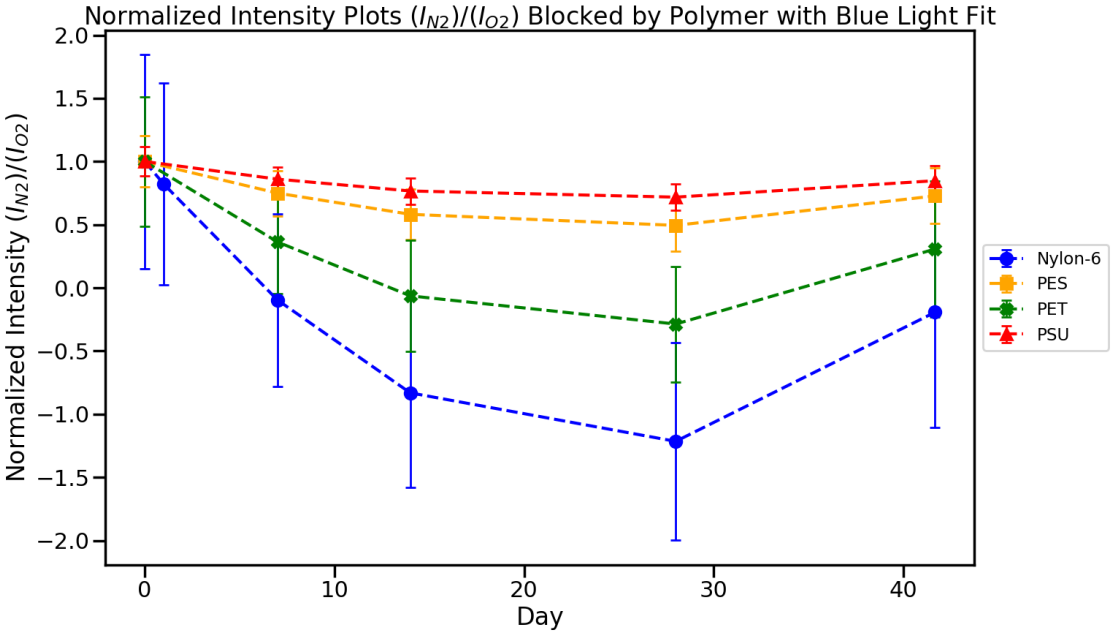

Figure 11: Normalized emission intensities: I_{N_2}/I_{O_2} after subtracting blue light overlap fitted values.

Table 12: ANOVA effects test report for the blue light overlap fitted $I_{N_2}/I_{N_{20}}$ response.

Expanded Estimates

Nominal factors expanded to all levels

Term	Estimate	Std Error	t Ratio	Prob>|t|	Lower 95%	Upper 95%
Intercept	58.132255	6.546151	8.88	<.0001*	44.983923	71.280587
Polymer[Nylon-6]	-62.10917	6.417568	-9.68	<.0001*	-74.99923	-49.2191
Polymer[PES]	14.580616	7.089078	2.06	0.0449*	0.3417843	28.819447
Polymer[PET]	-45.73634	6.557799	-6.97	<.0001*	-58.90807	-32.56461
Polymer[PSU]	93.264892	6.873639	13.57	<.0001*	79.458781	107.071
Day Cts	-1.151435	0.289642	-3.98	0.0002*	-1.733198	-0.569672
(Day Cts-17.84)*(Day Cts-17.84)	0.0837641	0.022489	3.72	0.0005*	0.0385939	0.1289344

Table 13: Tukey-HSD test report for the blue light overlap fitted I_{N_2}/I_{N_2} response.

Level				Least Sq Mean
PSU	A			130.8555
PES		B		52.1713
PET			C	-8.1457
Nylon-6			C	-24.5185

Levels not connected by same letter are significantly different.

Based on the results in Table 12 and 16, the effects showed the same significance before the fit, based on all reported p-values being less than 0.05. The Tukey-HSD test also had the same levels of significance as before. The primary importance of the fit was that different spectrometer integration times could be applied to prevent peak cutoff due to over-saturation. Also, different integration times entailed varying levels of blue excitation light saturation. Thus, the subtraction program eliminates the variability caused by blue light overlap. Moreover, applying the fit can then result in sensitivity values being more accurate to their true values. For example, prior to fit, the initial sensitivity I_{N_2}/I_{O_2} for the PSU(PdTFPP)-PCL system was approximated at 20.2, and after applying the fit, the value was approximated at 178.1. Xue et al. showed an initial sensitivity of 106.7 for PSU(PdTFPP)-PCL, also much higher than 20.2 [3]. Despite this, the 106.7 is clearly still far less than 178.1. Nonetheless, the program still offers promising capability, and may offer more utility in future work.

Another caveat of the program output was the near parabolic shape of the curves. We would not expect the end points of sensitivity to increase. This is probably due to the propagation of error induced by subtracting the blue light fit value from each intensity measurement and then taking the quotient of I_{N_2}/I_{O_2}. To quantify this, a lack of fit F-test was performed in JMP, and the results are shown in Table 14. The p-value<0.05 indicates a significant lack of fit. Therefore, this indicates that data variation was not properly accounted for in the statistical model, implying that more samples need to be used and perhaps modification to the fit algorithm is necessary in future work.

Table 14: Lack of fit test for post blue light overlap fitted model.

Lack Of Fit

Source	DF	Sum of Squares	Mean Square	F Ratio
Lack Of Fit	15	24043.963	1602.93	3.1855
Pure Error	35	17612.028	503.20	**Prob > F**
Total Error	50	41655.991		0.0024*
				Max RSq
				0.9341

Stern-Volmer plots were also constructed from the emission intensity data in order to further evaluate sensor sensitivity and performance. Since measurements were taken in three different oxygen concentration environments for each sample set, it was possible to plot the Stern-Volmer plots by normalizing the intensities by the values measured in pure nitrogen: (I/I_0). Plots were constructed for each polymer host, where the data from the initial and final time points time measurements are shown. We expected that plotting these values against oxygen content would yield linear data series. The plots can be found in Figures 12-13.

A Stern-Volmer plot with a high slope indicates high sensitivity and a high degree of linearity indicates good probe-matrix compatibility, making better device calibration possible [3]. The slopes with normalized intensity as the ordinate and oxygen percent as the abscissa were the following in order from high to low: PSU(PdTFPP)-PCL - 24.6, PES(PdTFPP)-PCL - 11.6,

Nylon-6(PdTFPP)-PCL 7.4, PET(PdTFPP)-PCL 6.3. Allowing the slope magnitudes to represent sensitivity, this trend is similar to the I_{N_2}/I_{O_2} sensitivity trend as earlier demonstrated. The primary difference is that the Nylon-6 sensitivity is slightly higher than that for PET. However, the results from the I_{N_2}/I_{O_2} sensitivity data did reveal that the levels between PET and Nylon-6 were insignificant, so we cannot fully claim that the PET sensitivity is in fact different. Also, the two slopes were similar, as were the I_{N_2}/I_{O_2} sensitivity level magnitudes.

The R^2 values were used to evaluate linearity in each case. Deviations from linearity are typically caused by the presence of varying probe populations in the polymer matrix as a result of poor compatibility. The different populations contribute different levels of emission intensity to the overall intensity, therefore leading to nonlinear behavior [31]. The day 0 R^2 values were the following from high to low: PET(PdTFPP)-PCL - 0.959, PSU(PdTFPP)-PCL - 0.878, Nylon-6(PdTFPP)-PCL - 0.873, PES(PdTFPP)-PCL - 0.834. The percent change of R^2 from day 0 to 1000 hours were the following from low to high: PES(PdTFPP)-PCL - 27.5%, PSU(PdTFPP)-PCL - 38.0%, PET(PdTFPP)-PCL - 52.2%, Nylon-6(PdTFPP) - 80.0%. The initial R^2 values show that the PET(PdTFPP)-PCL system initially offered a high potential for proper calibration. However, the percent change in R^2 reveal the change in performance after photobleaching. The PSU(PdTFPP)-PCL system had the smallest change after 1000 hours of excitation of 27.5% and the Nylon-6 bleached most heavily, resulting in a percent change of 80.0%. Based on the results, the system selected for a sensor design will depend on the oxygen detection sensitivity requirements and the desired longevity of the device.

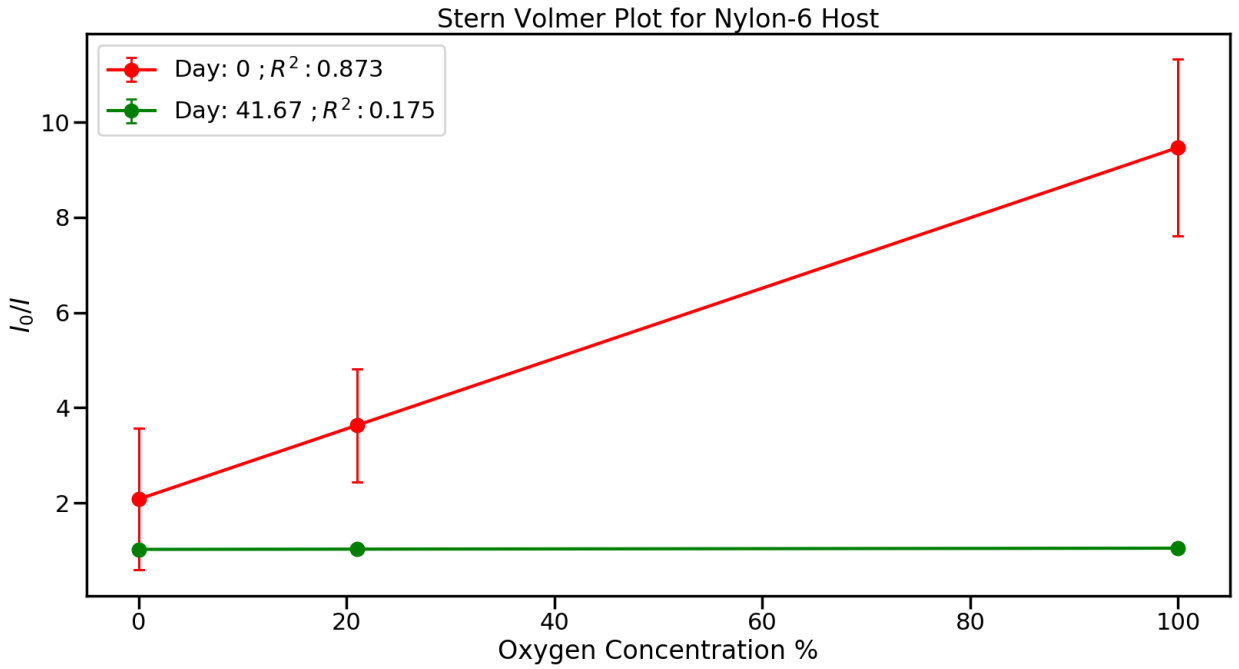

(a) Stern-Volmer plot for aging experiment with Nylon-6 host.

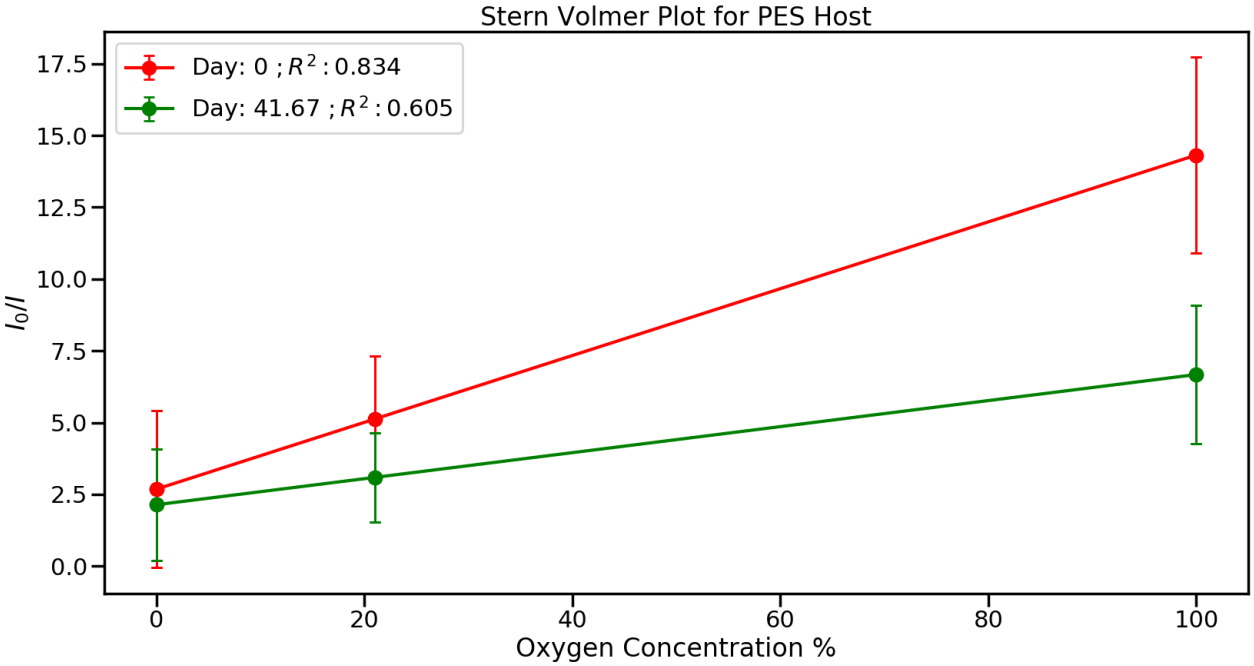

(b) Stern-Volmer plot for aging experiment with PES host.

Figure 12: Short and long term normalized intensity plots for PdTFPP dye aggregation experiment group.

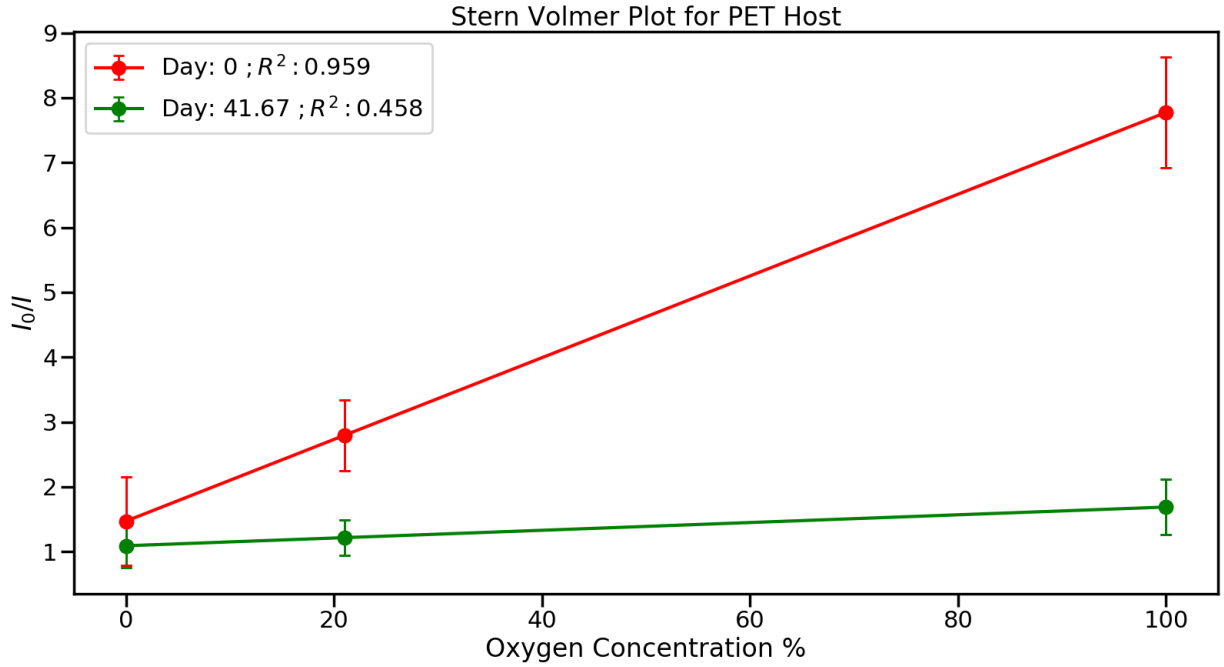

(a) Stern-Volmer plot for aging experiment with PET host.

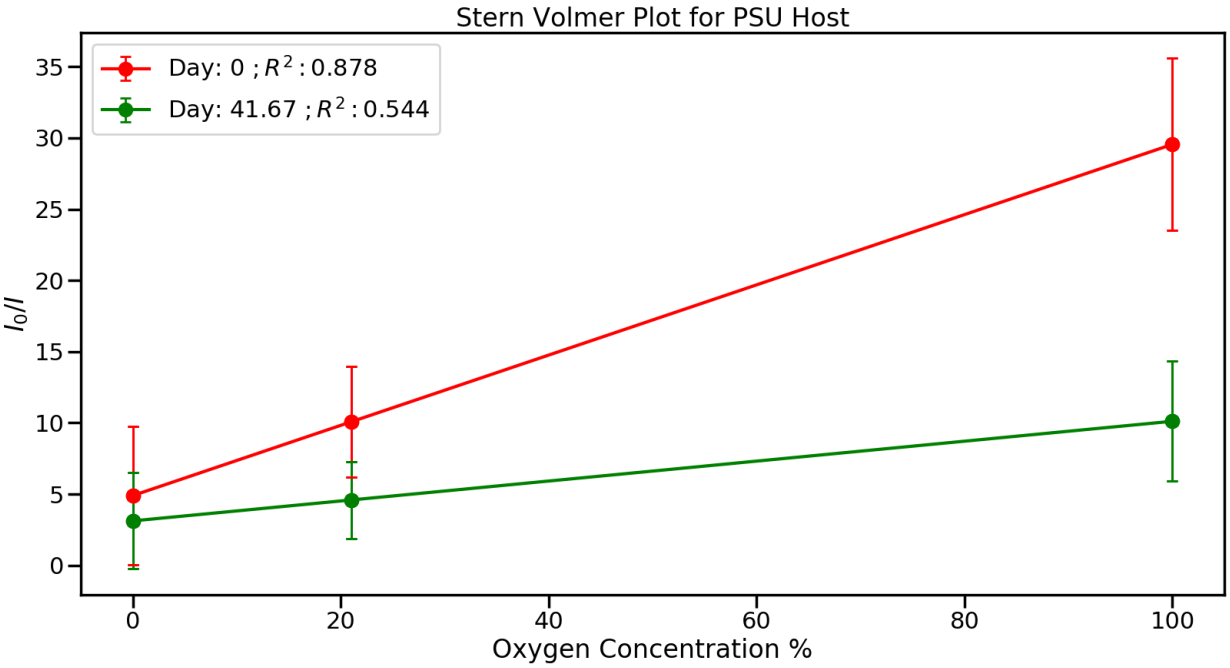

(b) End normalized curve behavior for PdTFPP aggregation experiment group.

Figure 13: Stern-Volmer plot for aging experiment with PSU host.

3.3 Results for Exploring β-Carotene as a Singlet Oxygen Quencher

The analysis methods used for the spectral data from this experiment were similar to that of the aging experiment except that they concerned shorter times. The aim was to examine if incorporating β-Carotene as an additive could significantly reduce the sensor degradation caused by photobleaching. To holistically examine this, the sensitivity plot and normalized sensitivity plot of I_{N_2}/I_{O_2} were first plotted and shown in Figures 14 and 15. All plots displayed were constructed using a discrete statistical model in the same way as the polymer aging experiment results. All supplemental statistics can be found in Appendix C. The raw decay curves in a pure nitrogen environment can be found in Appendix B.

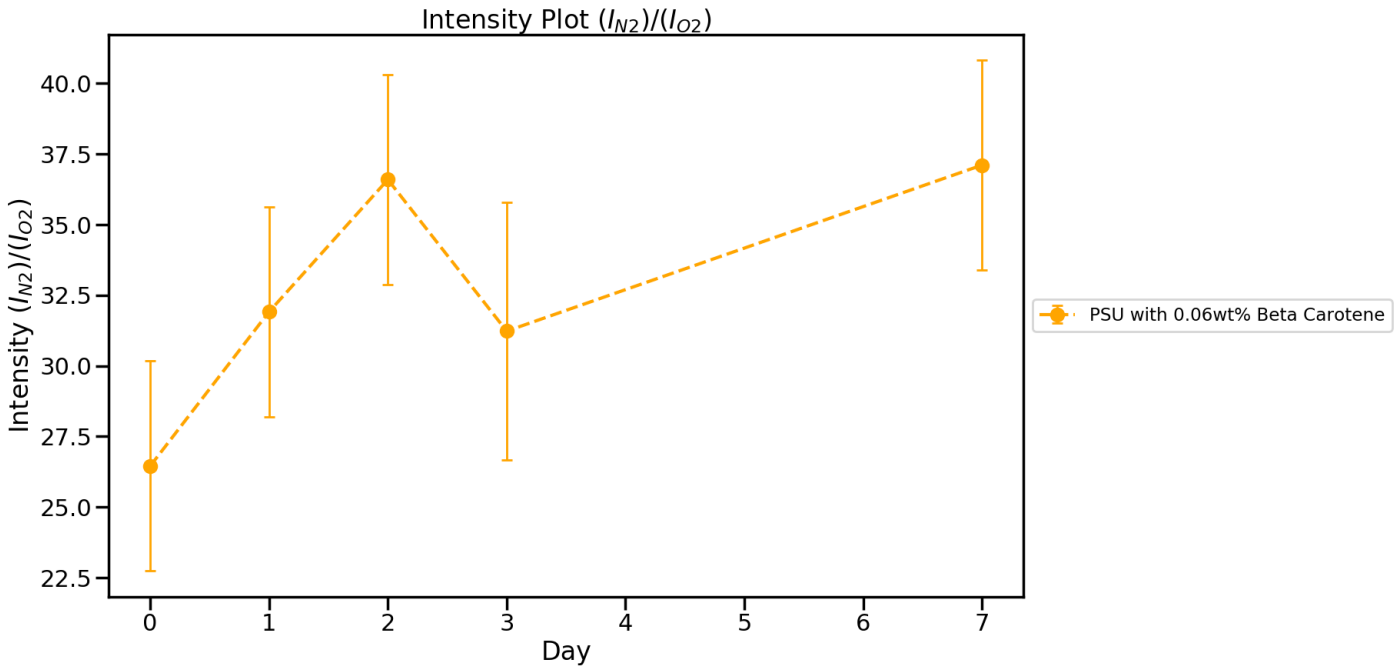

Figure 14: Emission intensities sensitivity: I_{N_2}/I_{O_2} in PSU-PCL system with 0.5 wt.% $Ru(dpp)_3Cl_2$ and 0.06 wt.% β-Carotene added.

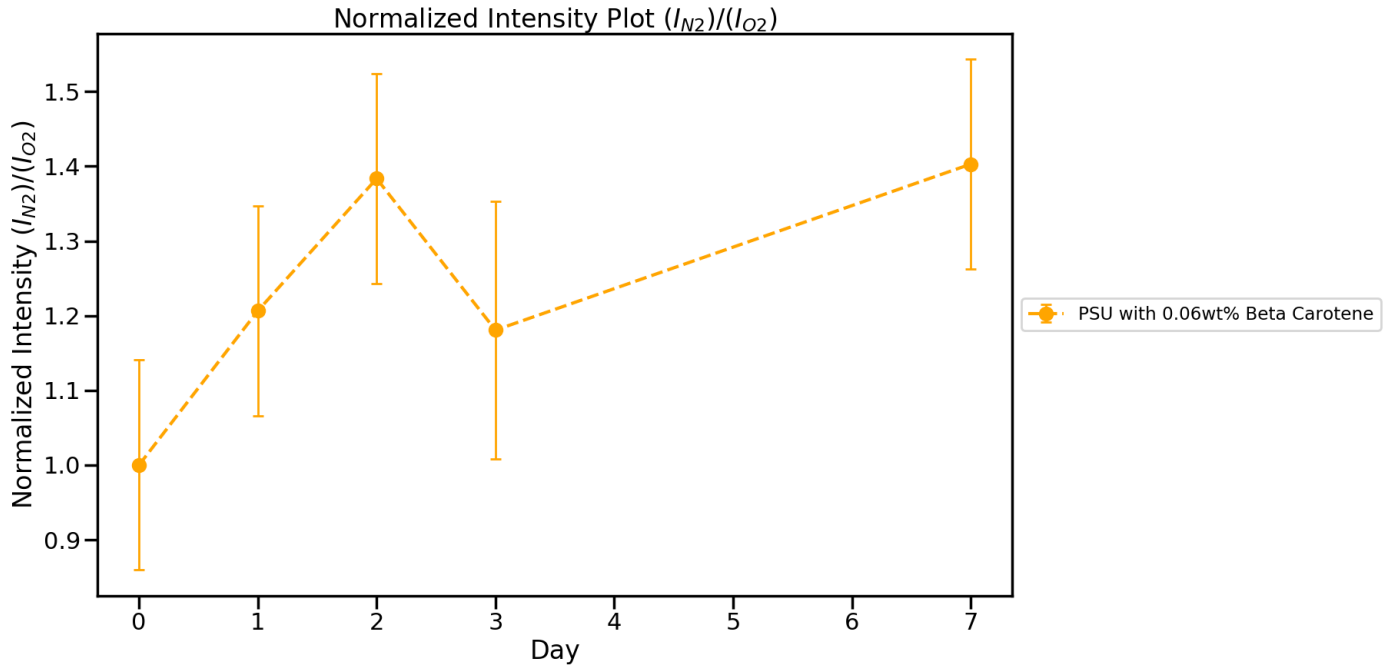

Figure 15: Normalized emission intensities sensitivity: I_{N_2}/I_{O_2} in PSU-PCL system with 0.5 wt.% $Ru(dpp)_3Cl_2$ and 0.06 wt.% β-Carotene.

At first, it appeared that the sensitivity overall increased at the end of the week-long period. However, this does not mean that it significantly increases. Therefore, an effects significance test was performed on each level of the discrete effect of day on measured sensitivity, and the results are displayed in Table 15. The hypothesized discrete model followed Equation (6), where y represents the sensitivity response, β represents the fitted intercept, the τ values are the discrete day effects, and ϵ is the term for random error.

$$y = \beta + \tau_{Day0} + \tau_{Day1} + \tau_{Day2} + \tau_{Day3} + \tau_{Day7} + \epsilon \tag{6}$$

The results show that none of the levels of day are significant, based on all p-values > 0.05. Therefore, even though the sensitivity appears to increase, the trend cannot be concluded based on the statistical evidence.

Table 15: ANOVA effects test report for each day effect on the $I_{N_2}/I_{N_{20}}$ response with β-Carotene.

Expanded Estimates

Nominal factors expanded to all levels

Term	Estimate	Std Error	t Ratio	Prob>|t|	Lower 95%	Upper 95%
Intercept	1.1994894	0.07368	16.28	<.0001*	1.03532	1.3636588
Day Discrete[0]	-0.199489	0.14736	-1.35	0.2056	-0.527828	0.1288494
Day Discrete[1]	0.0246422	0.14736	0.17	0.8705	-0.303697	0.352981
Day Discrete[2]	0.1929071	0.14736	1.31	0.2198	-0.135432	0.5212459
Day Discrete[3]	-0.236367	0.14736	-1.60	0.1398	-0.564705	0.0919722
Day Discrete[7]	0.2183067	0.14736	1.48	0.1693	-0.110032	0.5466455

A second look was taken at the data in Figures 14 and 15 by applying the blue light overlap fitting program and re-plotting the results. We speculated that removing the contribution of light intensity from excitation source could reveal important results. The regular and normalized sensitivity plots can be found in Figures 16 and 17.

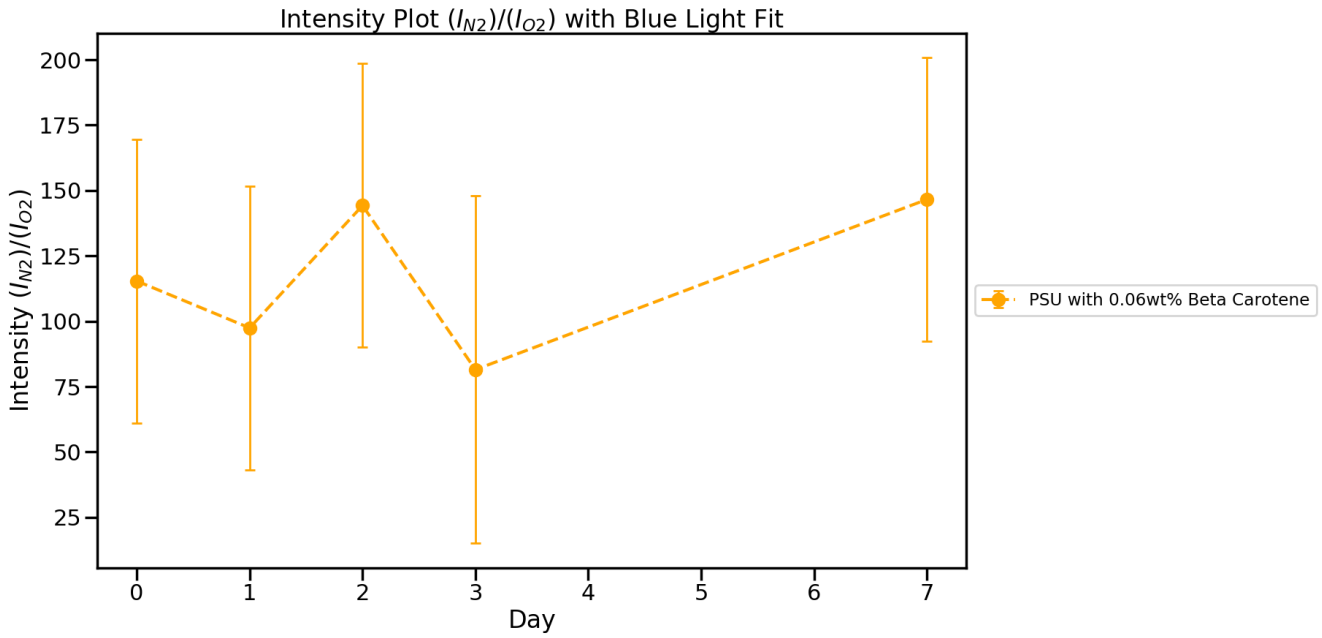

Figure 16: Emission intensities: $I_{N_2}/I_{N_{20}}$ in PSU-PCL system with 0.5 wt.% $Ru(dpp)_3Cl_2$ dye and 0.06 wt.% β-Carotene after applying the blue light overlap fitting program.

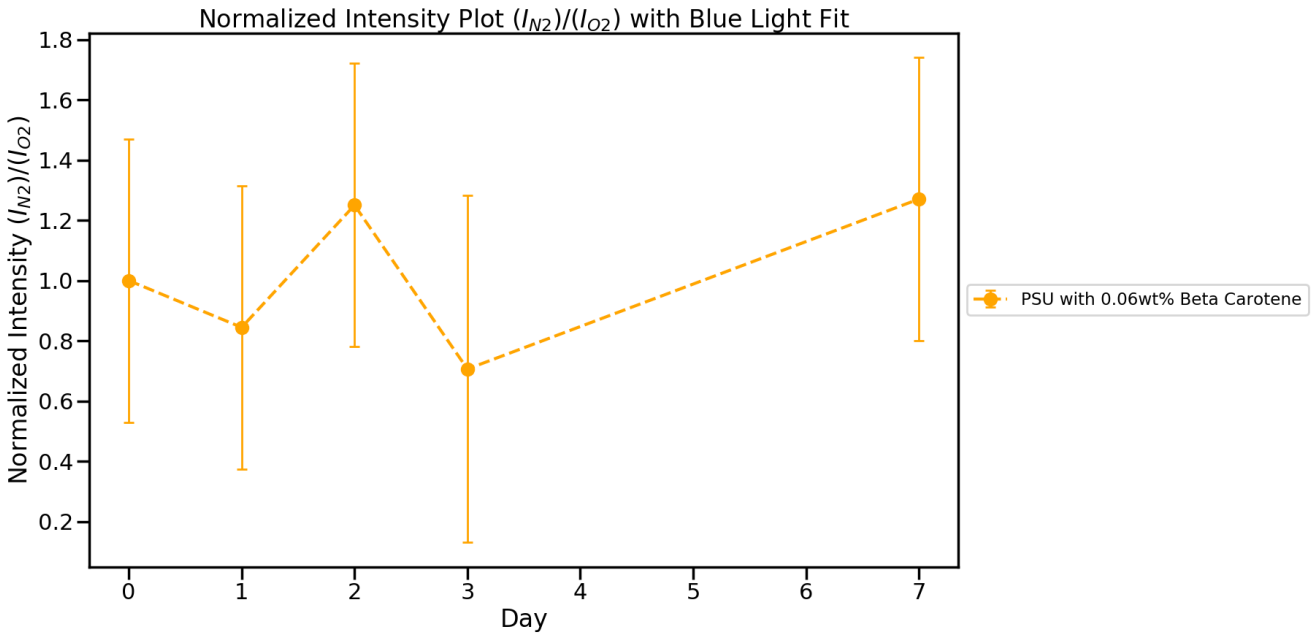

Figure 17: Normalized Emission intensities: $I_{N_2}/I_{N_{20}}$ in PSU-PCL system with 0.5 wt.% $Ru(dpp)_3Cl_2$ dye and 0.06 wt.% β-Carotene after applying the blue light overlap fitting program.

The same effects test on each level of day was performed after the applied blue light fit, and the results are displayed in Table 16. The results indicate Days 1,3, and 7 are significant, with p-values < 0.05. Although, the sensitivity at day 7 was not significantly difrerent from the day 0 value. This suggests that sensitivity was not significantly improved. The initial day 0 fitted 146.6 sensitivity for PSU(PdTFPP/BC)-PCL is lower than the 178.1 from the aging tests for PSU(PdTFPP)-PCL. It is possible that the -Carotene shields the core and dampens the emissions by acting as a light barrier or causing light scattering. After exposure to excitation, the -Carotene dissolves after quenching singlet oxygen, then exposing the inner core. We therefore hypothesize that after sufficient time, the sensitivity would finally reach values closer to 178.1 and exhibit similar behavior as the aging test results from that point forward. These claims are supported by the observation of the orange β-Carotene layer dissolving and exposing the light pink PSU(PdTFPP)-PCL layer shown in Figure D.3 in Appendix D.

Table 16: ANOVA effects test report for each day effect on the $I_{N_2}/I_{N_{20}}$ response with β-Carotene after applying blue light fit.

Expanded Estimates

Nominal factors expanded to all levels

Term	Estimate	Std Error	t Ratio	Prob>|t|	Lower 95%	Upper 95%
Intercept	0.9311728	0.026792	34.76	<.0001*	0.870566	0.9917796
Day Discrete[0]	0.0688272	0.051724	1.33	0.2160	-0.048181	0.1858355
Day Discrete[1]	-0.136448	0.051724	-2.64	0.0270*	-0.253456	-0.019439
Day Discrete[2]	0.0330556	0.051724	0.64	0.5387	-0.083953	0.1500639
Day Discrete[3]	-0.146246	0.06045	-2.42	0.0387*	-0.282993	-0.009499
Day Discrete[7]	0.1808107	0.051724	3.50	0.0068*	0.0638024	0.297819

As a final evaluation of sensitivity and resulting sensor performance, a Stern-Volmer plot was constructed in Figure 18. After the week-long period, the R^2 value improves slightly from 0.866 to 0.896, indicating a nominal increase. The slope gets slightly greater, indicating slightly better sensitivity. However, this is likely insignificant. To support any claim about improving sensing performance, more samples should be tested for a longer time period. As a basis of comparison, a control should be included in future experiments. For instance, if the sensitivity ratios and Stern-Volmer slopes were higher than the control values, the evidence would be stronger.

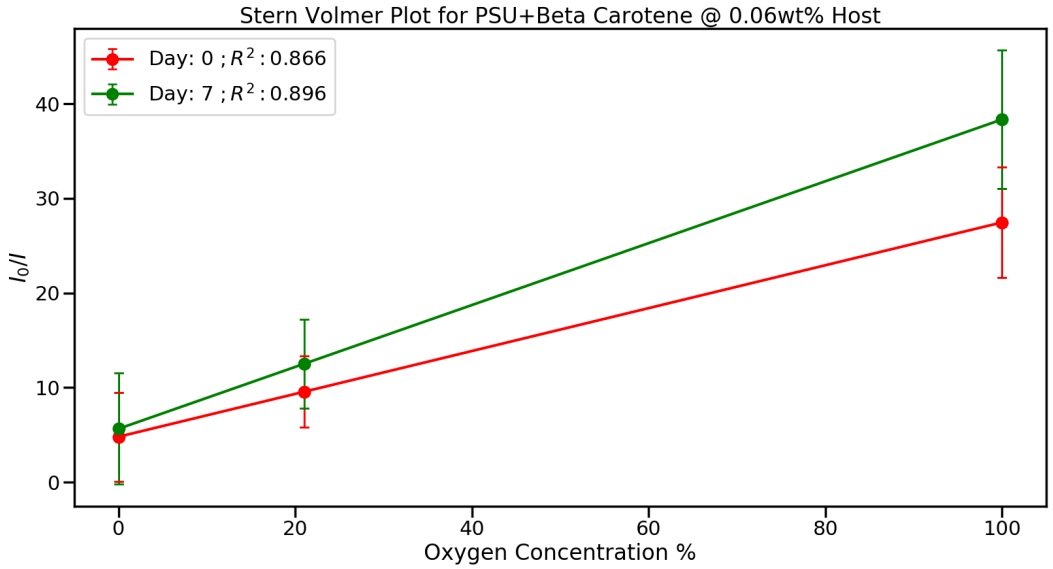

Figure 18: Stern-Volmer plot for PSU host with PdTFPP dye system containing 0.06wt.% β-Carotene.

3.4 Lifetime Analysis Results

For all data sets produced by each sample group, the phosphorescent lifetime was estimated by fitting an exponential function to the data using the SciPy library and Python 3 code. By using the exponential argument fit coefficient, we were able to compile estimates for the lifetimes for each polymer host and aging level. A sample plot that displays the fit generated by the code is shown in Figure 19. All source code, including Jupyter notebooks, can be retrieved from the following Git repository: *https://github.com/rarnold97/Research.git*.

After applying the fits, the lifetimes were compiled and grouped by polymer host and whether or not the host had been aged under continuous excitation. The values were then contrasted performing a Tukey-HSD test in JMP software. The results are displayed graphically and through a connecting letters reports. Levels with the same letter indicate they are not significant from each other. A plot containing the lifetime estimates can be found in Figure 20, while the connecting letters report can be found in Figure 21. A more rigorous level comparison, including p-values, can be located in Appendix C. Note, all computed lifetimes are in units of μs. Also, all $Ru(dpp)_3Cl_2$ dye loads are 0.5 wt.%, except in the 'PSU High' level, where the dye load is 3 wt.%.

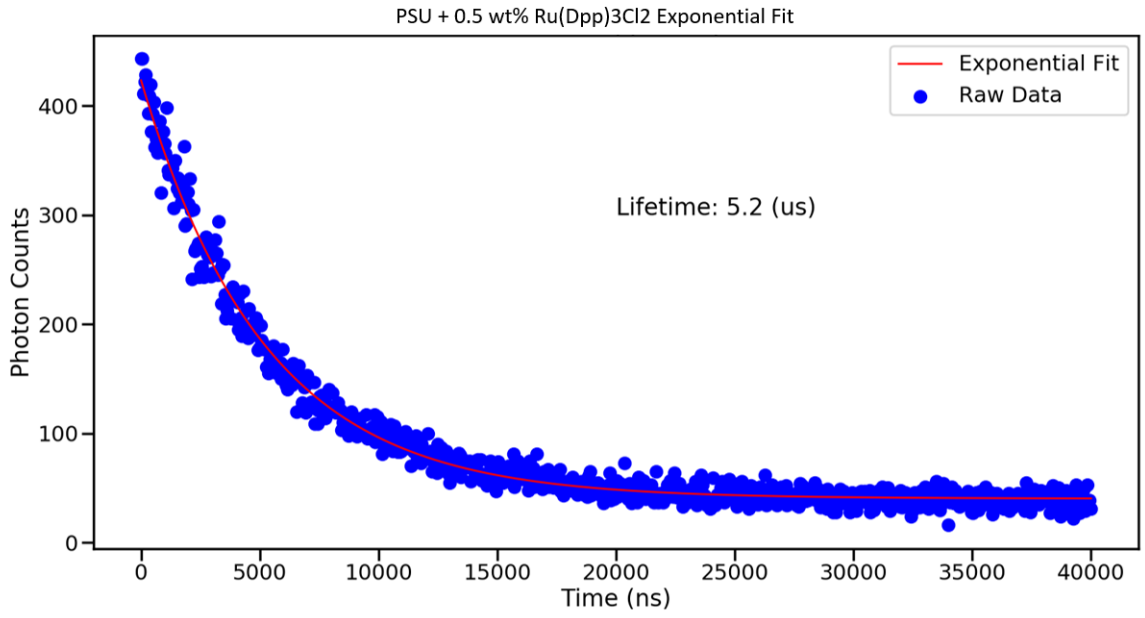

Figure 19: Exponential fit applied to Mini-Tau data output using a sample from the PSU + 0.5wt.% $Ru(dpp)_3Cl_2$ configuration.

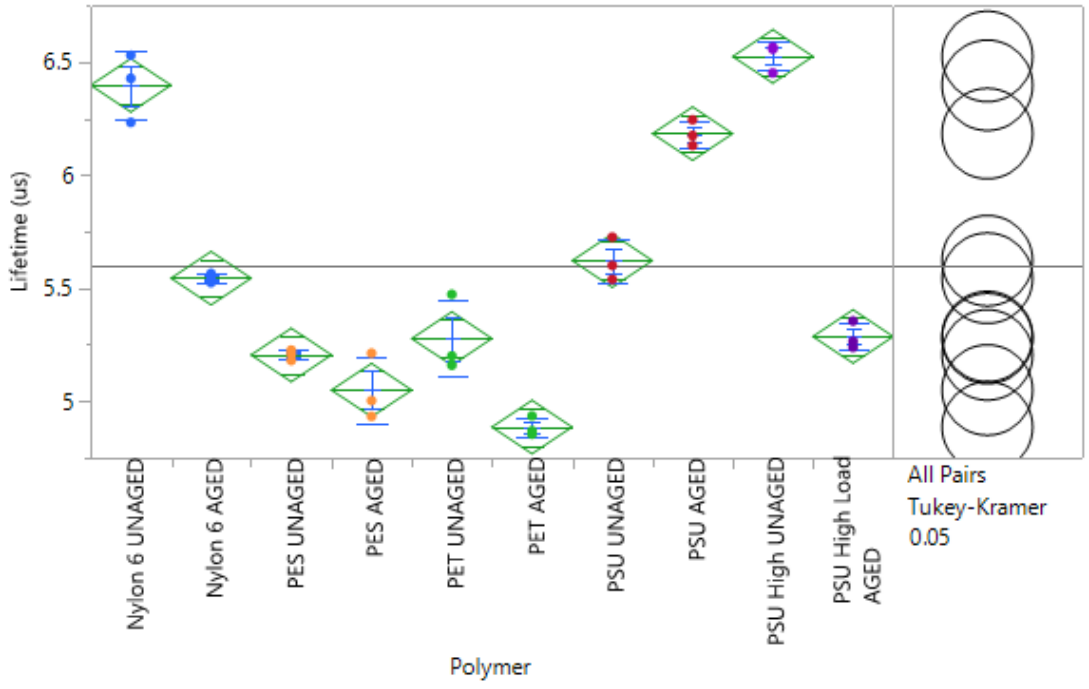

Figure 20: Computed lifetimes at each polymer level, both unaged and aged.

Connecting Letters Report

Level							Mean
PSU High UNAGED	A						6.5268777
Nylon 6 UNAGED	A	B					6.3989686
PSU AGED		B					6.1850294
PSU UNAGED			C				5.6224235
Nylon 6 AGED			C	D			5.5446958
PSU High Load AGED				D	E		5.2863312
PET UNAGED				D	E		5.2774073
PES UNAGED					E		5.2047815
PES AGED					E	F	5.0492321
PET AGED						F	4.8855694

Levels not connected by same letter are significantly different.

Figure 21: Connecting letters report demonstrating statistical significance between levels.

In addition the previous statistical comparison, a Tukey-HSD test comparing the percent changes in lifetime before and after aging across all levels of polymer was performed using JMP software. The intent was to determine if sensor molecule degradation caused by photobleaching had significant effects on lifetime. A similar discrete level plot and connecting letters report are provided in Figures 22 and 23 respectively.

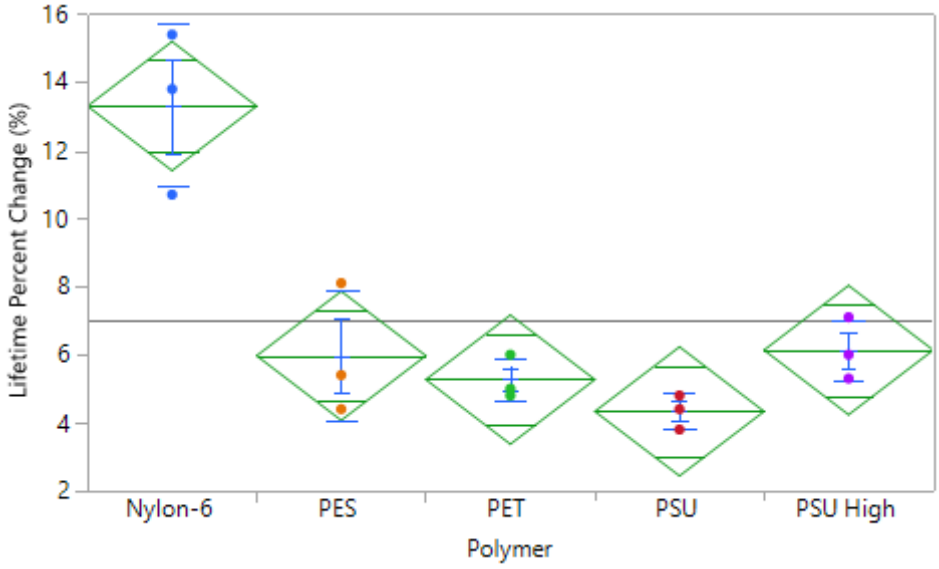

Figure 22: Computed lifetime percent changes at each polymer level.

Connecting Letters Report

Level			Mean
Nylon-6	A		13.300000
PSU High		B	6.133333
PES		B	5.966667
PET		B	5.266667
PSU		B	4.333333

Levels not connected by same letter are significantly different.

Figure 23: Connecting letters report demonstrating statistical significance between lifetime percent changes at each polymer level.

Based on the results from Table 21, the following unaged polymer levels were significant from each other, where the polymers within pairs were insignificant also letting *Ru dye* represent $Ru(dpp)_3Cl_2$: PSU(0.5 wt.% Ru dye)-PCL , [PSU(3 wt.% Ru dye)-PCL, Nylon-6(0.5 wt.% Ru dye)-PCL], [PET(0.5 wt.% Ru dye)-PCL, PES(0.5 wt.% $Ru(dpp)_3Cl_2$)-PCL]. This shows that the probe-matrix interaction has an effect on the lifetime. According to Table 23, the results for the percent lifetime change indicate that only the Nylon-6($Ru(dpp)_3Cl_2$)-PCL level was significant from the other levels in lifetime after continuous excitation. All levels, however, had confidence intervals larger than 0 percent, indicating that lifetime did significantly change after continuous excitation. This was likely a result of the spectrometer reading less photon counts due to the presence of inactive photobleached sensor molecules.

The results show that the lifetime for the unaged PSU(0.5 wt.% $Ru(dpp)_3Cl_2$)-PCL is significantly less than for the PSU(3 wt.% $Ru(dpp)_3Cl_2$)-PCL sample group. This can be explained by the fact that the higher dye load has more sensor molecules, meaning there were more excited sensor molecules contributing to the photon count bins measured by the spectrometer. However, after aging, the opposite was true, supporting the claim that aggregate populations enhanced the photobleaching rate, resulting in less active molecules in the higher dye load sample after aging. In general, the lifetimes slightly decreased after aging for all samples excluding PSU(0.5 wt.% $Ru(dpp)_3Cl_2$)-PCL, indicating photobleaching had a

significant effect on lifetime. Finally, the higher than average lifetime decrease in Nylon-6(0.5 wt.% $Ru(dpp)_3Cl_2$)-PCL sample may be indicative of the unique interaction with that particular system that causes unusually high levels of bleaching. The unaged Nylon-6(0.5 wt.% $Ru(dpp)_3Cl_2$)-PCL system did have one of the highest lifetimes, meaning the excited sensor molecules were more prone to singlet oxygen attack. Furthermore, this could be a contributing factor in the rapid bleaching of Nylon-6(0.5 wt.% $Ru(dpp)_3Cl_2$)-PCL.

4 Conclusions

In this work, we were able to identify several significant parameters that contributed to photobleaching rates and sensor performance. In the application of a biomedical oxygen sensing design, high sensitivity and sensor device performance are required. Moreover, we were able to identify polymer hosts containing luminescent oxygen sensing probes in an electrospun core-shell configuration that offer high levels of sensitivity and promising sensing capability. In addition, it was clear that certain polymers offered varying degrees of longevity, which is one of many important design considerations that must be take into account. Adding a singlet oxygen quencher in the form of β-Carotene to the design did not significantly improve sensor device performance. Finally, we were able to demonstrate that phosphorescent lifetime was significantly affected by host polymer matrix and photobleaching upon continuous light excitation.

The aggregation experiment demonstrated that temperature had a significant affect on normalized intensity, supporting the claim that probe-matrix solubility contributes to the distribution of aggregate sensor molecule populations. Upon testing different probe concentrations, it was clear that self-quenching occurred at higher concentrations, resulting in an overall net decrease in signal intensity. Thus, the final design should have lower concentrations that still produce a high resolution signal. From the results, 0.5 and 3 wt.% dye

loads were the most promising for a final design.

From the aging experiments, the PSU(PdTFPP)-PCL system had the overall highest stability over a long period of time, based on its high sensitivity and lowest relative decrease in signal over time due to photobleaching. PSU(PdTFPP)-PCL would be an adequate candidate for a final design, especially in applications were long-term oxygen detection is required. PET(PdTFPP)-PCL had the highest R^2 value in the Stern-Volmer plots, making it offer promising calibration potential in a final sensor device. Based on this and the fact that PET is highly biocompatible, it is another suitable candidate for sensing device design [32].

The experiment exploring β-Carotene as a singlet oxygen quencher at first glance indicated that sensitiviy was improved after adding it to a PSU(PdTFPP)-PCL system, but the statistical evidence was not strong enough to support that conclusion. Moreover, the data provided motivation to perform further experimentation to gather more conclusive results. If β-Carotene can truly improve sensitivity under long-term light exposure, it could enhance device longevity. Future experiments should use a higher replicate number with a longer aging duration and a better control group to compare to, since the electrospinning solvent was pure chloroform, as opposed to DCM/HFP used in the PSU(PdTFPP)-PCL samples that were part of the polymer aging experiment.

The phosphorescent lifetime measurements were significantly different across a range of different core polymer hosts, indicating that probe-matrix compatibility is important when designing an oxygen sensing device; this was also supported by the aggregation and polymer aging experiments. Photobleaching did have a significant affect on the lifetime percent change as well. The Nylon-6(PdTFPP)-PCL group also showed a substantial decrease in lifetime after aging, supporting the claim that this particular host experienced a unique interaction that caused enhanced photobleaching that is worth further investigation.

In future work, we believe using a higher replicate number and using samples from more than one electrospun scaffold to ensure a truly random design with less data variation. One of

the key issues throughout all the experiments was high data variation, which caused sub-optimal fit qualities in the applied statistical models. Only three replicates were used in all experiments. Significantly increasing this number and using more than one elctrospun fiber scaffold could help reduce data variation and ensure better randomness to improve statistical model validity, thereby producing more conclusive results in future work.

5 Notation/Terminology

(BC): beta carotene - $C_{40}H_{56}$

(Chloroform): dichloromethane.

(DABCO): 1,4-Diazabicyclo[2.2.2]octane.

(DCM): methylene chloride.

(ECM): extracellular matrix.

(HFP): 1,1,1,3,3,3 - hexafluoro-2-propanol.

(HVPS): high voltage power supply.

(ISC): intersystem crossing.

(LUMO): lowest unoccupied molecular orbital.

(PCL): polycaprolactone.

(PdTFPP): Pd (II) meso-tetra(pentafluorophenyl) porphine.

(PES): Polyethersulfone.

(PET): polyethylene terephthalate.

(PSU): polysulfone.

(PtTFPP): Pt (II) meso-tetra(pentafluorophenyl) porphine.

($Ru(dpp)_3Cl_2$): tris (4,7-diphenyl-1,10-phenanthroline) ruthenium(II) dichloride.

(S_0): ground state, singlet electron spin configuration.

(S_1): excited state, singlet eletron spin configuration.

(T_1): excited state, triplet electron spin configuration.

(τ_0): phosphorescent lifetime

(K_{SV}): overall quenching rate constant.

(k_2): bimolecular rate constant.

(I_{N_2}/I_{O_2}): Measure of oxygen sensitivity. In some other texts, represented asI_0/I_{100}.

References

[1] Geankoplis, Christie John *Transport Processes and Separation Process Principles*, Prentice Hall, Upper Saddle River, New Jersey fourth edition, pages: 625-690 2003

[2] Xue, R., Nelson, M. T., Teixeira, S. A., Viapiano, M. S., & Lannutti, J. J. (2016). Cancer cell aggregate hypoxia visualized in vitro via biocompatible fiber sensors. Biomaterials, 76, 208–217. https://doi.org/10.1016/j.biomaterials.2015.10.055

[3] Xue, R., Ge, C., Richardson, K., Palmer, A., Viapiano, M., & Lannutti, J. J. (2015). Microscale sensing of oxygen via encapsulated porphyrin nanofibers: Effect of indicator and polymer "core" permeability. ACS Applied Materials and Interfaces, 7(16), 8606–8614. https://doi.org/10.1021/acsami.5b00403

[4] Wendorff, J. H., Agarwal, S., & Greiner, A. (2012). Front Matter. Electrospinning, Materials, Processing, and Applications. WILEY-VCH, Weinhelm, Germany. Pages: 29-66

[5] Doshi, J., & Reneker, D. H. (1993). Electrospinning process and applications of electrospun fibers. Conference Record - IAS Annual Meeting (IEEE Industry Applications Society), 3, 1698–1703. https://doi.org/10.1109/ias.1993.299067

[6] Amao, Y. (2003). Probes and Polymers for Optical Sensing of Oxygen. Microchimica Acta, 143(1), 1–12. https://doi.org/10.1007/s00604-003-0037-x

[7] Quaranta, M., S. Borisov, and I. Klimant, Indicators for optical oxygen sensors. Bioanalytical Reviews, 2012. 4(2-4): p. 115-157.

[8] Seery, Michael. (2012). Photodynamic Therepy: An Overview. Chem Soc Rev, 2011, 40, 340: Sections A, B, C.1, C.4, D, F.2, F.3. https://photochemistry.wordpress.com/author/photochemistry/

[9] Demas, J.N., B.A. DeGraff, and W. Xu, Modeling of Luminescence Quenching-Based Sensors: Comparison of Multisite and Nonlinear Gas Solubility Models. Analytical Chemistry, 1995. 67(8): p. 1377-1380.

[10] Grist, S.M., L. Chrostowski, and K.C. Cheung, Optical Oxygen Sensors for Applications in Microfluidic Cell Culture. Sensors, 2010. 10(10): p. 9286-9316.

[11] Wang, X. dong, Chen, H. xu, Zhao, Y., Chen, X., Wang, X. ru, & Chen, X. (2010). Optical oxygen sensors move towards colorimetric determination. TrAC - Trends in Analytical Chemistry, 29(4), 319–338. https://doi.org/10.1016/j.trac.2010.01.004

[12] Presley, K. F., Cheong, S., Cochran, A., Tilley, R. D., Collins, J. E., & Lannutti, J. J. (2016). Upconverter-powered oxygen sensing in electrospun polymeric bilayers. Sensors and Actuators, B: Chemical, 235, 197–205. https://doi.org/10.1016/j.snb.2016.04.182

[13] Preslety, K. F., Cheong, S., Shahhosseini, M., Arnold, R. M., Graff, A., Castro, C. E., Tilley, R. D., Ariotti, N., & Lannutti, J.J. (2019) Performance and Photostability of oxygen sensing nanofibers: electrospinning solvent and polymer matrix.

[14] A. Diaspro, G. Chirico, C. Usai, P. Ramoino, J. Dobrucki, Photobleaching, Handb. Biol. Confocal Microsc. (2006) 690–702. doi:doi: 10.1007/978-0-387-45524-2_39.

[15] Enko, B., Borisov, S. M., Regensburger, J., Bäumler, W., Gescheidt, G., & Klimant, I. (2013). Singlet oxygen-induced photodegradation of the polymers and dyes in optical sensing materials and the effect of stabilizers on these processes. Journal of Physical Chemistry A, 117(36), 8873–8882. https://doi.org/10.1021/jp4046462

[16] Mills, A. (1998). Controlling the sensitivity of optical oxygen sensors. Sensors and Actuators, B: Chemical, 51(1–3), 60–68. https://doi.org/10.1016/S0925-4005(98)00211-1

[17] R. Xue, P. Behera, M.S. Viapiano, J.J. Lannutti, Rapid response oxygen-sensing nanofibers, Mater. Sci. Eng. C. 33 (2013) 3450–3457. doi:10.1016/j.msec.2013.04.030.

[18] S.M. Borisov, P. Lehner, I. Klimant, Novel optical trace oxygen sensors based on platinum(II) and palladium(II) complexes with 5,10,15,20-meso-tetrakis-(2,3,4,5,6-pentafluorphenyl)-porphyrin covalently immobilized on silica-gel particles, Anal. Chim. Acta. 690 (2011) 108–115. doi:10.1016/j.aca.2011.01.057.

[19] J. Moan, K. Berg, The photodegradation of porphyrins in Cells can be used to estimate the lifetime of singlet oxygen, Photochem. Photobiol. 53 (1991) 549–553. doi:10.1111/j.1751-1097.1991.tb03669.x.

[20] Stratton, S. P., Schaefer, W. H., & Liebler, D. C. (1993). Isolation and Identification of Singlet Oxygen Oxidation Products of -Carotene. Chemical Research in Toxicology, 6(4), 542–547. https://doi.org/10.1021/tx00034a024

[21] C.S. Chu, Y.L. Lo, Ratiometric fiber-optic oxygen sensors based on sol-gel matrix doped with metalloporphyrin and 7-amino-4-trifluoromethyl coumarin, Sensors Actuators, B Chem. 134 (2008) 711–717. doi:10.1016/j.snb.2008.06.022.

[22] National Center for Biotechnology Information. PubChem Database. beta-Carotene, CID=5280489, https://pubchem.ncbi.nlm.nih.gov/compound/beta-Carotene (accessed on Dec. 29, 2019)

[23] National Center for Biotechnology Information. PubChem Database. PdTFPP, CID=3867957, https://pubchem.ncbi.nlm.nih.gov/compound/PdTFPP (accessed on Dec. 29, 2019)

[24] National Center for Biotechnology Information. PubChem Database. CID=5190808, https://pubchem.ncbi.nlm.nih.gov/compound/5190808 (accessed on Dec. 29, 2019)

[25] Caymen Chemical. Item No.16117. Tris(4,7-diphenyl-1,10-phenanthroline)ruthenium II dichloride complex. https://www.caymanchem.com/product/16117 (accessed on Dec. 29, 2019)

[26] Montgomery, D. C. (2012). Design and Analysis of Experiments Eighth Edition. In Design (Vol. 2). https://doi.org/10.1198/tech.2006.s372

[27] Hartmann, P., Leiner, M. J. P., Kohlbacher, P. (1998). Photobleaching of a ruthenium complex in polymers used for oxygen optodes and its inhibition by singlet oxygen quenchers. Sensors and Actuators B, 51, 196–202. https://doi.org/10.1016/S0925-4005(98)00188-9

[28] Matweb Material Property Data (1996-2020), Matweb LLC., Data Accessed: January 2020, https://www.matweb.com

[29] S. Grenoble, M. Gouterman, G. Khalil, J. Callis, L. Dalton, Pressure-sensitive paint (PSP): Concentration quenching of platinum and magnesium porphyrin dyes in polymeric films, J. Lumin. 113 (2005) 33–44. doi:10.1016/j.jlumin.2004.08.049.

[30] A.K. Bansal, W. Holzer, A. Penzkofer, T. Tsuboi, Absorption and emission spectroscopic characterization of platinum-octaethyl-porphyrin (PtOEP), Chem. Phys. 330 (2006) 118–129. doi:10.1016/j.chemphys.2006.08.002.

[31] J. Demas, B. DeGraff, W. Xu, Modeling of luminescence quenching-based sensors: comparison of multisite and nonlinear gas solubility models, Anal. Chem. 67 (1995) 1377–1380. doi:10.1021/ac00104a012.

[32] Chaparro, F. J., Presley, K. F., Coutinho da Silva, M. A., Mandan, N., Colachis, M. L., Posner, M., … Lannutti, J. J. (2019). Sintered electrospun poly(-caprolactone)–poly(ethylene terephthalate) for drug delivery. Journal of Applied Polymer Science, 136(26), 1–14. https://doi.org/10.1002/app.47731

Appendix A: Oxygen Sensing Probes and Singlet Oxygen Quencher Chemical Structures

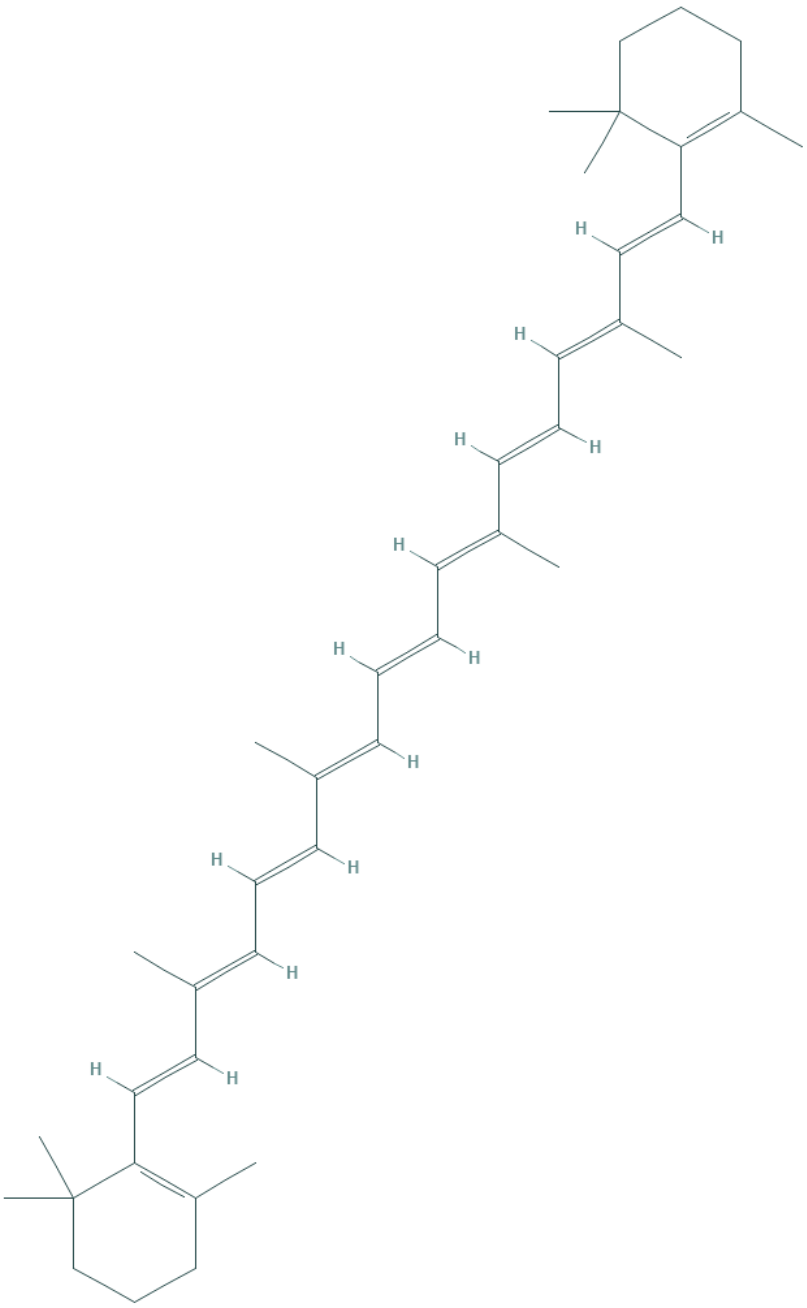

Figure A.1: Chemical structure of singlet oxygen quenching candidate $\beta-$Carotene [22].

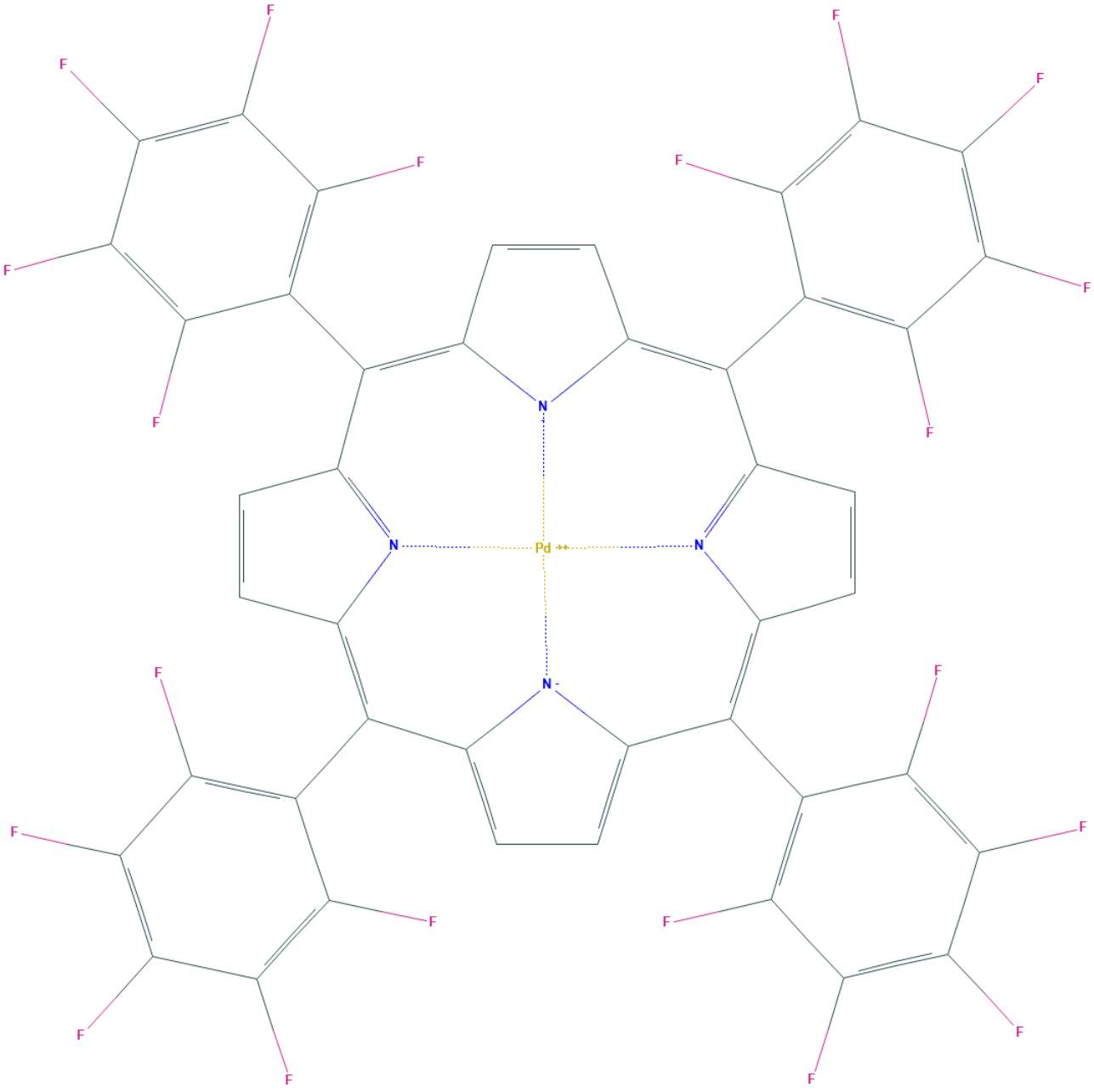

Figure A.2: Chemical structure of oxygen sensing probe PdTFPP [23].

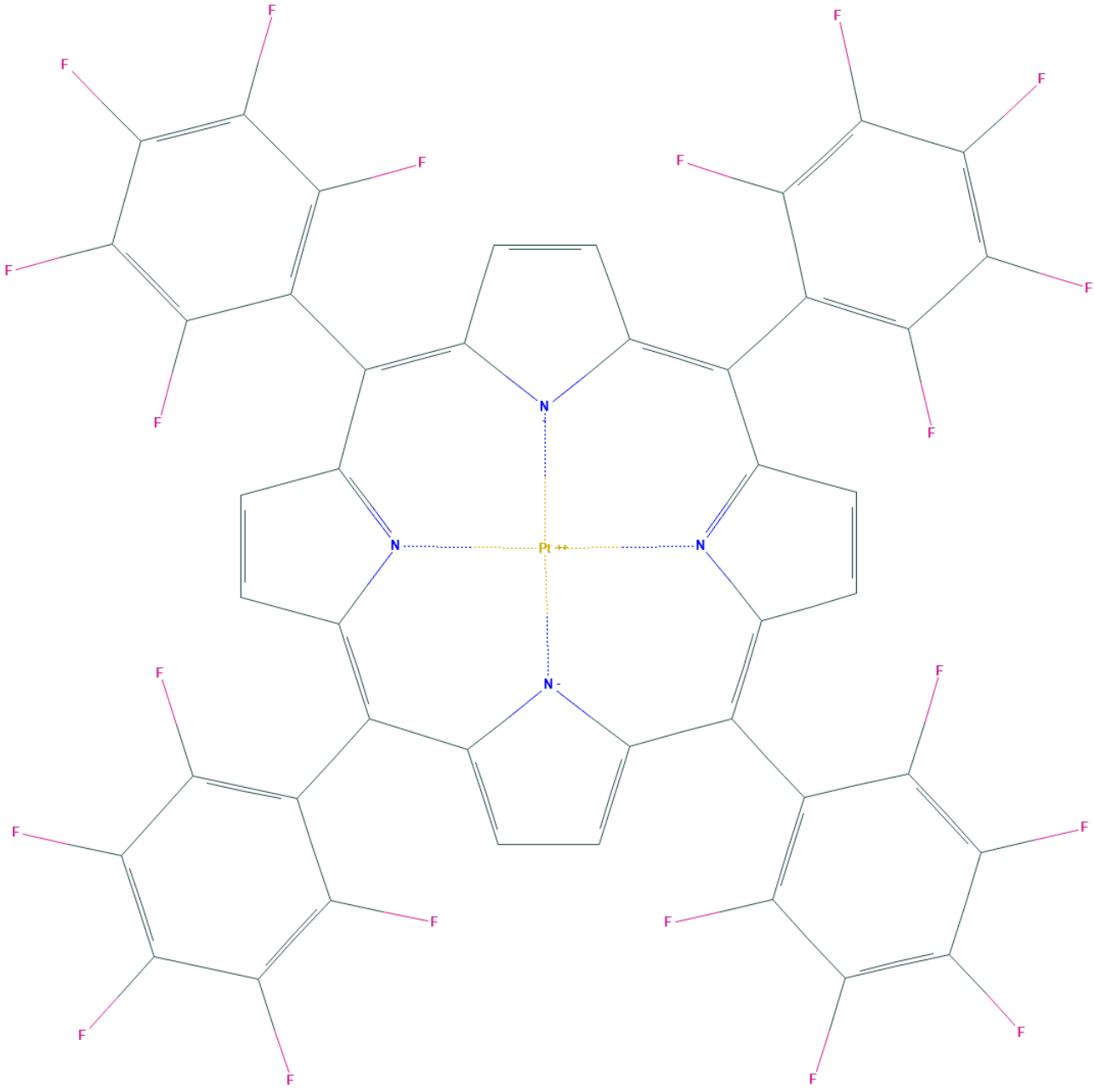

Figure A.3: Chemical structure of oxygen sensing probe PtTFPP [24].

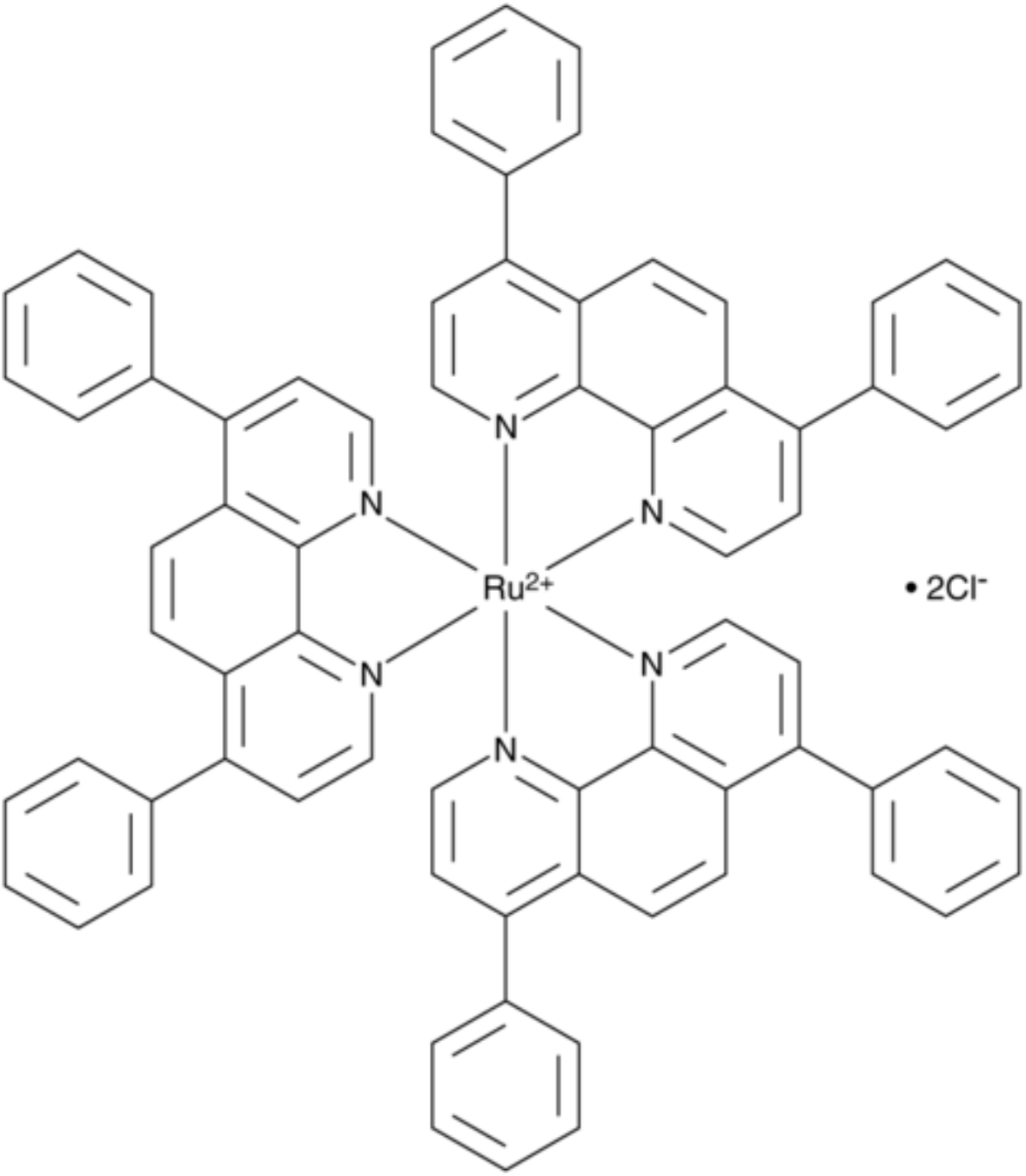

Figure A.4: Chemical structure of oxygen sensing probe $Ru(dpp)_3Cl_2$ [25].

Appendix B: Supplemental Figures

Decay Curves in Air Environment from Aggregation Experiment.

∘C".pdf ∘C".png ∘C".jpg ∘C".mps ∘C".jpeg ∘C".jbig2 ∘C".jb2 ∘C".PDF ∘C".PNG ∘C".JPG ∘C".JPEG ∘C".J

(a) Decay of 0.1 wt.% PdTFPP dye load at T=37°C.

∘C".pdf ∘C".png ∘C".jpg ∘C".mps ∘C".jpeg ∘C".jbig2 ∘C".jb2 ∘C".PDF ∘C".PNG ∘C".JPG ∘C".JPEG ∘C".J

(b) Decay of 0.1 wt.% PdTFPP dye load at T=50°C.

Figure B.1: Decay curves in air for 0.1wt.% PdTFPP Aggregation Experiment Group.

∘C".pdf ∘C".png ∘C".jpg ∘C".mps ∘C".jpeg ∘C".jbig2 ∘C".jb2 ∘C".PDF ∘C".PNG ∘C".JPG ∘C".JPEG ∘C".J

(a) Decay of 0.5 wt.% PdTFPP dye load at T=37°C.

∘C".pdf ∘C".png ∘C".jpg ∘C".mps ∘C".jpeg ∘C".jbig2 ∘C".jb2 ∘C".PDF ∘C".PNG ∘C".JPG ∘C".JPEG ∘C".J

(b) Decay of 0.1 wt.% PdTFPP dye load at T=50°C.

Figure B.2: Decay curves in air for 0.5wt.% PdTFPP Aggregation Experiment Group.

∘C".pdf ∘C".png ∘C".jpg ∘C".mps ∘C".jpeg ∘C".jbig2 ∘C".jb2 ∘C".PDF ∘C".PNG ∘C".JPG ∘C".JPEG ∘C".J

(a) Decay of 3 wt.% PdTFPP dye load at T=37°C.

∘C".pdf ∘C".png ∘C".jpg ∘C".mps ∘C".jpeg ∘C".jbig2 ∘C".jb2 ∘C".PDF ∘C".PNG ∘C".JPG ∘C".JPEG ∘C".J

(b) Decay of 3 wt.% PdTFPP dye load at T=50°C.

Figure B.3: Decay curves in air for 3 wt.% PdTFPP Aggregation Experiment Group.

∘C".pdf ∘C".png ∘C".jpg ∘C".mps ∘C".jpeg ∘C".jbig2 ∘C".jb2 ∘C".PDF ∘C".PNG ∘C".JPG ∘C".JPEG ∘C".J

(a) Decay of 10 wt.% PdTFPP dye load at T=37°C.

∘C".pdf ∘C".png ∘C".jpg ∘C".mps ∘C".jpeg ∘C".jbig2 ∘C".jb2 ∘C".PDF ∘C".PNG ∘C".JPG ∘C".JPEG ∘C".J

(b) Decay of 10 wt.% PdTFPP dye load at T=50°C.

Figure B.4: Decay curves in air for 10 wt.% PdTFPP Aggregation Experiment Group.

∘C".pdf ∘C".png ∘C".jpg ∘C".mps ∘C".jpeg ∘C".jbig2 ∘C".jb2 ∘C".PDF ∘C".PNG ∘C".JPG ∘C".JPEG ∘C".J

(a) Decay of 0.1 wt.% PtTFPP dye load at T=37°C.

∘C".pdf ∘C".png ∘C".jpg ∘C".mps ∘C".jpeg ∘C".jbig2 ∘C".jb2 ∘C".PDF ∘C".PNG ∘C".JPG ∘C".JPEG ∘C".J

(b) Decay of 0.1 wt.% PtTFPP dye load at T=50°C.

Figure B.5: Decay curves in air for 0.1wt.% PtTFPP Aggregation Experiment Group.

∘C".pdf ∘C".png ∘C".jpg ∘C".mps ∘C".jpeg ∘C".jbig2 ∘C".jb2 ∘C".PDF ∘C".PNG ∘C".JPG ∘C".JPEG ∘C".J

(a) Decay of 0.5 wt.% PtTFPP dye load at T=37°C.

∘C".pdf ∘C".png ∘C".jpg ∘C".mps ∘C".jpeg ∘C".jbig2 ∘C".jb2 ∘C".PDF ∘C".PNG ∘C".JPG ∘C".JPEG ∘C".J

(b) Decay of 0.5 wt.% PtTFPP dye load at T=50°C.

Figure B.6: Decay curves in air for 0.5wt.% PtTFPP Aggregation Experiment Group.

∘C".pdf ∘C".png ∘C".jpg ∘C".mps ∘C".jpeg ∘C".jbig2 ∘C".jb2 ∘C".PDF ∘C".PNG ∘C".JPG ∘C".JPEG ∘C".J

(a) Decay of 3 wt.% PtTFPP dye load at T=37°C.

∘C".pdf ∘C".png ∘C".jpg ∘C".mps ∘C".jpeg ∘C".jbig2 ∘C".jb2 ∘C".PDF ∘C".PNG ∘C".JPG ∘C".JPEG ∘C".J

(b) Decay of 3 wt.% PtTFPP dye load at T=50°C.

Figure B.7: Decay curves in air for 3 wt.% PtTFPP Aggregation Experiment Group.

∘C".pdf ∘C".png ∘C".jpg ∘C".mps ∘C".jpeg ∘C".jbig2 ∘C".jb2 ∘C".PDF ∘C".PNG ∘C".JPG ∘C".JPEG ∘C".J

(a) Decay of 10 wt.% PtTFPP dye load at T=37°C.

∘C".pdf ∘C".png ∘C".jpg ∘C".mps ∘C".jpeg ∘C".jbig2 ∘C".jb2 ∘C".PDF ∘C".PNG ∘C".JPG ∘C".JPEG ∘C".J

(b) Decay of 10 wt.% PdTFPP dye load at T=50°C.

Figure B.8: Decay curves in air for 10 wt.% PtTFPP Aggregation Experiment Group.

Decay Curves in Pure N_2 Environment from Polymer Aging Experiment.

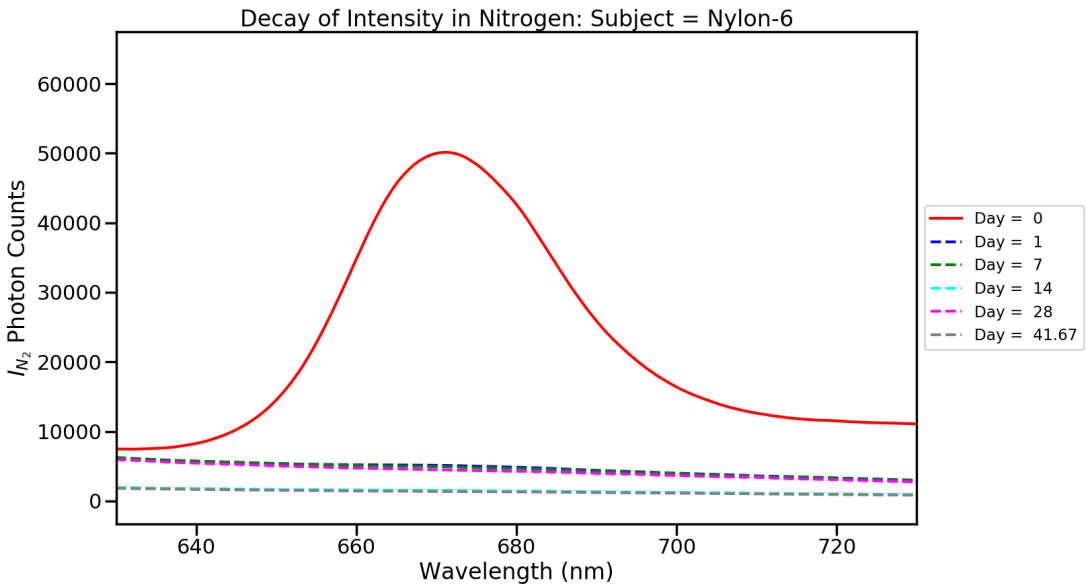

(a) Decay of PdTFPP dye emission curves for Nylon-6 host.

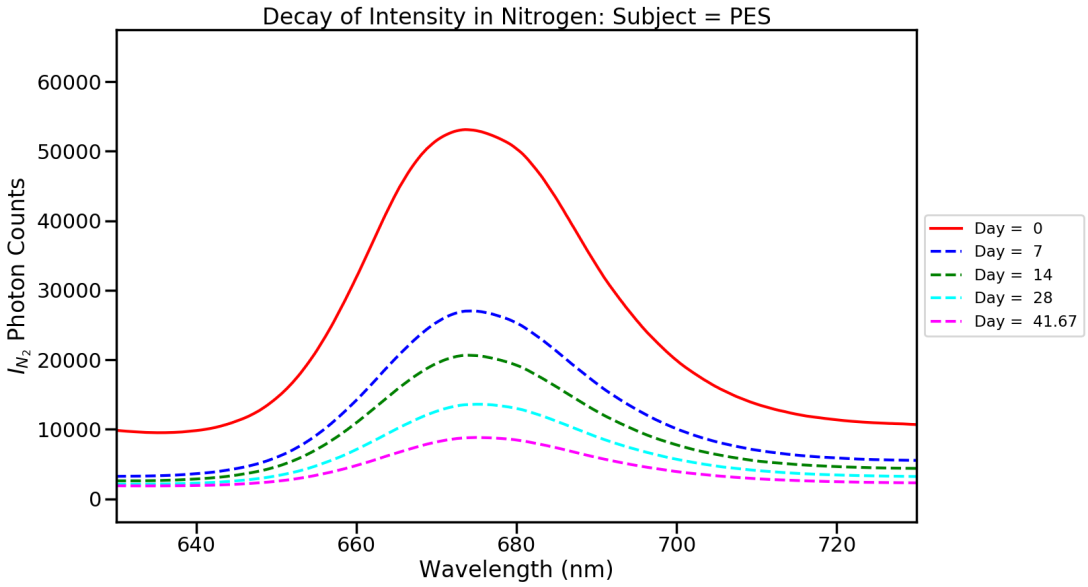

(b) Decay of PdTFPP dye emission curves for PES host.

Figure B.9: Decay of PdTFPP dye emission curves in pure N_2 environment for hosts Nylon-6 and PES.

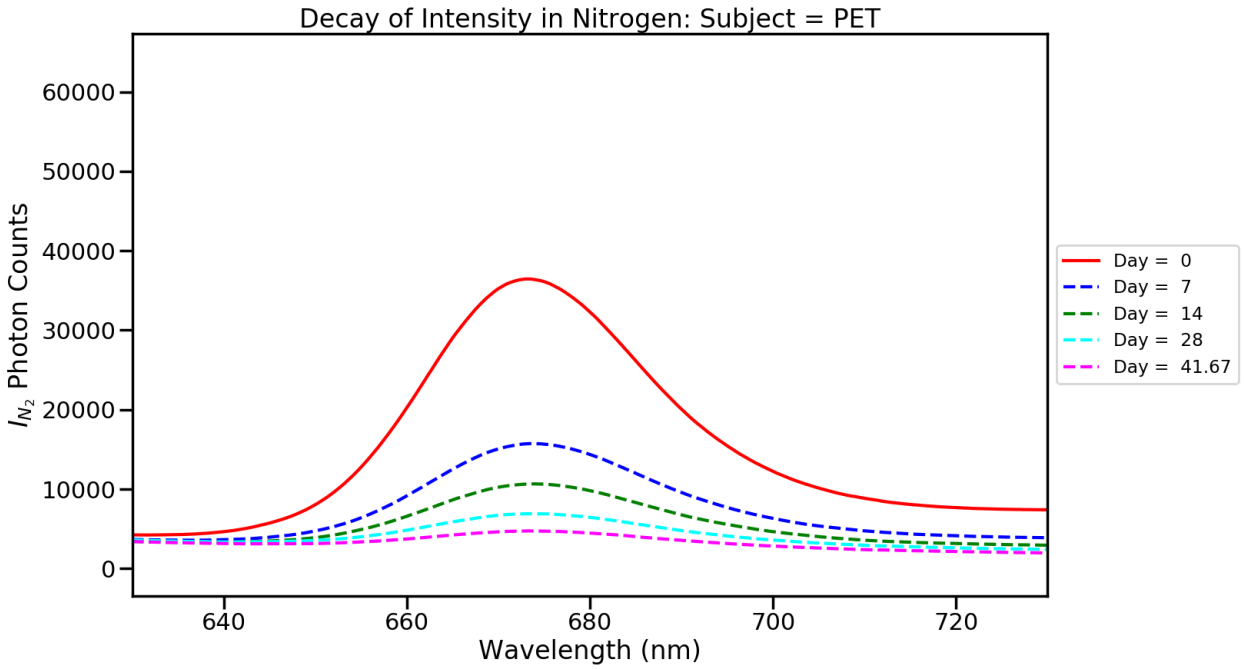

(a) Decay of PdTFPP dye emission curves for PET host.

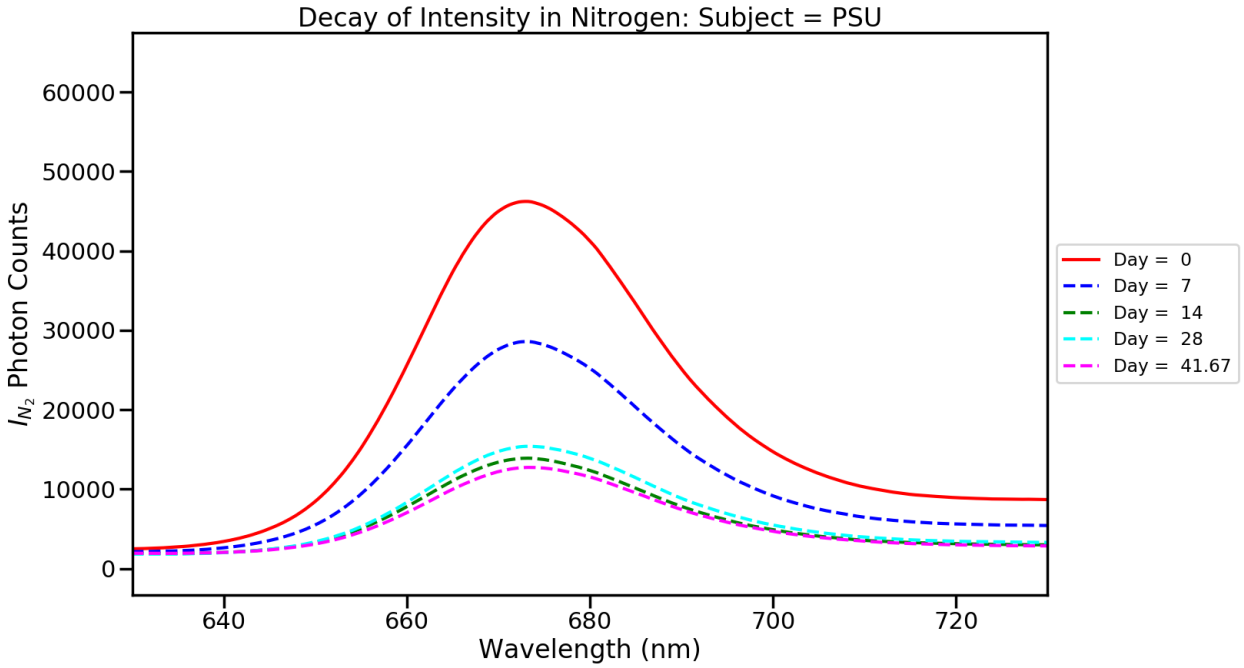

(b) Decay of PdTFPP dye emission curves for PSU host.

Figure B.10: Decay of PdTFPP dye emission curves in pure N_2 environment for hosts PET and PSU.

Decay Curves in Pure N_2 Environment from β-Carotene experiment.

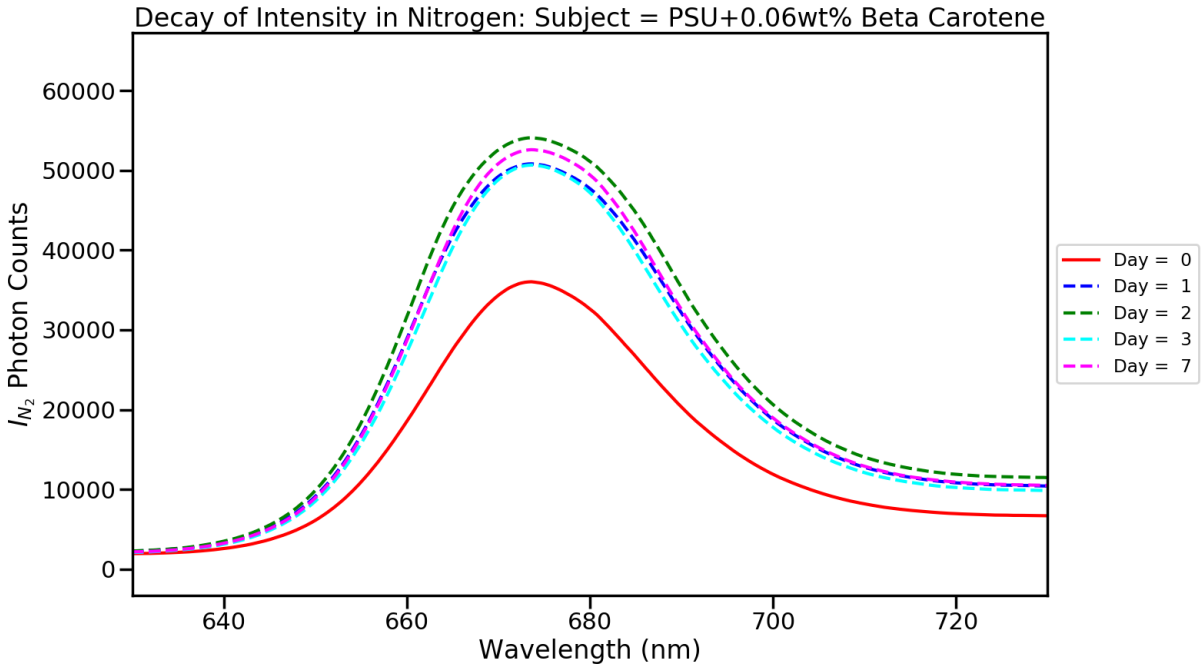

Figure B.11: Decay of PdTFPP dye emission curves in pure N_2 with PSU host and 0.06wt.% β-Carotene.

Decay Curves in Pure N_2 Environment from Lifetime experiment.

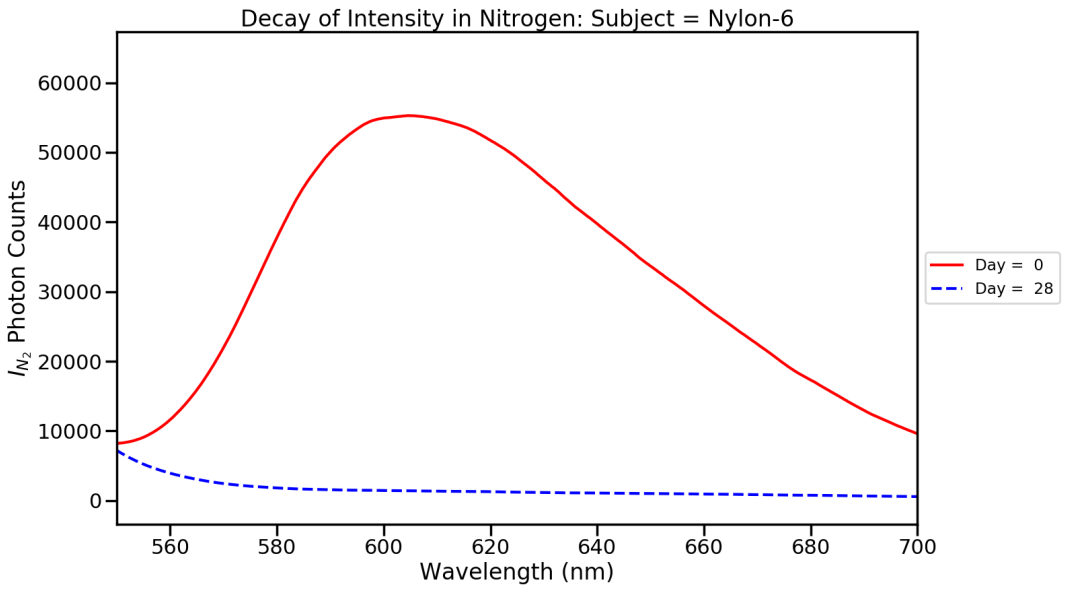

(a) Decay of 0.5 wt.% $Ru(dpp)_3Cl_2$ dye load emission curves with Nylon-6 host.

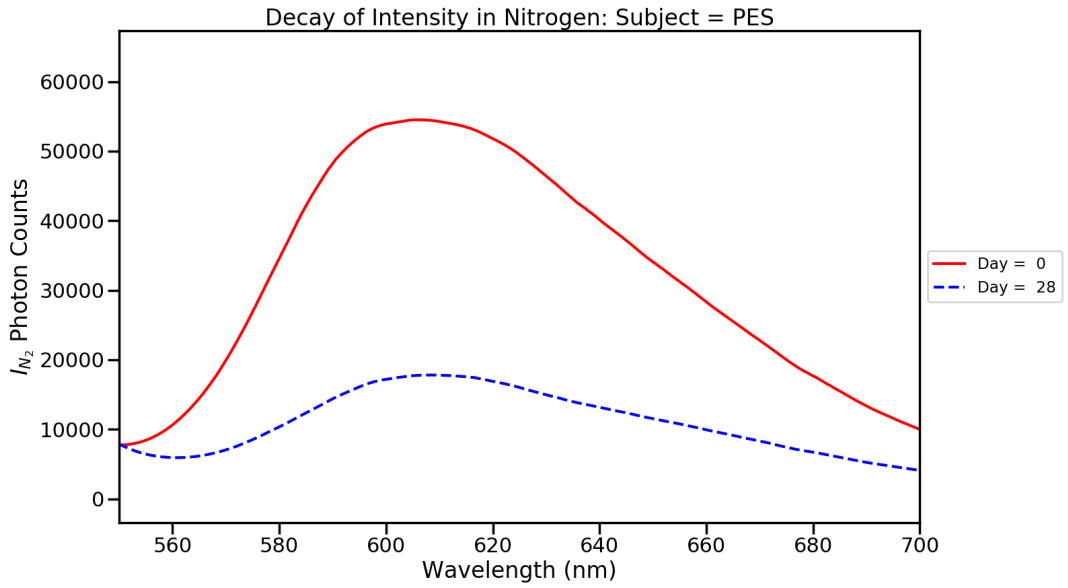

(b) Decay of 0.5 wt.% $Ru(dpp)_3Cl_2$ dye load emission curves with PES host.

Figure B.12: Decay of PdTFPP dye emission curves in pure N_2 environment with hosts PET and PSU.

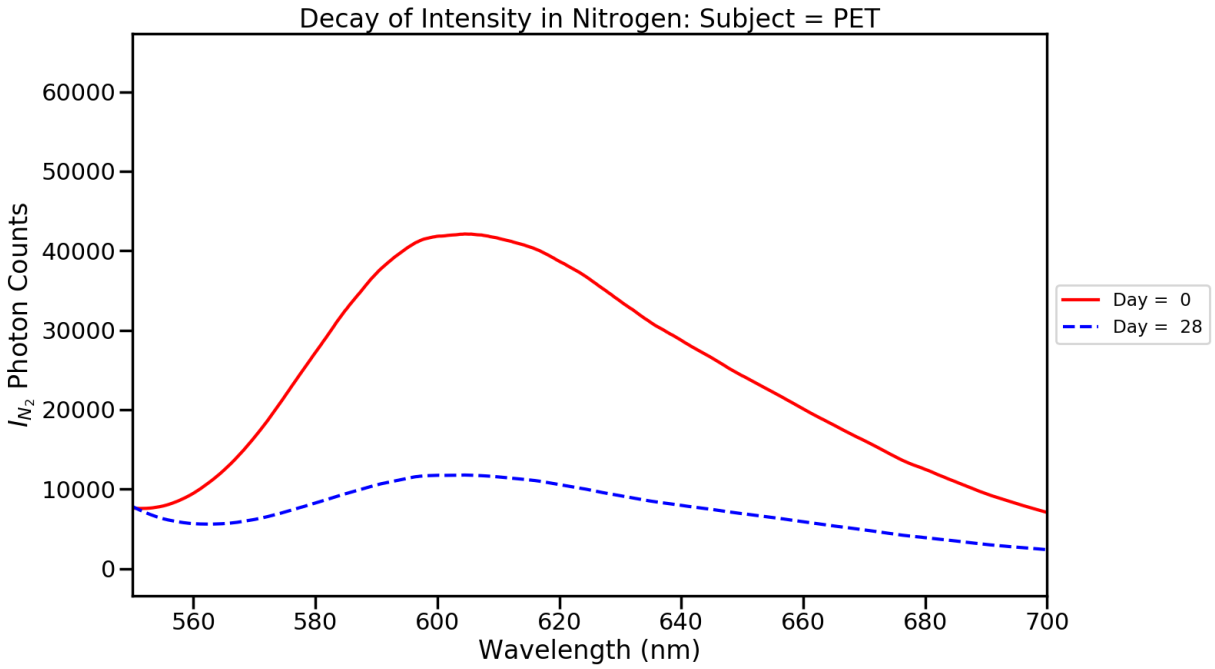

(a) Decay of 0.5 wt.% $Ru(dpp)_3Cl_2$ dye load emission curves with PET host.

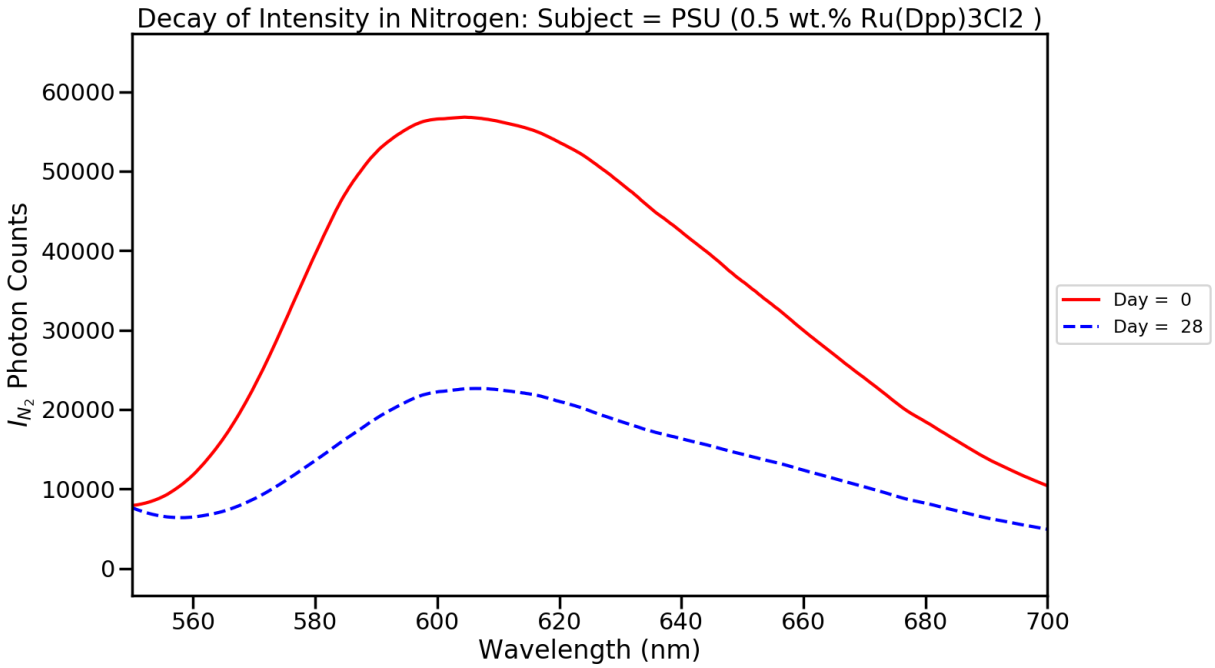

(b) Decay of 0.5 wt.% $Ru(dpp)_3Cl_2$ dye load emission curves with PSU host.

Figure B.13: Decay of 0.5 wt.% $Ru(dpp)_3Cl_2$ dye load emission curves for PSU and PET hosts.

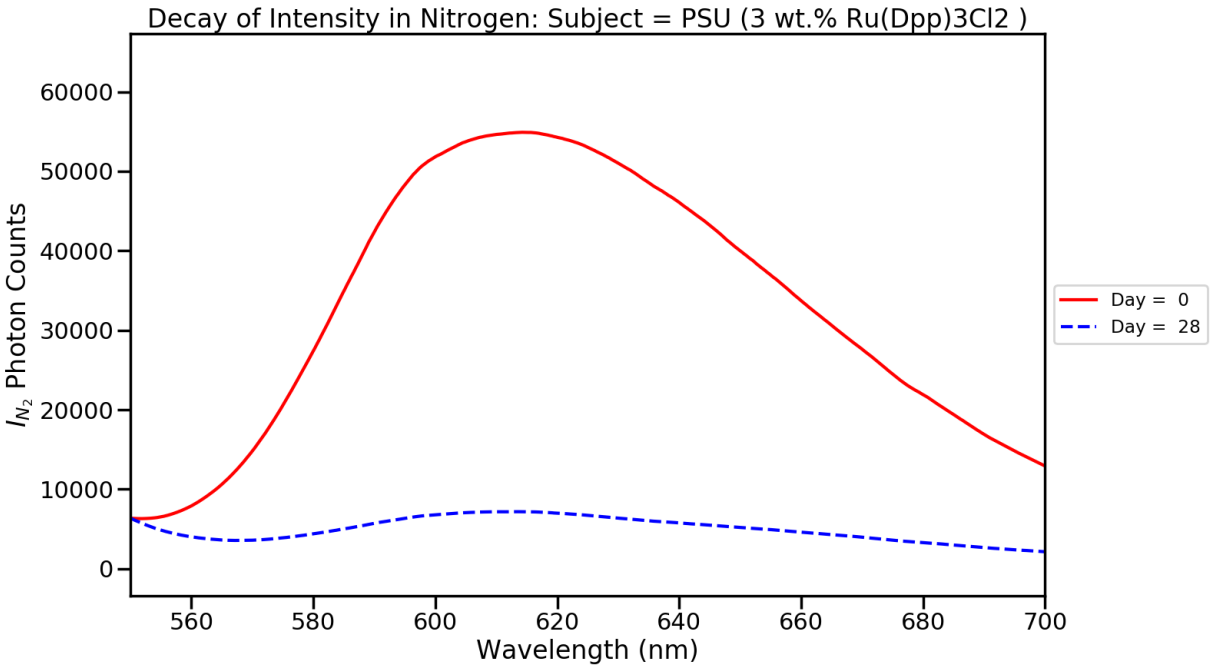

Figure B.14: Decay of 3 wt.% $Ru(dpp)_3Cl_2$ dye load emission curves with PSU host.

Appendix C: Supplemental Statics Tables and Analyses.

Aggregation Experiment Supplemental Statistics

Table C.1: Summary of model fit for I_{Air}/I_{Air_0} with PtTFPP dye response in aggregation experiment.

Summary of Fit	
RSquare	0.579001
RSquare Adj	0.494094
Root Mean Square Error	0.05722
Mean of Response	0.959488
Observations (or Sum Wgts)	144

Table C.2: ANOVA table for I_{Air}/I_{Air_0} with PtTFPP dye response in aggregation experiment.

Analysis of Variance				
Source	DF	Sum of Squares	Mean Square	F Ratio
Model	24	0.53583995	0.022327	6.8192
Error	119	0.38961573	0.003274	Prob > F
C. Total	143	0.92545569		<.0001*

Table C.3: Summary of model fit for I_{Air}/I_{Air_0} with PdTFPP dye response in aggregation experiment.

Summary of Fit	
RSquare	0.450042
RSquare Adj	0.416433
Root Mean Square Error	0.049831
Mean of Response	0.969402
Observations (or Sum Wgts)	192

Table C.4: ANOVA table for I_{Air}/I_{Air_0} with PdTFPP dye response in aggregation experiment.

Analysis of Variance				
Source	DF	Sum of Squares	Mean Square	F Ratio
Model	5	1840.0608	368.012	39.1514
Error	48	451.1862	9.400	Prob > F
C. Total	53	2291.2470		<.0001*

Table C.5: Expanded effect tests for I_{Air}/I_{Air_0} with PtTFPP dye response in aggregation experiment.

Term	Estimate	Std Error	t Ratio	Prob>|t|	Lower 95%	Upper 95%
Intercept	0.9594878	0.004768	201.22	<.0001*	0.9500461	0.9689295
Day[0]	0.0405122	0.012616	3.21	0.0017*	0.0155318	0.0654926
Day[1]	0.0139471	0.012616	1.11	0.2712	-0.011033	0.0389275
Day[3]	0.0330624	0.012616	2.62	0.0099*	0.008082	0.0580428
Day[14]	-0.000541	0.012616	-0.04	0.9659	-0.025521	0.0244393
Day[28]	-0.024569	0.012616	-1.95	0.0538	-0.049549	0.0004115
Day[365]	-0.040846	0.012616	-3.24	0.0016*	-0.065827	-0.015866
Day[41.67]	-0.038364	0.012616	-3.04	0.0029*	-0.063345	-0.013384
Day[7]	0.0167988	0.012616	1.33	0.1855	-0.008182	0.0417793
Dye Load Group[0.5wt%Pt]	-0.011349	0.006743	-1.68	0.0950	-0.024702	0.0020032
Dye Load Group[10wt%Pt]	-0.048669	0.006743	-7.22	<.0001*	-0.062022	-0.035317
Dye Load Group[3wt%Pt]	0.0600185	0.006743	8.90	<.0001*	0.0466659	0.0733711
Temperature[37]	0.0157629	0.004768	3.31	0.0013*	0.0063212	0.0252046
Temperature[50]	-0.015763	0.004768	-3.31	0.0013*	-0.025205	-0.006321
Dye Load Group[0.5wt%Pt]*Day[0]	0.0113494	0.017841	0.64	0.5259	-0.023978	0.046677
Dye Load Group[0.5wt%Pt]*Day[1]	-0.02768	0.017841	-1.55	0.1234	-0.063008	0.0076473
Dye Load Group[0.5wt%Pt]*Day[3]	0.0169623	0.017841	0.95	0.3437	-0.018365	0.05229
Dye Load Group[0.5wt%Pt]*Day[14]	0.0029459	0.017841	0.17	0.8691	-0.032382	0.0382736
Dye Load Group[0.5wt%Pt]*Day[28]	-0.026912	0.017841	-1.51	0.1341	-0.06224	0.0084156
Dye Load Group[0.5wt%Pt]*Day[365]	0.0286167	0.017841	1.60	0.1114	-0.006711	0.0639443
Dye Load Group[0.5wt%Pt]*Day[41.67]	-0.025179	0.017841	-1.41	0.1608	-0.060507	0.0101487
Dye Load Group[0.5wt%Pt]*Day[7]	0.019897	0.017841	1.12	0.2670	-0.015431	0.0552246
Dye Load Group[10wt%Pt]*Day[0]	0.0486691	0.017841	2.73	0.0073*	0.0133415	0.0839967
Dye Load Group[10wt%Pt]*Day[1]	-0.01191	0.017841	-0.67	0.5057	-0.047237	0.023418
Dye Load Group[10wt%Pt]*Day[3]	-0.013592	0.017841	-0.76	0.4477	-0.04892	0.0217356
Dye Load Group[10wt%Pt]*Day[14]	-0.007704	0.017841	-0.43	0.6667	-0.043032	0.0276234
Dye Load Group[10wt%Pt]*Day[28]	-0.001018	0.017841	-0.06	0.9546	-0.036345	0.0343101
Dye Load Group[10wt%Pt]*Day[365]	-0.018285	0.017841	-1.02	0.3075	-0.053612	0.017043
Dye Load Group[10wt%Pt]*Day[41.67]	0.0057925	0.017841	0.32	0.7460	-0.029535	0.0411201
Dye Load Group[10wt%Pt]*Day[7]	-0.001953	0.017841	-0.11	0.9130	-0.037281	0.0333742
Dye Load Group[3wt%Pt]*Day[0]	-0.060018	0.017841	-3.36	0.0010*	-0.095346	-0.024691
Dye Load Group[3wt%Pt]*Day[1]	0.03959	0.017841	2.22	0.0284*	0.0042624	0.0749177
Dye Load Group[3wt%Pt]*Day[3]	-0.00337	0.017841	-0.19	0.8505	-0.038698	0.0319574
Dye Load Group[3wt%Pt]*Day[14]	0.0047583	0.017841	0.27	0.7902	-0.030569	0.0400859
Dye Load Group[3wt%Pt]*Day[28]	0.0279296	0.017841	1.57	0.1201	-0.007398	0.0632573
Dye Load Group[3wt%Pt]*Day[365]	-0.010332	0.017841	-0.58	0.5636	-0.04566	0.0249956
Dye Load Group[3wt%Pt]*Day[41.67]	0.0193864	0.017841	1.09	0.2794	-0.015941	0.054714
Dye Load Group[3wt%Pt]*Day[7]	-0.017944	0.017841	-1.01	0.3166	-0.053271	0.0173841

Table C.6: Expanded effect tests for I_{Air}/I_{Air_0} with PtTFPP dye response in aggregation experiment.

Term	Estimate	Std Error	t Ratio	Prob>|t|	Lower 95%	Upper 95%
Intercept	0.9694016	0.003596	269.56	<.0001*	0.9623055	0.9764978
Day[0]	0.0305984	0.009515	3.22	0.0015*	0.0118236	0.0493731
Day[1]	0.0051319	0.009515	0.54	0.5903	-0.013643	0.0239066
Day[3]	-0.019841	0.009515	-2.09	0.0385*	-0.038616	-0.001066
Day[14]	-0.000385	0.009515	-0.04	0.9678	-0.01916	0.0183898
Day[28]	-0.013508	0.009515	-1.42	0.1574	-0.032283	0.0052668
Day[365]	0.0079085	0.009515	0.83	0.4070	-0.010866	0.0266833
Day[41.67]	0.000754	0.009515	0.08	0.9369	-0.018021	0.0195287
Day[7]	-0.010659	0.009515	-1.12	0.2641	-0.029434	0.0081159
Dye Load Group[0.1_wt%_PdTFPP]	0.0474158	0.006229	7.61	<.0001*	0.0351249	0.0597068
Dye Load Group[0.5_wt%_PdTFPP]	-0.028293	0.006229	-4.54	<.0001*	-0.040584	-0.016002
Dye Load Group[10_wt%_PdTFPP]	-0.048365	0.006229	-7.76	<.0001*	-0.060656	-0.036074
Dye Load Group[3_wt%_PdTFPP]	0.0292418	0.006229	4.69	<.0001*	0.0169508	0.0415327
Temperature[37]	0.0113921	0.003596	3.17	0.0018*	0.0042959	0.0184882
Temperature[50]	-0.011392	0.003596	-3.17	0.0018*	-0.018488	-0.004296

Polymer Aging Experiment Supplemental Statistics

Table C.7: Summary of model fit for I_{N_2}/I_{O_2} response in aging experiment.

Summary of Fit	
RSquare	0.803083
RSquare Adj	0.78257
Root Mean Square Error	3.065895
Mean of Response	7.914999
Observations (or Sum Wgts)	54

Table C.8: ANOVA table for I_{N_2}/I_{O_2} response in aging experiment.

Analysis of Variance				
Source	DF	Sum of Squares	Mean Square	F Ratio
Model	5	1840.0608	368.012	39.1514
Error	48	451.1862	9.400	Prob > F
C. Total	53	2291.2470		<.0001*

Table C.9: Overall effects test for $I_{N_2}/I_{O_{20}}$ response in aging experiment.

Effect Tests

Source	Nparm	DF	Sum of Squares	F Ratio	Prob > F
Polymer	3	3	1569.5560	55.6597	<.0001*
Day Cts	1	1	431.0253	45.8552	<.0001*
Day Cts*Day Cts	1	1	34.8596	3.7086	0.0601

Table C.10: Lack of fit F-test for $I_{N_2}/I_{O_{20}}$ statistical model in aging experiment.

Lack Of Fit

Source	DF	Sum of Squares	Mean Square	F Ratio
Lack Of Fit	14	293.59343	20.9710	4.5244
Pure Error	34	157.59279	4.6351	Prob > F
Total Error	48	451.18621		0.0002*
				Max RSq
				0.9312

Table C.11: Summary of model fit for $I_{N_2}/I_{O_{20}}$ after blue light fit response in aging experiment.

Summary of Fit

RSquare	0.844054
RSquare Adj	0.828459
Root Mean Square Error	28.86382
Mean of Response	52.34551
Observations (or Sum Wgts)	56

Table C.12: ANOVA table for $I_{N_2}/I_{O_{20}}$ after blue light fit response in aging experiment.

Analysis of Variance

Source	DF	Sum of Squares	Mean Square	F Ratio
Model	5	225461.36	45092.3	54.1246
Error	50	41655.99	833.1	Prob > F
C. Total	55	267117.35		<.0001*

Table C.13: Overall effects test for $I_{N_2}/I_{O_{20}}$ after blue light fit response in aging experiment.

Effect Tests

Source	Nparm	DF	Sum of Squares	F Ratio	Prob > F
Polymer	3	3	206489.23	82.6169	<.0001*
Day Cts	1	1	13166.28	15.8036	0.0002*
Day Cts*Day Cts	1	1	11558.13	13.8733	0.0005*

Table C.14: Lack of fit F-test for $I_{N_2}/I_{O_{20}}$ after blue light fit statistical model in aging experiment.

Lack Of Fit

Source	DF	Sum of Squares	Mean Square	F Ratio
Lack Of Fit	15	24043.963	1602.93	3.1855
Pure Error	35	17612.028	503.20	Prob > F
Total Error	50	41655.991		0.0024*
				Max RSq
				0.9341

β-Carotene as Singlet Oxygen Quencher Experiment Supplemental Statistics

Table C.15: Summary of model fit for $I_{N_2}/I_{O_{20}}$ response with β- Carotene.

Summary of Fit

RSquare	0.400245
RSquare Adj	0.160343
Root Mean Square Error	0.285362
Mean of Response	1.199489
Observations (or Sum Wgts)	15

Table C.16: ANOVA table for $I_{N_2}/I_{O_{20}}$ response with β-Carotene.

Analysis of Variance

Source	DF	Sum of Squares	Mean Square	F Ratio
Model	4	0.5434302	0.135858	1.6684
Error	10	0.8143127	0.081431	Prob > F
C. Total	14	1.3577429		0.2329

Table C.17: Summary of model fit for $I_{N_2}/I_{O_{20}}$ after blue light fit response with β- Carotene.

Summary of Fit	
RSquare	0.707102
RSquare Adj	0.576926
Root Mean Square Error	0.098934
Mean of Response	0.941619
Observations (or Sum Wgts)	14

Table C.18: ANOVA table for $I_{N_2}/I_{O_{20}}$ after blue light fit response with β-Carotene.

Analysis of Variance				
Source	DF	Sum of Squares	Mean Square	F Ratio
Model	4	0.21266902	0.053167	5.4319
Error	9	0.08809224	0.009788	Prob > F
C. Total	13	0.30076126		0.0167*

Lifetime Experiment Supplemental Statistics

Table C.19: Lifetime ANOVA table with null hypothesis that none of the levels of percent difference across polymer are significant.

Analysis of Variance					
Source	DF	Sum of Squares	Mean Square	F Ratio	Prob > F
Polymer	4	154.87333	38.7183	17.8207	0.0002*
Error	10	21.72667	2.1727		
C. Total	14	176.60000			

Table C.20: Lifetime percent change level difference statistical summary with p-values.

Ordered Differences Report

Level	- Level	Difference	Std Err Dif	Lower CL	Upper CL	p-Value
Nylon-6	PSU	8.966667	1.203513	5.00581	12.92753	0.0002*
Nylon-6	PET	8.033333	1.203513	4.07247	11.99419	0.0004*
Nylon-6	PES	7.333333	1.203513	3.37247	11.29419	0.0009*
Nylon-6	PSU High	7.166667	1.203513	3.20581	11.12753	0.0010*
PSU High	PSU	1.800000	1.203513	-2.16086	5.76086	0.5870
PES	PSU	1.633333	1.203513	-2.32753	5.59419	0.6653
PET	PSU	0.933333	1.203513	-3.02753	4.89419	0.9321
PSU High	PET	0.866667	1.203513	-3.09419	4.82753	0.9470
PES	PET	0.700000	1.203513	-3.26086	4.66086	0.9749
PSU High	PES	0.166667	1.203513	-3.79419	4.12753	0.9999

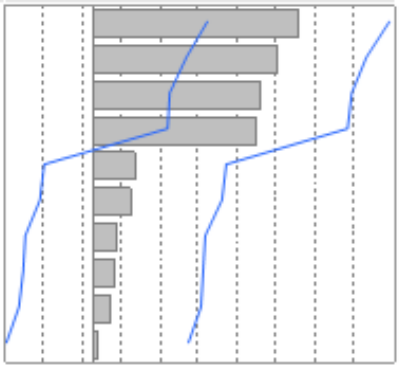

Table C.21: Lifetime ANOVA table with null hypothesis that none of the levels of polymer or age are significant.

Analysis of Variance

Source	DF	Sum of Squares	Mean Square	F Ratio	Prob > F
Polymer	9	9.0469414	1.00522	104.5883	<.0001*
Error	20	0.1922233	0.00961		
C. Total	29	9.2391648			

Table C.22: Lifetime polymer and age level difference statistical summary with p-values.

Ordered Differences Report

Level	- Level	Difference	Std Err Dif	Lower CL	Upper CL	p-Value
PSU High UNAGED	PET AGED	1.641308	0.0800465	1.35785	1.924762	<.0001*
Nylon 6 UNAGED	PET AGED	1.513399	0.0800465	1.22995	1.796853	<.0001*
PSU High UNAGED	PES AGED	1.477646	0.0800465	1.19419	1.761099	<.0001*
Nylon 6 UNAGED	PES AGED	1.349737	0.0800465	1.06628	1.633190	<.0001*
PSU High UNAGED	PES UNAGED	1.322096	0.0800465	1.03864	1.605550	<.0001*
PSU AGED	PET AGED	1.299460	0.0800465	1.01601	1.582913	<.0001*
PSU High UNAGED	PET UNAGED	1.249470	0.0800465	0.96602	1.532924	<.0001*
PSU High UNAGED	PSU High Load AGED	1.240547	0.0800465	0.95709	1.524000	<.0001*
Nylon 6 UNAGED	PES UNAGED	1.194187	0.0800465	0.91073	1.477641	<.0001*
PSU AGED	PES AGED	1.135797	0.0800465	0.85234	1.419251	<.0001*
Nylon 6 UNAGED	PET UNAGED	1.121561	0.0800465	0.83811	1.405015	<.0001*
Nylon 6 UNAGED	PSU High Load AGED	1.112637	0.0800465	0.82918	1.396091	<.0001*
PSU High UNAGED	Nylon 6 AGED	0.982182	0.0800465	0.69873	1.265635	<.0001*
PSU AGED	PES UNAGED	0.980248	0.0800465	0.69679	1.263701	<.0001*
PSU AGED	PET UNAGED	0.907622	0.0800465	0.62417	1.191075	<.0001*
PSU High UNAGED	PSU UNAGED	0.904454	0.0800465	0.62100	1.187908	<.0001*
PSU AGED	PSU High Load AGED	0.898698	0.0800465	0.61524	1.182152	<.0001*
Nylon 6 UNAGED	Nylon 6 AGED	0.854273	0.0800465	0.57082	1.137726	<.0001*
Nylon 6 UNAGED	PSU UNAGED	0.776545	0.0800465	0.49309	1.059999	<.0001*
PSU UNAGED	PET AGED	0.736854	0.0800465	0.45340	1.020308	<.0001*
Nylon 6 AGED	PET AGED	0.659126	0.0800465	0.37567	0.942580	<.0001*
PSU AGED	Nylon 6 AGED	0.640334	0.0800465	0.35688	0.923787	<.0001*
PSU UNAGED	PES AGED	0.573191	0.0800465	0.28974	0.856645	<.0001*
PSU AGED	PSU UNAGED	0.562606	0.0800465	0.27915	0.846059	<.0001*
Nylon 6 AGED	PES AGED	0.495464	0.0800465	0.21201	0.778917	0.0002*
PSU UNAGED	PES UNAGED	0.417642	0.0800465	0.13419	0.701095	0.0014*
PSU High Load AGED	PET AGED	0.400762	0.0800465	0.11731	0.684215	0.0022*
PET UNAGED	PET AGED	0.391838	0.0800465	0.10838	0.675291	0.0027*
PSU UNAGED	PET UNAGED	0.345016	0.0800465	0.06156	0.628470	0.0099*
PSU High UNAGED	PSU AGED	0.341848	0.0800465	0.05839	0.625302	0.0107*
Nylon 6 AGED	PES UNAGED	0.339914	0.0800465	0.05646	0.623368	0.0113*
PSU UNAGED	PSU High Load AGED	0.336092	0.0800465	0.05264	0.619546	0.0126*
PES UNAGED	PET AGED	0.319212	0.0800465	0.03576	0.602666	0.0197*
Nylon 6 AGED	PET UNAGED	0.267289	0.0800465	-0.01616	0.550742	0.0748
Nylon 6 AGED	PSU High Load AGED	0.258365	0.0800465	-0.02509	0.541818	0.0928
PSU High Load AGED	PES AGED	0.237099	0.0800465	-0.04635	0.520553	0.1520
PET UNAGED	PES AGED	0.228175	0.0800465	-0.05528	0.511629	0.1849
Nylon 6 UNAGED	PSU AGED	0.213939	0.0800465	-0.06951	0.497393	0.2487
PES AGED	PET AGED	0.163663	0.0800465	-0.11979	0.447116	0.5811
PES UNAGED	PES AGED	0.155549	0.0800465	-0.12790	0.439003	0.6431
PSU High UNAGED	Nylon 6 UNAGED	0.127909	0.0800465	-0.15554	0.411363	0.8344
PSU High Load AGED	PES UNAGED	0.081550	0.0800465	-0.20190	0.365003	0.9873
PSU UNAGED	Nylon 6 AGED	0.077728	0.0800465	-0.20573	0.361181	0.9909
PET UNAGED	PES UNAGED	0.072626	0.0800465	-0.21083	0.356079	0.9943
PSU High Load AGED	PET UNAGED	0.008924	0.0800465	-0.27453	0.292377	1.0000

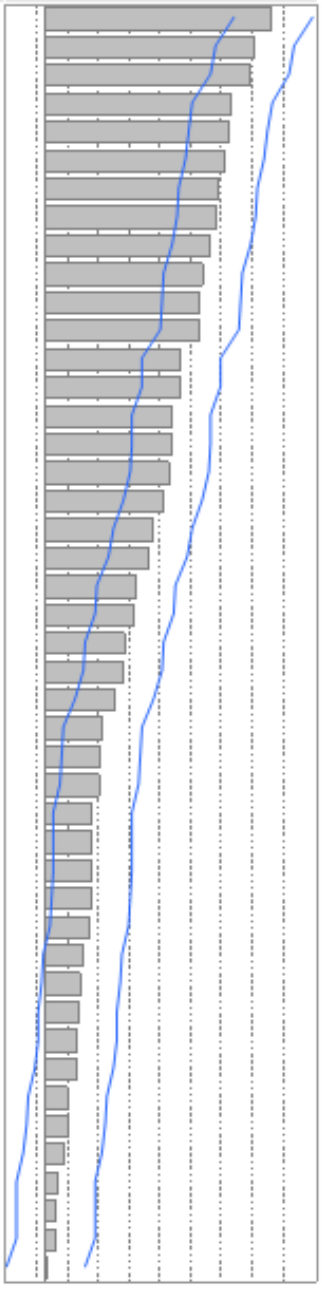

Appendix D: Sample Photobleaching Images.

Photobleached Samples from Polymer Aging Experiment

(a) PES-PCL + 0.5 wt.% PdTFPP sample replicates aged for 1 day and 1000 hours under continuous excitation.

(b) PET-PCL + 0.5 wt.% PdTFPP sample replicates aged for 1 day and 1000 hours under continuous excitation.

(c) PSU-PCL + 0.5 wt.% PdTFPP sample replicates aged for 1 day and 1000 hours under continuous excitation.

(d) Nylon-6-PCL + 0.5 wt.% PdTFPP sample replicates aged for 1 day and 1000 hours under continuous excitation.

Figure D.1: Select photobleached samples from polymer aging experiment. Photobleaching occurred in green. Light pink outer rims represent portions of samples that remained unbleached.

Photobleached Samples from Lifetime Experiment

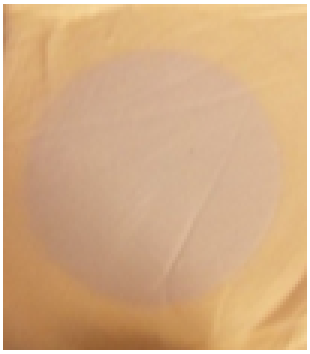

(a) Nylon-6-PCL + 0.5 wt.% $Ru(dpp)_3Cl_2$ lifetime sample aged for 28 days under continuous excitation.

(b) PSU-PCL + 0.5 wt.% $Ru(dpp)_3Cl_2$ lifetime sample aged for 28 days under continuous excitation.

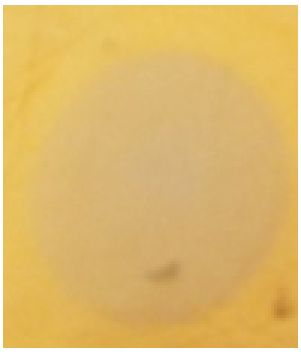

(c) PSU-PCL + 3 wt.% $Ru(dpp)_3Cl_2$ lifetime sample aged for 28 days under continuous excitation.

Figure D.2: Select photobleached samples from lifetime experiment. Photobleaching occurred in circular blue regions contrasted with original non-bleached orange regions.

Photobleached Samples from Experiment Exploring β-Carotene

Figure D.3: PSU-PCL + 0.5 wt.% $Ru(dpp)_3Cl_2$ + 0.06 wt.% β-Carotene sample replicates aged for 1 week under continuous excitation. The orange region is indicative of β-Carotene additive. The light pink region is indicative of PdTFPP. The faint green regions are the photobleached areas.

Appendix E: Polymer Material Properties

Table E.1: Oxygen permeability values for all experimented core polymers [28]

Polymer	**Oxygen Permeability** $\left[\frac{(cm^3-mm)}{(m^2-day-atm)}\right]$
Nylon-6	1.2
PES	14.6
PET	0.223
PSU	91

Table E.2: Mechanical properties of experimented core polymers [28].

Polymer	**Modulus of Elasticity (GPa)**	**Rockwell Hardness M**
Nylon-6	2.59	85.0
PES	7.5	92.5
PET	3.14	92.2
PSU	5.18	77.3

Appendix F: Electrospun Fiber Morphology

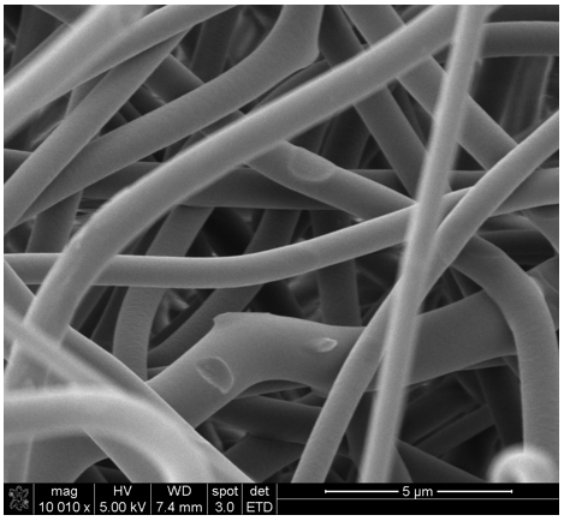

(a) Nanofiber morphology taken from an SEM for Nylon-6 host from polymer aging experiment.

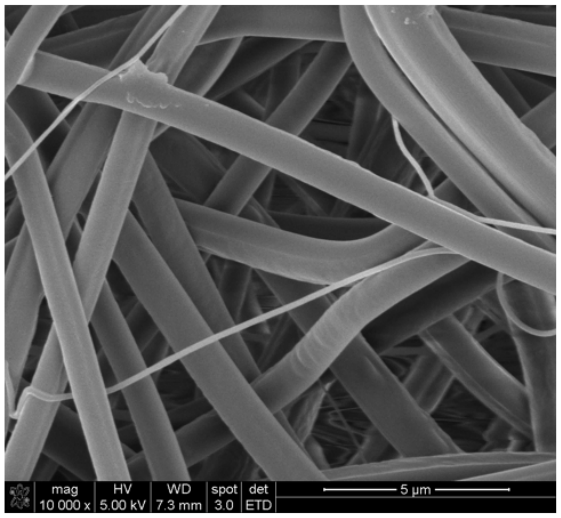

(b) Decay of 0.5 wt.% $Ru(dpp)_3Cl_2$ dye load emission curves with PES host.

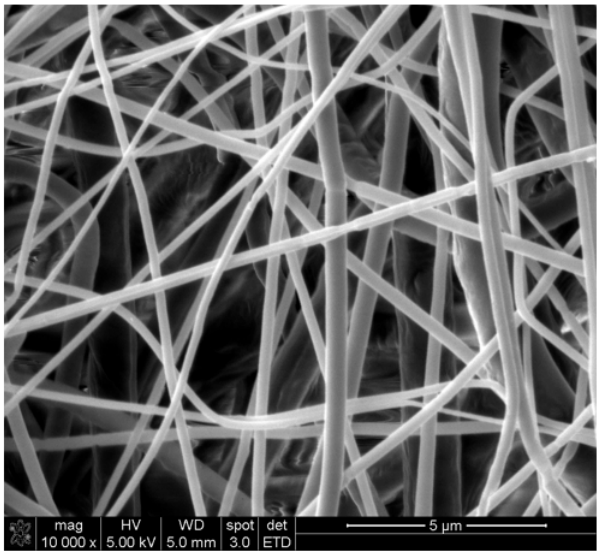

(c) Nanofiber morphology taken from an SEM for Nylon-6 host from polymer aging experiment.

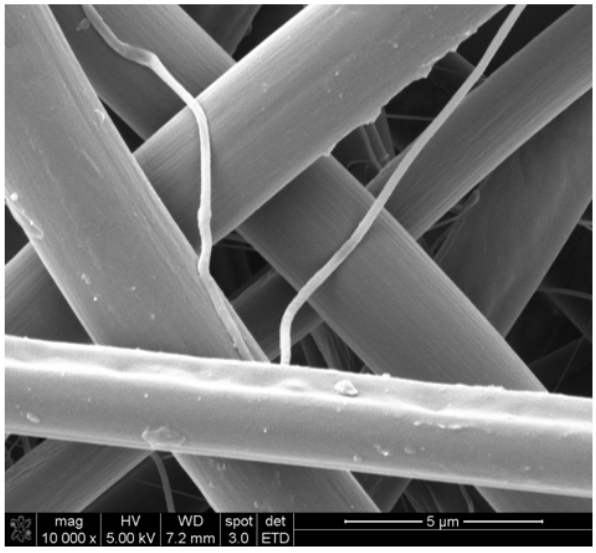

(d) Decay of 0.5 wt.% $Ru(dpp)_3Cl_2$ dye load emission curves with PES host.

Figure F.1: Nanofiber morphology images gathered from an SEM, obtained from samples used in polymer aging experiment.

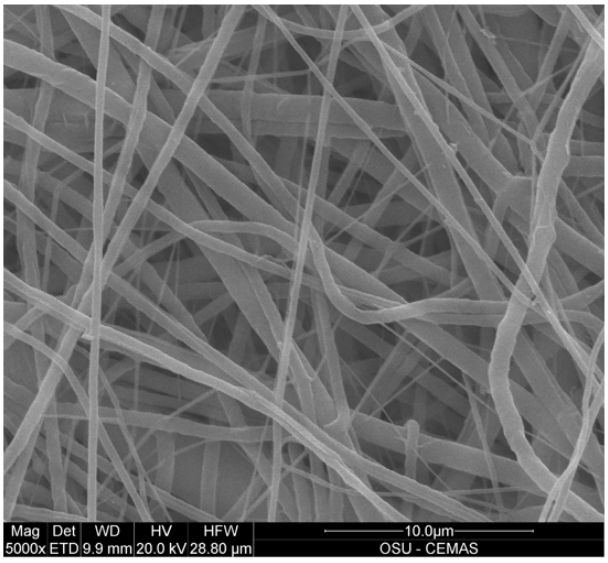

(a) Nanofiber morphology taken from an SEM for Nylon-6 host from the lifetime experiment.

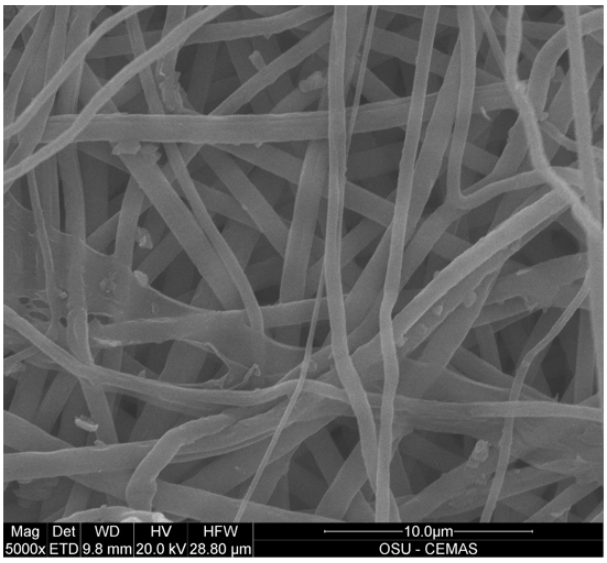

(b) Nanofiber morphology taken from an SEM for PES host from the lifetime experiment.

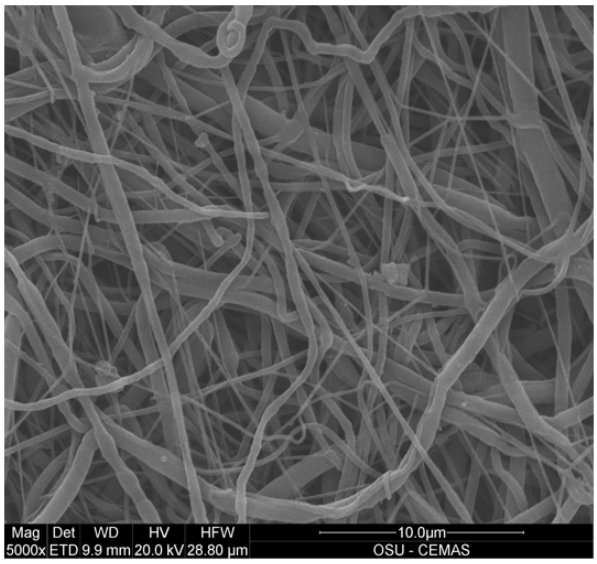

(c) Nanofiber morphology taken from an SEM for PET host with 0.5wt.% $Ru(dpp)_3Cl_2$ dye load from the lifetime experiment.

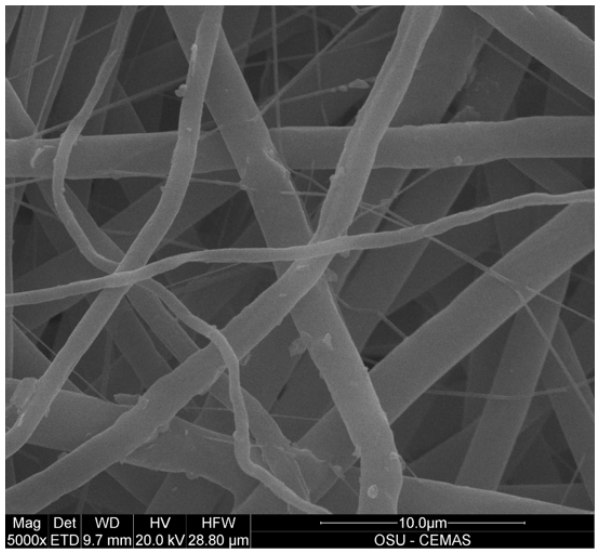

(d) Nanofiber morphology taken from an SEM for PSU host from the lifetime experiment.

Figure F.2: Nanofiber morphology images taken from an SEM for PES, PET, PSU, and Nylon-6 hosts with 0.5wt.% $Ru(dpp)_3Cl_2$ dye load from the lifetime experiment.

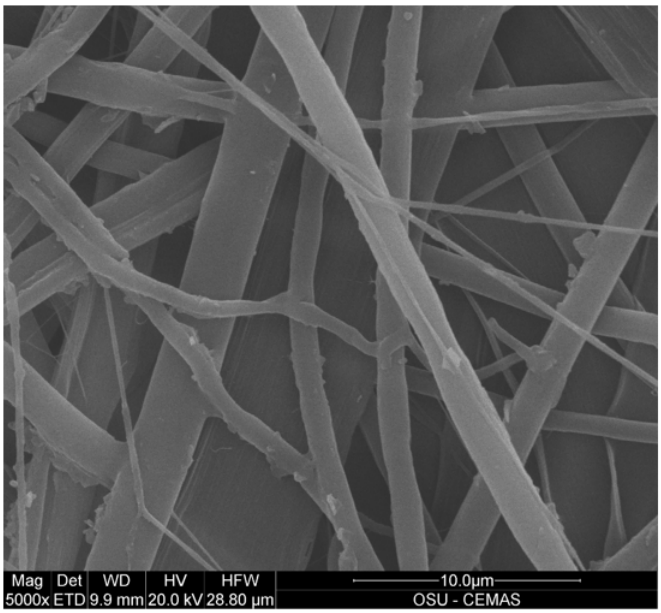

Figure F.3: Nanofiber morphology taken from an SEM for PSU host with 3wt.% $Ru(dpp)_3Cl_2$ dye load from the lifetime experiment.